8-2019

Linkage of Climate Diagnostics in Predictions for Crop Production: Cold Impacts in Taiwan and Thailand

Parichart Promchote
Utah State University

LINKAGE OF CLIMATE DIAGNOSTICS IN PREDICTIONS FOR CROP PRODUCTION: COLD IMPACTS IN TAIWAN AND THAILAND

by

Parichart Promchote

A dissertation submitted in partial fulfillment
of the requirements for the degree

of

DOCTOR OF PHILOSOPHY

in

Climate Science

Approved:

Shih-Yu Simon Wang, Ph.D. Major Professor	Paul G. Johnson, Ph.D. Committee Member
Roger Kjelgren, Ph.D. Committee Member	Earl Creech, Ph.D. Committee Member
Hernan Tejeda, Ph.D. Committee Member	Yuan Shen, Ph.D. Committee Member

Richard S. Inouye, Ph.D.
Vice Provost for Graduate Studies

UTAH STATE UNIVERSITY
Logan, Utah

2019

ABSTRACT

Linkage of Climate Diagnostics in Predictions for Crop Production:

Cold Impacts in Taiwan and Thailand

by

Parichart Promchote, Doctor of Philosophy

Utah State University, 2019

Major Professor: Dr. S.-Y. Simon Wang
Department: Plants, Soils, and Climate

This research presents three case studies of low temperature anomalies that occurred during the winter–spring seasons influenced extreme events and crop production. We investigate causes and effects of each climate event and developed prediction methods for crops based on the climate diagnostic information. The first study diagnosed driven environmental-factors associated with the 2011 great flood in Thailand which resulted in total crop loss. The flood was caused by abnormally high monsoon rainfall over the Chao Phraya River basin (CPRB) and low drainage capacity because of anomalous high soil-moisture, increased Gulf of Thailand sea level, and other management factors. Increased premonsoon rainfall in March, strengthened by prominent northeasterly cold winds coming from East Asia, was a key element to increase soil moisture. Increases in the premonsoon rainfall are projected in the future because of influences from rising anthropogenic greenhouse gases over the CPRB. The second

study investigated climate circulation and indices related to wet-and-cold (WC) events that lead to significant crop damage in Taiwan. We developed empirical-dynamical models by using observed indices of western North Pacific (WNP), Niño 3.4, and Arctic Oscillation and predicted indices of WNP and Pacific meridional mode (PMM) from Climate Forecast System Version 2 (CFSv2) outputs. The prediction was suitable for 6 months leading up to the occurrence of the WC events. Our final study extends from the second study and aims to predict chronic crop damage from climate change by using a crop simulation model, ORYZA(v3) and RCP 8.5 scenario from Coordinated Regional Climate Downscaling Experiment (CORDEX). The long-term prediction of rice growth and yield for different regions of Taiwan illustrated an earlier maturation of 6–11 days by 2045. Yield was predicted to be reduced by 3.3–10% or increased by 8.5–18% without or with rising CO_2 effects respectively. The three studies, while different in location and circumstances, were influenced by similar climate phenomena. These findings are useful to support plans to adapt cropping in these specific study sites. The same methodologies can be applied across Thailand, Taiwan, and other areas with similar agro-climatology.

(156 pages)

PUBLIC ABSTRACT

Linkage of Climate Diagnostics in Predictions for Crop Production:

Cold Impacts in Taiwan and Thailand

Parichart Promchote

This research presents three case studies of low temperature anomalies that occurred during the winter–spring seasons and their influence on extreme events and crop production. We investigate causes and effects of each climate event and developed prediction methods for crops based on the climate diagnostic information. The first study diagnosed the driven environmental-factors, including climate pattern, climate change, soils moisture, and sea level height, associated with the 2011 great flood in Thailand and resulting total crop loss. The second study investigated climate circulation and indices that contributed to wet-and-cold (WC) events leading to significant crop damage in Taiwan. We developed empirical–dynamical models based on prominent climate indices to confidently predict WC events as much as 6 months before they occur. The final study extends from the second study and predict chronic damage to rice crops from climate change by using a crop simulation model. The long-term prediction of rice growth and yield effectively illustrated both decreases and increases in yield depending on climate scenarios. The three studies are different in location and circumstances but the methodologies can be applied across Thailand, Taiwan, and other areas with similar agro-climatology.

ACKNOWLEDGMENTS

I would like to thank the Royal Thai Government for a full graduate scholarship and Faculty of Agriculture, Kasetsart University (KU) for support and providing me a great opportunity to pursue my education. I would also like to thank Dr. Ming-Hwi Yao for his help to access Taiwan's weather data and rice data from field experiments at Taiwan Agricultural Research Institute, Taichung. The research could not have been achieved without the collaboration from National Chung Hsing University.

I would like to give my gratitude to my other committee members, Drs. Roger Kjelgren, Earl Creech, Hernan Tejeda, and Yuan Shen, for their assistance throughout the entire process of the study. Very importantly, I would especially express my gratefulness to my major advisor, Simon Wang and co-major advisor, Paul Johnson for their guidance, encouragement, support, warm heart, and appreciable work together throughout my academic track at USU.

Finally, special thanks are given to my family, friends, colleagues at USU, dean Sutkhet Nakasathien, colleagues from Department of Agronomy-KU, Mr. Wichai Pakayanon and other staff of the Royal Thai Embassy at Washington D.C. I could not have done it without all of you.

Parichart Promchote

CONTENTS

Page

ABSTRACT iii

PUBLIC ABSTRACT v

ACKNOWLEDGMENTS vi

LIST OF TABLES x

LIST OF FIGURES xi

CHAPTER

I. INTRODUCTION 1

II. THE 2011 GREAT FLOOD IN THAILAND: CLIMATE DIAGNOSTICS AND IMPLICATIONS FROM CLIMATE CHANGE 5

Abstract 5
Introduction 6
Data and methods 8

Methodology 8
Data sources 10

Results and discussion 12

Rainfall distribution and changes 12
Role of soil moisture and sea level 15
Impact of tropical cyclones 17
Weather and climate patterns 18
Model attribution analysis 21

Concluding remarks 22
Acknowledgments 24
References 24
Table and figures 32

III. A SEASONAL PREDICTION FOR THE WET–COLD SPELLS LEADING TO WINTER CROP DAMAGE IN NORTHWESTERN TAIWAN WITH A COMBINED EMPIRICAL–DYNAMICAL APPROACH 42

Abstract 42
Introduction 43
Methods and data sets 45

Crop damage and weather events 46
Meteorological data and climate indices 47
CFSv2 reforecast 48

Results and discussion 49

Relation of crop damage and wet–cold events 49
Climate patterns associated with the wet–cold spells 51
Predictive skill evaluation 53
Discussion 57

Concluding remarks 58
Acknowledgments 60
Supporting information 61
References 61
Tables and figures 70

IV. PROJECTED RICE GROWTH AND YIELD IN TAIWAN UNDER CHANGING COLD SEASON 81

Abstract 81
Introduction 82
Material and methods 84

Study areas 84
Data collection 85
Observed rice data 85
Observed weather data 85
Projected climate data 85
Simulation framework 86
Step (A): ORYZA(v3) calibration, validation, and evaluation 86
Step (B): downscaling of outputs from climate model 87
Step (C): simulation of potential rice growth and yield 88

Results 88

ORYZA(v3) performance 88
Response of rice phenology on warming trend 89
Spikelet sterility because of temperature 90

Potential change of rice yield in the future without rising CO_2 91
Effects of rising CO_2 on rice yield 92

Discussion 93

Effects of temperature 93
Effects of CO_2 95
Simulation bias in validation 96

Conclusions 97
Supporting information 98
References 98
Figures 105

V. CONCLUSIONS 115

APPENDICES 117

APPENDIX A. SUPPORTING INFORMATION FOR CHAPTER 3 118

APPENDIX B. SUPPORTING INFORMATION FOR CHAPTER 4 121

APPENDIX C. PERMISSIONS AND RELEASE LETTERS 132

License Agreement I: Materials for Chapter 2 132
License Agreement II: Materials for Chapter 3 134
Permission to Reprint from Co-author: Chapter 3 138

CURRICULUM VITAE 139

LIST OF TABLES

Table Page

2-1 CMIM5 specifics as used in this study 32

3-1 Abbreviations used to categorize weather events 70

3-2 Correlation coefficients (*r*) between each JF-mean of weather event and climate index 71

4-S1 Lists of equations and names of CORDEX models used in this study 121

4-S2 Phenological development parameters used with TNG67 rice variety for parameterization of ORYZA(v3) model 123

4-S3 Statistics for observed and simulated outputs for TNG67 rice variety from calibration of ORYZA(v3) model 123

4-S4 Statistics for observed and simulated outputs for TNG67 rice variety from validation of ORYZA(v3) model 124

4-S5 Correlation coefficients between accumulated growing degree days and simulated rice yield for 1986–2045 (*, ** indicate significance of the coefficients exceeding 99% and 99.9% confidence interval) 125

4-S6 Correlation coefficients between accumulated radiation and simulated rice yield for 1986–2045 (*, ** indicate significance of the coefficients exceeding 99% and 99.9% confidence interval) 126

LIST OF FIGURES

Figure Page

2-1 Map of Thailand and the CPRB (shaded area of terrain) with blue boxes highlighting northern Thailand or upper CPRB (indicated by "a"), central Thailand or lower CPRB (indicated by "b"), and the Gulf of Thailand (indicated by "c"). The red box marks the location of Bangkok 33

2-2 (a),(b) The 63-yr average (1951–2013) monthly rainfall overlaid with the 6 flood years for the upper (top) and lower CPRB (bottom). (c),(d) Cumulative rainfall of each flood year and the 63-yr average for the upper (top) and lower (bottom). The above-and below-normal rainfall in 2011 is indicated by yellow- and blue-filled areas, respectively.....34

2-3 (a) Premonsoon (January–April) rainfall overlaid with the linear trend of the period 1980–2013 (red) and the 5-yr moving average (orange) for the upper CPRB. (b) As in (a), but for the lower CPRB. Linear trend slopes are highly significant with $r^2 = 0.33$ and 0.32, $p < 0.01$, for the upper and lower CPRB, respectively. (c),(d) As in (a),(b), but for the monsoon season (May-October). (e),(f) Linear trend slopes of monthly rainfall for the periods of 1951–2013, 1951–79, and 1980–2013 in the upper and lower CPRB, respectively.....35

2-4 Monthly distribution of soil moisture computed from the 1951–2014 average overlaid with 6 flood years for the (a) upper and (b) lower CPRB. The above-normal soil moisture content in 2011 is indicated by the yellow area. Premonsoon soil moisture for the (c) upper and (d) lower CPRB overlaid with the linear trend after 1980 (red) and the 5-yr moving average (orange).....36

2-5 (a) Monthly distribution of sea level height in the Gulf of Thailand from the long-term (1993–2013) average and overlaid with 6 flood years. The anomaly of 2011 sea level height from normal is indicated by the yellow area. (b) Flood-period sea level height (July–December) overlaid with the linear trend. The linear trend slope was highly significant with $r^2 = 0.67$, $p < 0.01$.....37

2-6 Tropical cyclone tracks that could have affected Thailand from both the Bay of Bengal (blue) and western North Pacific (yellow) over the period 1975–2014 during (a) January-June and (b) July–December. Red lines indicate 2011 tropical cyclones.....38

2-7 (a) The 6-hourly *u* wind at 850 mb during 1–31 Mar for each year since 1985, averaged over 13°–20°N across the CPRB from 95° to 110°E (the light-blue dashed contours represent –8 ms^{-1}). (b) As in (a), but for the *v* wind at 250 mb 39

2-8 The 850-mb wind (vectors) and SST anomalies (shading) computed from (a) 2011 and (b) epoch between the period of 1997–2013 and 1980-96 for Southeast Asia in the premonsoon season [January–April (JFMA)]. (c),(d) As in (a),(b), but for the global domain 40

2-9 Pre-monsoon rainfall derived from the observation and CMIP5 ensembles of GHG, AER, NAT and ALL forcings superimposed with 5-year moving average (black) and post-1980 linear trend (orange) constructed for the (a) upper CPRB and (b) lower CPRB. Normalization of time series is given by [(value of variable x_i – sample mean μ)/sample std dev σ]. Annual mean is plotted against the overall mean as the zero line. The anomaly means above the overall mean are plotted as positive and anomaly means below the overall mean are plotted negative. The r^2 and p values are given for those that are significant 41

3-1 Map of Taiwan with terrain elevation above mean sea level and location of Miaoli city 72

3-2 Daily temperature (yellow lines-top side), precipitation (blue lines-bottom side), and damaged crops (opened-circles) in November–March 1989–2016. Blue-dashed line boxes indicate wet spells and red-solid line boxes indicate cold spells 73

3-3 Crop damage intensity (a) and (b)–(g) frequency of weather events in January–February 1989–2016 (χ^2 is derived from Pearson's chi-squared test; Φ_c is Phi and Cramér's V) 74

3-4 Regression coefficient (shading) and correlation coefficient (contours) of (a) SST and (b) SLP computed against a time-series of cold days in January–February 1990–2016. Hatched areas indicate the significance of correlation coefficients exceeding 95% confidence interval. White box in (a) denotes the areas for PMM′ computation 75

3-5 Composite analysis for year 0 with (a) wet-cold event, (b) dry-cold event, and (c) difference between wet-cold and dry-cold events computed for the 850-mb wind (vector) with SST anomalies (shading) in January–February. (d) through (f) are the same as (a) through (b), but computed for SLP (shading). White contours

indicate statistical significance exceeding 80% confidence interval as determined by a two-tailed Student's *t* test. Red boxes indicate the location of Taiwan 76

3-6 Composite analysis for year-1 with (a) wet-cold event, (b) dry-cold event, and (c) difference between wet-cold and dry-cold events computed for the 850-mb wind (vector) with SST anomalies (shading) in January–February. (d) through (f) are the same as (a) through (b), but computed for SLP (shading). White contours indicate statistical significance exceeding 80% confidence interval as determined by a two-tailed Student's *t* test. Red boxes indicate the location of Taiwan 77

3-7 Observed wet and cold (WC) days (bars) in January–February and the estimated WC days (lines) derived from two regression models by using historical data (WNP, Niño 3.4, AO) and data in year 0; (a) CFS-WNP with CFS-PMM′ derived from CFSv2-lead month 6, (b) CFS-WNP with CFS-PMM' derived from CFSv2-lead month 1, (c) CFS-WNP with CFS-PMM′ derived from CFSv2-lead month 0, (d) WNP with PMM′, and (e) WNP with PMM-SST. Correlation coefficients (*r*) with ** are significant, exceeding 99% confidence interval 78

3-8 (a) through (c) show correlation coefficients (*r*) between WNP and CFS-WNP (lead month 0–6) in January–February (JF), January (J), and February (F). (d) through (f) are the same as (a) through (c) but computed for PMM-SST and CFS-PMM′. (g) shows *r*-values between observed-WC days and estimated-WC days derived from regression model 1 by using WNP with PMM-SST (Obs.), WNP with PMM′ (PMM′), and CFS-WNP with CFS-PMM′ (0–6). (h) is the same as (g) but derived the estimation from model 2. Correlation coefficients (*r*) with * are significant exceeding 99% confidence interval 79

3-9 Unstandardized and standardized (numbers in parentheses) regression coefficients among climate indices determined the wet-cold (WC) days using regression model 2. Unstandardized coefficients were estimated from the original scores of each climate index in the regression model, while standardized coefficients (path coefficients) were estimated from the standard scores (*z*-scores). The *z*-scores of each climate index are given by [(raw score x_i – population mean μ) / population standard deviation σ]. The error variance of the model is given as *e* 80

4-1 Panel (a) show location of Taiwan (red box) and study areas; Ilan (circle), Taichung (square), and Chaiyi (triangular), and panels (b1) –(b3) present climatology patterns of the three areas 105

4-2 Diagrams of methodological approaches to simulate rice growth and yield by using ORYZA(v3) rice model and outputs from CORDEX 106

4-3 ORYZA(v3) model calibration by using experimental data from 2009; observed (Obs) and simulated (Sim) (a) biomass, and (b) Leaf Area Index (LAI) 107

4-4 ORYZA(v3) model validation by using experiment data from 2009-2016; observed and simulated (a) yield, and (b) total above ground biomass; panel (c) shows scatter plots for yield and biomass (orange-circle marks are 2011, 2014 and 2015) 108

4-5 Time series of simulated growing degree days (GDD), lengths of vegetative (V-phase) and reproductive (R-phase) stages for three planting dates (15, 30, 45 day of year) constructed for (a) Taichung, (b) Chaiyi, and (c) Ilan; linear regression coefficients (Reg) and coefficient of determination (R^2) between year and V-phase present in each panel 109

4-6 Time series of simulated maturity date (day after emergence; DAE) and yield for three planting dates (15, 30, 45 day of year) constructed for (a) Taichung, (b) Chaiyi, and (c) Ilan; correlation coefficients (Cor) and linear regression coefficients (Reg) between maturity date and yield present in each panel (*, ** indicate significance of the coefficients exceeding 99% and 99.9% confidence interval) 110

4-7 Time series of simulated yield, number of spikelets, spikelet sterility factor because of low temperature (SF1) and spikelet fertility factor because of high temperature (SF2) for three planting dates (15, 30, 45 day of year) constructed for (a) Taichung, (b) Chaiyi, and (c) Ilan; numbers indicate significant correlation coefficients (exceeding 99% confidence interval) of SF2 and yield.....111

4-8 Simulated yield (with and without CO_2 effects) for three planting dates (15, 30, 45 day of year) and three periods (1986–2005, 2006–2025, 2026–2045) constructed for (a) Taichung, (b) Chaiyi and (c) Ilan; numbers indicate percentage of averaged-yield change compares to historical period (1986–2005) 112

4-9 Probability density function of simulated yield (without CO_2 effects) for three planting dates (15, 30, 45 day of year) and three periods (1986–2005, 2006–2025, 2026–2045) constructed for (a) Taichung, (b) Chaiyi and (c) Ilan; solid lines are averaged values from 3 models and dotted line are values of each model 113

4-10 Probability density function of simulated yield (with CO_2 effects) for three planting dates (15, 30, 45 day of year) and three periods (1986–2005, 2006–2025, 2026–2045) constructed for (a) Taichung, (b) Chaiyi and (c) Ilan; solid lines are averaged values from 3 models and dotted line are values of each model 114

3-S1 (a) Crop-damage intensity and (b) wet with cold event in January–February, which are the same as Figure 3. (c) Number of days with temperature below 10 ^{o}C and (d) mean temperature (T_{mean}) in January overlaid with the 5-year moving average (red lines) and linear trend (black). (e) Normalization of T_{mean} in January, which indicates anomaly means, is derived from [(value of T_{mean} x_i – sample mean μ)/sample standard deviation σ].....118

3-S2 Time series of PMM-SST and PMM′ (PMM-SST proxy) indicate that PMM′ has a high correlation coefficient (r = 0.937) with PMM-SST 119

3-S3 Regression coefficient (shading) of SST computed against a time-series of cold days in January–February 1990–2016 constructed over 32^{o}N-21^{o}S to 175^{o}E-95^{o}W and used as reference areas for PMM′ computation.....120

4-S1 Seasonal (January-June) observed-temperature (OBS) and projected-temperature from adjusted CORDEX constructed for (a) Taichung, (b) Chaiyi, and (c) Ilan; linear regression coefficients (Reg) and coefficient of determination (R^2) between year and temperature (Tmax, Tmin, Tmean) and presented in each panel 127

4-S2 Annual observed CO2 and projected CO2 from RCP 8.5 scenario.....128

4-S3 Probability density function of total growing degree days (GDD) from rice emergence to maturation for three-planting dates (15, 30, 45 day of year) and three periods (1986–2005, 2006–2025, 2026–2045) constructed for (a) Taichung, (b) Chaiyi, and (c) Ilan. The probability density distributions are derived with a bin size of 10 degree-days (^{o}C) 129

4-S4 Probability density function of total radiation from rice emergence to maturation for three-planting dates (15, 30, 45 day of year) and three periods (1986–2005, 2006–2025, 2026–2045) constructed for (a) Taichung, (b) Chaiyi, and (c) Ilan. The probability density distributions are derived with a bin size of 20 (Mj m^{-2}).....130

4-S5 Time series of yield, biomass and number of spikelets superimposed on (a) total radiation from panicle initiation to flowering stages (DVS0.65 to DVS1.0), (b) growing degree day (GDD) during vegetative phase (DVS0.4), and (c) precipitation and vapor pressure deficit (VPD) during DVS0.4; Panel (d) presents time series of yield bias (simulated – observed yields) and climate indices (WNP, PMM-SST, Niño 3.4, WNP*PMM-SST); number in each panel indicates significant correlation coefficients (r) exceeding 99% ($r > 0.83$) and 90% ($r > 0.62$) confidence interval. [Methods to obtain climate indices are followed Promchote et al., 2018; WNP is the western North Pacific, PMM-SST is the Pacific Meridional Mode - sea surface temperature] 131

CHAPTER 1

INTRODUCTION

Specific weather events or "extreme events" occur with the trend toward global warming. While high temperature anomalies are understandable, low temperature extremes not as intuitive. Climate scientists have explained changes in the atmospheric circulation related to elevated greenhouse gasses (GHGs) emissions, such as carbon dioxide (CO_2), that likely increase the number of high temperature events. The likelihood of unusually cold events is possible due to unusual patterns in the earth's atmosphere that are exacerbated by the prevalence of global warming. These extreme events represent "climate variability" but not of all associate climate change. Most climate variation is unique and specific for a space and time, from a short span (i.e., weekly, seasonal, interannual) to a longer period (i.e., decadal, interdecadal). Climate diagnostics, which apply a theoretical framework of climate systems and dynamics, using several analytical tools, is an appropriate method to identify nature and causes of climate variability for an individual case. Understanding extreme events can provide information to support the progress in climate forecast and can help to prevent risks and manage their impacts.

Crop production is a particular and important case that is highly vulnerable to climate extremes and climate change. National adaptation plans for crops, e.g. Thailand and Taiwan, are primarily established based on general climate impacts but are limited in predicting a particular event. Research studies predicting crop yields have commonly used observed/predicted meteorological parameters (e.g., temperature, precipitation) and well-known climate phenomenon (El Niño, La Niña, Pacific Decadal Oscillation, etc.)

without understanding whether those climate phenomena are involved. Therefore, numerous studies reported influences of high temperatures on crop production that is explained in terms of average temperature; however don't acknowledge those influences on cold events in the low latitudes.

Currently, cold events during winter and spring occur in the tropics, such as Thailand and other Indo-China countries, which influence on people's livelihoods, animals, and crops. Unusually cold events and snow have occurred in sub-tropical countries like Taiwan, leading to unprecedent crop loss in 2016. Therefore, it is essential to understand this climate variability and enable growers to prepare. Manipulation of climate diagnostic results to establish a prediction in crop risks and productivity is a challenge and is the motivation for this dissertation. The main objective of the study is to understand extreme events associated with cold anomalies in the tropics and sub-tropics and subsequently develop predictions for crop production. The study goal is accomplished by case analysis. Two prominent extreme events were selected, 2011 great flood in Thailand and unusual cold in 2016 in Taiwan. The third case focuses on future changes in climate on mean crop production and variability during the cold season in Taiwan.

The great flood in Thailand represents an impact of climate extremes that resulted in total crop loss, and no ability to predict for adaptation by the country's rice growers. Predictions can help make for a resilient cropping system under climate extremes and those predictions rely on climate projections and implications from climate change. The flood occurred during the monsoon season with high intensity and among the longest of

the country's flood events. Our research findings differ from other work by suggesting causes of substantially increased premonsoon rainfall in winter-spring because of cold spells and high sea levels in the Gulf of Thailand. We observed signals of climate change related the premonsoon rainfall that suggest potential flooding similar to the 2011 occurring in the future. Details of the analysis results and its implication from climate change are documented in Chapter 2.

The second study is of cold events in Taiwan that presents significant and abrupt damage in many crop species. The crop loss was mainly by physical injury from freeze and chilling stresses which are difficult to predict by any ecophysiological model. Our alternative method is prediction of climate events that results in the damage. Diagnostic results reveal that it is not only cold but cold combined with wet conditions that significantly caused the loss in 2016. Limitations of existing climate models are in their resolution and poor evaluation for some climate phenomenon over land. Thus, the combined empirical-dynamical models to predict wet and cold (WC) events were developed. Climate pattern attributed WC events, components and performance of the predicting models were presented in Chapter 3.

Extending from Chapter 3, the last study, or Chapter 4, determined winter crop response to climate change and variability in a future period. The probability of yield variability is investigated. This case study presents a latent effect (gradual change) of climate on crop growth and yield where predictions were directly made to crop productivity. Rice, a staple food, was selected for the study which is normally exposed to cold stress in the early growing season. The prediction was constructed based on an

existing crop simulation model and RCP 8.5 climate scenarios. The predicted results with and without CO_2 effects, performance of the model, and limitation in predictions are described in Chapter 4. Conclusions of all three case studies are given in Chapter 5.

CHAPTER 2

THE 2011 GREAT FLOOD IN THAILAND: CLIMATE DIAGNOSTICS AND IMPLICATIONS FROM CLIMATE CHANGE[1]

ABSTRACT

Severe flooding occurred in Thailand during the 2011 summer season, which resulted in more than 800 deaths and affected 13.6 million people. The unprecedented nature of this flood in the Chao Phraya River Basin (CPRB) was examined and compared with historical flood years. Climate diagnostics were conducted to understand the meteorological conditions and climate forcing that lead to the magnitude and duration of this flood. Neither the monsoon rainfall nor the tropical cyclone frequency anomalies alone was sufficient to cause the 2011 flooding event. Instead, a series of abnormal conditions collectively contributed to the intensity of the 2011 flood: anomalously high rainfall in the premonsoon season especially during March; record-high soil moisture content thorough the year; elevated sea level height in the Gulf of Thailand which constrained drainage; and other water management factors. In the context of climate change, the substantially increased premonsoon rainfall in CPRB after 1980 and the continual sea level rise in the river outlet have both played a role. The rainfall increase is associated with a strengthening of the premonsoon northeasterly winds that come from East Asia. Attribution analysis using phase 5 of the Coupled Model Intercomparison

[1] *The material for this chapter was recently published as*: Promchote, P., S.-Y. S. Wang, and P. G. Johnson, 2016: The 2011 great flood in Thailand: Climate diagnostics and implications from climate change. *J. Climate*, **29**, 367−379, doi:10.1175/JCLI-D-15-0310.1.

Project historical experiments pointed to anthropogenic greenhouse gases as the main external climate forcing leading to the rainfall increase. Together, these findings suggest increasing odds for potential flooding similar intensity to that of the 2011 flood.

1. Introduction

The Chao Phraya River Basin (CPRB) flows through densely populated areas in Thailand, including large areas of manufacturing industry in and around Bangkok (Fig. 2-1). The Chao Phraya River flows from the northern mountains of Thailand southward into the Gulf of Thailand. The lower CPRB and Bangkok cover a low-lying area, less than 2.5 m above mean sea level (MSL) and in some areas below mean sea level (Cooper 2014), and terrain like this slows down the river substantially. Having an area of 162,800 km^2, CPRB covers approximately 30% of the country (Aon Benfield 2012) and its episodic floods have impacted agriculture, economics and life in general to a great extent. The lower basin has undergone several large flooding events, including those in 1831, 1942, 1983, 1995, 1996, 2002, 2006 and 2011 (Aon Benfield 2012). The flood in 1995 was ranked the highest in terms of submerged area (444,000 km^2) while the 2011 flood ranked ninth (97,000 km^2; Gale and Saunders 2013). However, the 2011 flood lasted 158 days—longer than any other flood event in history and affecting the urban area. Damage and economic losses were unprecedented (Haraguchi and Lall 2014). As a result, the 2011 flood has been considered the worst in the last 50 years (Aon Benfield 2012; Rakwatin et al. 2013).

Previous studies suggested that the 2011 flood was caused by heavy rainfall in the northern and central CPRB (Thai Meteorological Department 2011; Aon Benfield 2012; Komori, et al. 2012; Gale and Saunders 2013; Rakwatin et al. 2013). The large rainfall amounts that accumulated from March to October were compounded by five tropical storms that affected Thailand from June through October (Thai Meteorological Department 2011). Gale and Saunders (2013) suggested that the above-normal summer monsoon rainfall in 2011 was related to anomalous low pressure and moderately positive Southern Oscillation Index (SOI), which is typically associated with La Niña. While the peak of the 2011 flood was not the highest, its duration was the longest in history (Koontanakulvong 2012). The extended period of flood is likely linked to high tides in the Gulf of Thailand that raised the river level to 2.6 m MSL (Rakwatin et al. 2013), together with land subsidence of Bangkok, which is sinking at a rate of 2–3 cm yr^{-1} (Aobpaet et al. 2009).

The lack of direct links of the 2011 flood with specific natural causes is concerning. For instance, van Oldenborgh et al. (2012) reported that the amount of rainfall in the CPRB was not unusual, and La Niña that occurred in 2011 did not have a prominent effect on the region. Gale and Saunders (2013) noted that there were substantially more tropical storms in 1995 than 2011 and yet the 1995 flood was not nearly as severe. Additionally, in 2011 the monsoon arrived on May 6, which is about 7 days earlier than normal (Thai Meteorological Department 2011). This early onset is in contrast with the projected 15-day delay in monsoon onset in Southeast Asia for the twenty-first century (Ashfag et al. 2009; Loo et al. 2015). As far as climate change is concerned, van

Oldenborgh et al. (2012) did not find any role of climate change in the 2011 flood as a result of the lack of significant trend in the monsoon precipitation in Thailand. As will be discussed in this paper, the mere focus on monsoon season precipitation undermines the substantial effect of premonsoon precipitation on soil moisture and sea level. Therefore, the objectives of this study were to 1) explore the climatic causes of the 2011 severe flood in CPRB along with a comparison with historical flood years and 2) diagnose the climate conditions, trends and their collective implication on future flood occurrence in the basin.

The paper is arranged as follows. Section 2 introduces the methodology. The outputs from our diagnostics are presented in five parts of Section 3: section 3a consides rainfall distribution and changes, section 3b evaluates the role of soil moisture and sea level, section 3c explores the impact of tropical cyclones, section 3d looks at weather and climate patterns, and section 3e conducts a model attribution analysis. Section 4 provides concluding remarks and a discussion of the implications on future flood occurrence in the CPRB.

2. Data and methods

a. Methodology

The conceptual framework to fulfill our objectives is to quantify the climatic factors involved in the imbalance of natural water supply and demand in the CPRB. Precipitation and tropical cyclones are the primary sources of water addition to the basin, while soil

moisture content and sea level height determine the capacity of natural discharge. Different from previous studies, we included soil moisture content and sea level height in our analysis and considered them as important factors for flooding in Thailand. To explore the role of climatic variations in the 2011 flood in CPRB, we conducted empirical analyses (e.g., linear regression and correlation) and analyzed climate model outputs. First, we examined atmospheric and surface conditions of 2011 and compared them with those of five historical flood years (1983, 1995, 1996, 2002, and 2006). Monthly distributions of rainfall, soil moisture content, and sea level height averaged over the upper and lower basins were analyzed. To assess the impacts of tropical cyclones on the precipitation and flooding in 2011, we analyzed tracks that potentially affect Thailand from either the Bay of Bengal or western North Pacific. In terms of climate dynamics, epoch differences of 850-mb wind field and sea surface temperature between 2011 and 1980–2013 were examined, both at regional and global domains. We also analyzed the springtime occurrence of rainstorms over CPRB using daily wind field. Trends were computed for rainfall, soil moisture content, sea level height, and tropical cyclone frequency in order to assess the role of climate change on the 2011 flood. To attribute the role of climate change in the long-term rainfall variations, we analyzed simulation outputs forced with various external climate forcings, following previous studies (Cho et al. 2015; Wang et al. 2015) that have used similar models for attributing climate extreme events in South Asia.

b. Data sources

We analyzed four meteorological variables (precipitation, tropical cyclones, wind, and sea surface temperature) and two relevant factors (soil moisture and sea level height). Daily precipitation was obtained from two sources: the Asian Precipitation–Highly Resolved Observational Data Integration Towards Evaluation of the Water Resources (APHODITE; http://www.chikyu.ac.jp/prep/), version 1101, which covered the Monsoon Asia region of 15°S–55°N, 60°E–150°E for the period of 1951–2007; and the Tropical Rainfall Measuring Mission (TRMM; http://disc2.nascom.nasa.gov/dods/3B42_V7_daily) daily precipitation for the period 1998–2014. Since APHRODITE and TRMM produced agreeable rainfall analysis over Monsoon Asia (Yatagi et al. 2012), both precipitation data sets were merged to create a longer, continuous dataset covering 1951–2014 with a spatial resolution of 0.25° x 0.25°. The merger was done by subjecting the two datasets to least-squares regression during their overlapping period. The regression function was then applied to the TRMM data to correct for the mean differences and systematic biases. We note that, although APHRODITE and TRMM datasets have correlated trends, magnitude differences do exist and the correction method eliminated those differences. We also analyzed monthly precipitation data from CRU time series (TS), version 3.21, to cross check the precipitation trend obtained from APHODITE and TRMM.

The 6-h-interval best-track records of tropical cyclones over the period of 1975–2014 were obtained from the Joint Typhoon Warning Center (JTWC; http://www.usno.navy.mil/NOOC/nmfc-ph/RSS/jtwc/best_tracks/) and UNISYS Weather (http://weather.unisys.

com). Monthly soil moisture (assimilation) data with a spatial resolution of 0.5° x 0.5° was obtained from the NOAA/OAR/ESRL Physical Sciences Division (PSD; http://www.esrl.noaa.gov/psd/data/gridded/data.cpcsoil.html). The dataset contains model-based water height equivalent (volume of water/soil surface area) over landmass (van den Dool et al. 2003; Fan and van den Dool 2004). The wind field of the period 1951-2014 was obtained from the NCEP–NCAR reanalysises at a spatial resolution of 2.5° x 2.5° (Kalnay et al. 1996). Sea level height data came from the Oceans and Atmosphere Flagship of Australian's Commonwealth Scientific and Industrial Research Organisation (CSIRO) and the Antarctic and Ecosystems (ACE) Cooperative Research Centre (CRC) as a combination of data from various satellites (http://www.cmar.csiro.au/sealevel/sl-data_cmar.html). The sea level data are monthly averages on a 1° x 1° grid applied with an inverse barometer correction, seasonal (annual and semiannual) signal removal, and glacial isostatic adjustment (GIA) correction (Church et al. 2004). NOAA extended reconstructed SST, version 3b (ERSST.v3b), data with a resolution 2° x 2° during the period of 1854–2014 were also used.

Finally, for the attribution analysis of external climate forcing, we analyzed precipitation outputs of 10 models from phase 5 of the Coupled Model Intercomparison Project (CMIP5) historical single-forcing experiments, which were driven by (i) only greenhouse gas forcing (GHG), (ii) only aerosol forcing (AERO), (iii) only natural forcing including volcanic and solar forcing (NAT), and (iv) all the forcing combined (ALL). These experiments were initialized from long stable preindustrial (1850) control run up to 2005. The specifics of these CMIP5 models are described in Table 2-1.

3. Results and Discussion

a. Rainfall distribution and changes

We compared the monthly and accumulated rainfall in 2011 with that of the other flood years (1983, 1995, 1996, 2002, and 2006) for two study areas, defined as the upper CPRB (16.0°–20.6°N, 97.5°–101.5°E; indicated by "a" in Fig. 2-1a) and the lower CPRB (13.5°–16.0°N, 98.5°–101.5°E; indicated by "b" in Fig. 2-1b), the division of which follows Molle (2007) and Rakwatin et al. (2013). Figures 2-2a and 2-2b illustrate the distribution of monthly rainfall averaged for the upper and lower CPRB, respectively, for these 6 flood years and the 63-year average (1951–2013). Rainfall in 2011 was above the 63-year average from January to July in the upper basin and until August in the lower basin. This excessive rainfall apparently occurred and accumulated before the flood started at the upper CPRB in late July. The usually dry month of March and the early monsoon season of May–July received significantly more rains than normal. According to the Thai Meteorological Department (2011), measured rainfall was higher than the 61-year average (1951–2011) by ~370% in March and ~110% in June, consistent with (and therefore verifying) our analysis using gridded data merged from TRMM and APHRODITE.

It is worth noting that monsoon rainfall in 2011 after July was not unusual—it was only slightly above normal in the upper CPRB (Fig. 2-2a). In fact, rainfall was below normal in the lower CPRB after August (Fig. 2-2b). This is contrary to most other events in which heavy monsoon rains (July–October) caused the flooding (Chokngamwong and

Chiu 2007; Thai Meteorological Department 2012), such as the monsoon season flooding in 1995 (Gale and Saunders 2012). In the lower CPRB, the highest amount of monsoon rainfall occurred in 1983, not 2011. In terms of annual accumulation of precipitation (Figs. 2-2c,d), the 2006 amount actually surpasses the 2011amount and yet it did not cause any serious flooding. Thus, rainfall accumulation alone is not a universal indicator for flooding in the CPRB. Likewise, heavy monsoon rains emphasized by previous studies (Thai Meteorological Department 2011; Aon Benfield 2012; Komori et al. 2012; Gale and Saunders 2013; Rakwatin et al. 2013) could not be held as a primary cause for flooding. In the case of 2011, wintertime and premonsoon rainfall anomalies in the upper CPRB appear to be critical.

The role of climate change in the abnormal rainfall of 2011 was investigated by plotting the rainfall trends separately for the premonsoon (January–April) and monsoon (May–October) periods over the recent 33 years (1980–2013). Figures 2-3a and 2-3b illustrate a significant increase in rainfall during the premonsoon season for both the upper (coefficient of determination $r^2 = 0.33$, $p < 0.01$) and lower ($r^2 = 0.32$, $p < 0.01$) CPRB. This trend coincides with the record rainfall received in the upper basin during the dry season of 2011. By comparison, the monsoon season rainfall exhibits a flat trend in the upper CPRB (Fig. 2-3c) and an insignificant upward trend in the lower CPRB (Fig. 2-3d). This lack of trend in the monsoon rainfall led van Oldenborgh et al. (2012) to conclude that climate change was not involved in the 2011 floods. However, Fig. 2-3c does suggest that the monsoon rainfall variability has amplified in recent decades with a strong decadal signal, as was noted by Kripalani and Kulkani (1997). According to the

literature, such rainfall variability might be associated with the Indian Ocean Dipole (Muangsong et al. 2014), SOI (Singhrattna et al. 2005), El Niño-Southern Oscillation (ENSO) (Singhrattna et al. 2005; Muangsong et al. 2014), or the Pacific quasi-decadal Oscillation (Wang and Gillies 2013). More importantly, Fig. 2-3c indicates that the highest monsoon rainfall in the upper CPRB occurred in 1994, a nonflood year. This observation suggests that premonsoon rainfall plays a more important role in the 2011 flood than monsoon rainfall.

To understand the seasonal difference in the long-term change, we derived the monthly trend of rainfall for three different periods: 1951–2013, 1951–1979 (an early era), and 1980–2013 (a recent era). The linear trend slopes of each month are plotted for the upper (Fig. 2-3e) and lower (Fig. 2-3f) CPRB. The results indicate that rainfall during the dry season (January–April and December) has increased considerably in the recent era, with the most dramatic change in March (i.e., a month of record rainfall in 2011). Although interdecadal variation is apparent and might involve natural causes, in the following section we will show that anthropogenic causes do apply. During the monsoon months, rainfall in either basin does not reveal any robust trends, with the exception of the lower basin (Fig. 2-3f) in which the early monsoon (May–July) rainfall has increased. Increased rainfall in this region of Thailand coincides with the finding of Wang et al. (2013) that early monsoon rainfall in the vicinity of Myanmar has increased partly as a result of anthropogenic aerosols.

b. Role of soil moisture and sea level

Despite the abnormal rainfall, change in the water budget of a basin system also directly influences flood potential. Here, we analyzed soil moisture content anomalies as an indicator for infiltration capacity and runoff (Nijssen et al. 2001). As soil moisture increases in the premonsoon season, rainfall infiltration and percolation in the monsoon season could be low, causing the river basin runoff to move more easily and/or quickly (Nijssen et al. 2001). The situation could worsen when the basin receives high rainfall during and after the monsoon onset. Figures 2-4a and 2-4b show the monthly distribution of soil moisture indicating the low point in April and high point in September. In 2011, soil moisture started to exceed normal in March and stayed above normal until October, amounting to as much as 11 cm above the long-term mean—the highest among all flood years. This continual surplus in soil moisture stands out from other flood years during which soil moisture was uniformly lower than normal, with the exception of 2006 when soil moisture was near normal. Arguably, the abnormally high soil moisture content in 2011 so early in the season facilitated the release of discharge when large rainfall events occurred in subsequent months, increasing runoff in the CPRB (Komori et al. 2012). The importance of concurrent increases in soil moisture and rainfall during the premonsoon season to the flood magnitude is clearly illustrated. In further examination, historical trends of premonsoon soil moisture (January–April) are shown in Figs. 2-4c and 2-4d for both basins. Although 2011 had the highest soil moisture after 1990, there was not an apparent trend in the soil moisture content of the CPRB during the past 3–4 decades. This observation echoes the pan-evaporation data in the CPRB showing a decrease throughout

the years since 1970 (Tebakari et al. 2005; Limjirakan and Limsakul 2012), which may be related to the increase in rainfall. Therefore, interannual variability in rainfall and temperature may explain the above-normal soil moisture anomaly in 2011. This relationship will be further analyzed in the weather and climate pattern section next.

Sea level height can affect drainage of surplus water from CPRB to the Gulf of Thailand (Rakwatin et al. 2013). When sea level at the mouth of CPRB rises, water flowing from the river into the Gulf of Thailand slows. Trisirisatayawong et al. (2011) have measured a tidal increase of 0.6–0.8 cm yr^{-1} near the coast of Bangkok and the mouth of the Chao Praya River. Under these circumstances, Dutta (2013) projected Bangkok to be increasingly vulnerable to flood. Therefore, we analyzed sea level fluctuation and its seasonal patterns within the domain of 6.1°–13.5°N and 99°–106° E, covering the Gulf of Thailand (Fig. 2-1c). Figure 2-5a shows monthly sea level height and the fact that 2011 was higher than the long-term average and all other flood years by a great margin, reaching 12.5 cm above normal in March and 5 cm in July and August. By late October as floodwater reached the inner metropolitan area of Bangkok, sea level height was about 4 cm above average, thereby obstructing drainage from CPRB and possibly prolonging the flood. This effect of sea level on drainage can be illustrated by comparing with the shorter flood duration in 2006 (Gale and Saunders 2013), as the sea level was near normal and would not have blocked the drainage as much as it did in 2011. The implication of this observation is important because, according to Fig. 2-5b, average sea level in the Gulf of Thailand has increased about 5 cm since 2003 and 8 cm since 1994. This trend is expected to continue under the warming climate.

Recall in Figs. 2-3a and 2-3b we showed that the premonsoon rainfall in the CPRB underwent a pronounced increase since 1980. Incidentally, Lacombe et al. (2012) suggested that the projected rainfall increases would induce local sea level rise by 2050. In addition, sea level variation in the tropical Pacific Ocean is regulated by ENSO events (Chang et al. 2013), and this coincides with the presence of La Niña in 2011 with increased sea level in the western Pacific and Indian Ocean—an interannual feature that adds to the changing climate and sea level trends.

c. Impact of tropical cyclones

Thailand is more prone to tropical cyclone strikes after July. In 2011, there were six tropical storms that impacted Indochina, and these were suggested as a contributor to the flooding (Aon Benfield 2012; Gale and Saunders 2013). However, only one tropical storm reached Thailand before the flooded period (i.e., before July), while the other five impacted Thailand during and after July (Nockten in July, Nesat and Haitang in September, Nalgae in October, and Washim in December) when the flood had already taken place. Thus, it is unlikely that tropical cyclones contributed much to the abnormal rainfall of the premonsoon season in any significant manner. As shown in Fig. 2-6, which depicts tropical cyclone tracks during the period of 1975–2014, mainland Southeast Asia undergoes frequent tropical cyclones coming from two sides: the Bay of Bengal and the western North Pacific. However, compared to other flood years, the timing and annual number of tropical cyclones in 2011 were not outstanding; in fact, the 2011 number (six cyclones) was lower than the average of 1975–2013 (seven cyclones). The fact that

rainfall in the post-July period of 2011 was not outstanding (cf. Fig. 2-3) suggests that the tropical cyclones that impacted Thailand, as depicted in Fig. 2-4b, may not contribute sufficiently to the flooding. We also note that the annual tropical cyclone numbers in the western North Pacific (13.5°–20.6°N, 97°–115°E) and the Northern Indian Ocean (13.5°–20.6°N, 90°–106°E) have not changed throughout the recent 40 years (analysis not shown). Therefore, we argue that the effect of tropical cyclones on the 2011 flood is minimal.

d. Weather and climate patterns

In this section, we analyzed the climate anomalies in 2011 and associated trends in the context of atmospheric circulations. The abnormal rainfall during winter and premonsoon seasons in the upper CPRB is likely driven by patterns of circulation anomalies. In Fig. 2-7a we show the 6-hourly *u* wind evolution at 850 mb as the time–longitude diagram for March each year, averaged over 13°–20°N across the CPRB from 95° to 110°E. Low-level zonal wind was analyzed in order to depict any change in the easterly flows that dominate the winter season (i.e., before the arrival of the monsoonal westerly winds). The month of March is shown here because it received the highest anomaly of rainfall in 2011. As shown in Fig. 2-7a, 2011 stands out as having the most pronounced easterly winds from the middle to end of March compared to all other years. This means that the relatively cool northeasterly monsoon that characterizes winter in the CPRB was much enhanced in 2011. This is further illustrated in Fig. 2-8a by the departure of 850-mb winds during January–April from the climatology (i.e., persistent increase in the

northeasterly flows coming from East Asia). The strengthened northeasterly flows interact with the mountains in western CPRB, enhancing orographic lift and subsequent rainfall generation. The cooler air temperature in spring 2011 over the CPRB (not shown) also acted to reduce evaporation and increase soil moisture.

In Fig. 2-7b, we show the 6-hourly 250-mb meridional *v* winds in the same time–longitude cross sections as Fig. 2-7a to examine the activity of synoptic waves passing through the CPRB. Although a rather strong trough passed over the basin in mid-March 2011, which produced substantial frontal rainfall (not shown), neither the magnitude nor frequency of the synoptic waves is unprecedented. This result indicates that strong low-level northeasterly wind played a crucial role in the increased precipitation of 2011 as it interacted with upper-level synoptic troughs and orography. Apparently, any long-term change in the circulation regimes affecting the CPRB likely is tied to the lower-tropospheric circulations more so than the upper level.

The large-scale circulation pattern and associated SST anomalies were examined in Fig. 2-8 for the period of January–April. At the regional domain (Fig. 2-8a), the enhanced winter monsoon manifested as northeasterly flows is accompanied by cold SST anomalies over the East Sea and the South China Sea, suggesting a strengthened East Asian winter monsoon. Meanwhile, in the Bay of Bengal the wind anomalies appear to be southwesterly accompanied by a local warming in the SST. The outcome of these two converging flows is that they collided near the western hills of the CPRB. When compared to the long-term change in the low-level wind and SST, depicted by the era difference between the years of 1951–1979 and 1980–2013 (Fig. 2-8b), similar wind

patterns appear: southwesterlies in the Bay of Bengal and (weak) northeasterlies along the East Asian coast. However, the SST near East Asia has increased persistently during the past three decades as a result of anthropogenic warming and a warming landmass (Luo et al. 2012; He and Zhou 2015).

By expanding our analysis to the global domain, it is found that the 2011 anomalies in the 850-mb winds and SST (Fig. 2-8c) exhibit a pattern generally consistent with the long-term change (Fig. 2-8d; i.e., era difference between 1997–2013 and 1980–1996), although around East Asia the colder SST and stronger winter monsoon northeasterlies stood apart from the global pattern as a pronounced regional feature. One possible explanation is that the well-developed La Niña during 2011 may enhance East Asian winter monsoon; this echoes the observation by Cheung et al. (2012) that the cold event of ENSO (i.e., La Niña) tends to enhance the Siberian high and lower the temperatures in East Asia. This observation is also apparent in 2011 by the robust anticyclone anomaly over Siberia (Fig. 2-8c), in contrast to its absence in the long-term change (Fig. 2-8d). The discrepancy here suggests that the stronger East Asian winter monsoon during 2011 is likely affected by interannual variability rather than a long-term trend. On the other hand, the Indian Ocean warming and the anomalous southwesterlies over the Bay of Bengal are part of the long-term change, and these may incidentally enhance the 2011 situation by transporting moisture towards the CPRB from the increasingly warmer water of the Bay of Bengal (Wang et al. 2013). This feature contributed to the increase in the wintertime precipitation over the CPRB as seen in Fig. 2-3, through convergent upslope winds from the east and moist flows from the southwest as revealed in Fig. 2-8b.

e. Model attribution analysis

The next important question is the extent to which the post-1980 rainfall increase resulted from anthropogenic climate change. As attribution analysis, premonsoon rainfall in the upper and lower CPRB as simulated by the CMIP5 ensembles are displayed in Figs. 2-9a and 2-9b with normalized scales. The ALL experiments produced the rainfall increase in both the upper and lower basins, though the increase in the upper CPRB is not significant. Only the GHG experiments reproduced the marked increase in rainfall after 1980, while the AERO and NAT experiments generated a flat trend. We therefore could reach a preliminary conclusion that anthropogenic GHG plays an important role in the increase of premonsoon rainfall, especially in the lower CPRB. Overall in the tropics, increased GHG would increase precipitation as the atmosphere holds more water; however, the precipitation processes in CPRB are manifold. Some implications are suggested: (i) an increase in radiative forcing, especially GHGs, can influence radiation balance on the surface, and, according to Singhratina et al. (2005), there is a significant correlation between surface temperature in March–May and rainfall in August–September over Thailand, likely due to the increased land–ocean gradient. (ii) Rainfall in northern Thailand has been reported to fluctuate in association with global temperature increases (Likasiria et al. 2014). However, our analysis indicated a less direct dynamical process—that the slight decrease in temperature after 1980 (not shown) is related to the discernable strengthening of the cool northeasterly winds (Fig. 2-8b) associated with the global SST and low-level circulation changes, both of which are tied to the GHG-induced global warming (e.g., Tokinaga et al. 2012). The GHG-induced Pacific SST pattern (e.g.,

Yeh et al. 2012) that resembles the La Niña structure manifest in Fig. 2-8d also helps strengthen a 2011-like anomalous wind pattern.

4. Concluding Remarks

The causes of the extreme floods in Thailand during 2011 were diagnosed in terms of the changes and variability in meteorological and surface conditions. The 2011 flood was different from most of the other flooding years in that it was driven by unusually high rainfall in the premonsoon (normally dry) season leading to unusually saturated soil moisture. Together with the lower basin's drainage being constrained by the large increase in sea level height in the Gulf of Thailand, the flood became not only widespread but also prolonged. Putting these yearly anomalies in the context of climate change, the effects of the substantially increased rainfall during the premonsoon season and sea level rise in the Gulf of Thailand were evident. The rainfall increase in CPRB is coupled with a mild strengthening of northeasterly winds prevailing in the premonsoon season, a feature associated with the documented global SST and circulation changes at the interdecadal timescale. In 2011, the northeasterly winds were further enhanced by La Niña. Attribution analysis using the CMIP5 single-forcing experiments indicated that anthropogenic GHG played an important role in producing the sustained increase of premonsoon rainfall over the CPRB. Additional analysis is necessary to further the understanding of the physical processes linking GHG increase in the global context to the

eventual increase in the regional rainfall, such as utilizing the full archive of daily CMIP5 outputs to examine and attribute the weather pattern change over CPRB.

Apart from climatic causes, the extreme flood in 2011 also could result from other factors that involve human activities and civil engineering, such as types of land cover, land-use change, (Sriwongsitanon and Taesombat 2011; Jothityangkoon et al. 2013), interactions between a river channel and its natural and/or constructed flood plain (Trigg et al. 2013), and impacts of reservoir operation (Mateo et al. 2014). Water management factors appeared to exacerbate the scale of the 2011 flood, such as inefficient drainage canals with broken dykes, together with challenges in managing large dams of the Bhumipol and Sirikit reservoirs (Aon Benfield 2012; Rakwatin 2013; Haraguchi and Lall 2014; Mateo et al. 2014). As Komori et al. (2012) pointed out, had the water been drained from these reservoirs earlier in the monsoon season (instead of storing it as is common practice), 1 x 10^9 m^3 of flood water could have been stored in the reservoirs during the monsoon season.

Regardless, given the results in this study that the increases in both local rainfall and sea level height are tied to anthropogenic GHG, the potential for flooding events similar to the 2011 intensity will increase. Of particular concern is the inevitable increase in sea level in the Gulf of Thailand, which will make the lower CPRB prone to longer-duration floods. On the other hand, such flooding occurrence would not be sudden and can be progressively monitored. Thus, future water management can benefit from monitoring the premonsoon and monsoon onset rainfall, soil moisture, and sea level height; this could help determine the timing and volume to drain water from reservoirs in order to mitigate

flood at its onset stage. Solving these many puzzles is by no means trivial and will require a truly cross-disciplinary approach.

Acknowledgements. The first author is supported by the Royal Thai Government through a graduate scholarship. This research was partially supported by the Utah Agricultural Experiment Station (8821), Utah State University. CPC soil moisture data were provided by the NOAA/OAR/ESRL PSD, and sea level height data were provided by the CSIRO Oceans and ACE CRC.

REFERENCES

Aobpaet, A., M. Caro Cuenca, A. Hopper, and I. Trisirisatayawong, 2009: Land subsidence evaluation using InSAR time series analysis in Bangkok metropolitan area. *Proc. Fringe 2009,* Frascati, Italy, European Space Agency, ESA SP-677. [Available online at http://earth.eo.esa.int/workshops /fringe09/proceedings/papers/ s12_6aob.pdf].

Aon Benfield, 2012: 2011 Thailand floods event recap report: Impact forecasting—March 2012. Aon Corporation Rep., 38 pp. [Available online at http://thoughtleadership.aonbenfield.com/Documents/20120314_impact_forecasting_thailand_flood_event_recap.pdf].

Ashfaq, M., Y. Shi, W. Tung, R. J. Trapp, X. Gao, J. S. Pal, and N. S. Diffenbaugh, 2009: Suppression of South Asian summer monsoon precipitation in the 21st century. *Geophys. Res. Lett*., **36**, L01704, doi:10.1029/2008GL036500.

Chang, Y.-T., L. Du, S.-W. Zhang, and P.-F. Huang, 2013: Sea level variations in the tropical Pacific Ocean during two types of recent El Niño events. *Global Planet. Change,* **108**, 119–127, doi:10.1016/j.gloplacha.2013.06.001.

Cheung, H. M., W. Zhou, H. Y. Mok, and M. C. Wu, 2012: Relationship between Ural–Siberian Blocking and the East Asian Winter Monsoon in Relation to the Arctic Oscillation and the El Niño–Southern Oscillation. *J. Climate,* **25**, 4242–4257, doi:10.1175/JCLI-D-11-00225.1.

Cho, C., R. Li, S.-Y. Wang, J.-H. Yoon, and R. R. Gillies, 2015: Anthropogenic footprint of climate change in the June 2013 northern India flood. *Climate Dyn.*, **46**, 797–805, doi:10.1007/s00382-015-2613-2.

Chokngamwong, R., and L. S. Chiu, 2008: Thailand daily rainfall and comparison with TRMM products. *J. Hydrometeor.*, **9**, 256–266, doi:10.1175/2007JHM876.1.

Church, J. A., N. J. White, R. Coleman, K. Lambeck, and J. X. Mitrovica, 2004: Estimates of the regional distribution of sea level rise over the 1950 to 2000 period. *J. Climate,* **17**, 2609–2625, doi:10.1175/1520-0442(2004)017<2609:EOTRDO>2.0.CO;2.

Cooper, R. T., 2014: Open data flood mapping of Chao Phraya River basin and Bangkok metropolitan region. *Br. J. Environ. Climate Change*, **4**, 186–216, doi:0.9734/ BJECC/ 2014/11872.

Dutta, D., 2011: An integrated tool for assessment of flood vulnerability of coastal cities to sea-level rise and potential socio-economic impacts: A case study in Bangkok, Thailand. *Hydrol. Sci. J.,* **56**, 805–823, doi:10.1080/02626667.2011.585611.

Fan, Y., and H. van den Dool, 2004: Climate Prediction Center global monthly soil moisture data set at 0.5º resolution for 1948 to present. *J. Geophys. Res.,* **109**, D10102, doi:10.1029/ 2003JD004345.

Gale. E. L., and M. A. Saunders, 2013: The 2011 Thailand flood: Climate causes and return periods. *Weather*, **68**, 233–237, doi:10.1002/wea.2133.

Haraguchi, M., and U. Lall, 2014: Flood risks and impacts: A case study of Thailand's floods in 2011 and research questions for supply chain decision making. *Int. J. Disaster Risk Reduct.*, **14**, 256–272, doi:10.1016/j.ijdrr.2014.09.005.

He, C., and T. Zhou, 2015: Responses of the western North Pacific subtropical high to global warming under RCP4.5 and RCP8.5 scenarios projected by 33 CMIP5 models: The dominance of tropical Indian Ocean–tropical western Pacific SST gradient. *J. Climate*, **28**, 365–380, doi:10.1175/JCLI-D-13-00494.1.

Jothityangkoon, C., C. Hirunteeyakul, K. Boonrawd, and M. Sivapalan, 2013: Assessing the impact of climate and land use changes on extreme floods in a large tropical catchment. *J. Hydrol*., **490**, 88–105, doi:10.1016/j.jhydrol.2013.03.036.

Kalnay, E., and Coauthors, 1996: The NCEP/NCAR 40-Year Reanalysis Project. *Bull. Amer. Meteor. Soc*., **77**, 437–471, doi:10.1175/1520-0477(1996)077<0437: TNYRP>2.0.CO;2.

Komori, D., and Coauthors, 2012: Characteristics of the 2011 Chao Phraya River flood in Central Thailand. *Hydrol. Res. Lett.,* **6**, 41–46, doi:10.3178/HRL.6.41.

Koontanakulvong, S., 2012: Thailand flood 2011: Causes and future management system. Society for Social Management Systems Rep., 9 pp. [Available online at http://kutarr .lib.kochi-tech.ac.jp/dspace/bitstream/10173/1021/1/sms12-4498.pdf.]

Kripalani, R. H., and A. Kulkarni, 1997: Rainfall variability over South-east Asia−connections with Indian monsoon and ENSO extremes: New perspectives. *Int. J. Climatol.,* **17**, 1155–1168, doi:10.1002/(SICI)1097-0088(199709)17:11<1155:: AID-JOC188>3.0.CO;2-B.

Lacombe, G., C. T. Hoanh, and V. Smakhtin, 2012: Multi-year variability or unidirectional trends? Mapping long-term precipitation and temperature changes in continental Southeast Asia using PRECIS regional climate model. *Climate Change*, **113**, 285–299, doi:10.1007/s10584-011-0359-3.

Likasiria, C., E. Duangdaia, and R. Pongvuthithumb, 2014: Mathematical model on the effects of global climate change and decreasing forest cover on seasonal rainfall in northern Thailand. *Ecol. Modell.,* **272**, 388–393, doi:10.1016/j.ecolmodel.2013. 10.022.

Limjirakan, S., and A. Limsakul, 2012: Trends in Thailand pan evaporation from 1970 to 2007. *Atmos. Res.,* **108**, 122–127, doi:10.1016/j.atmosres.2012.01.010.

Loo, Y. Y., L. Billa, and A. Singh, 2014: Effect of climate change on seasonal monsoon in Asia and its impact on variability of monsoon rainfall in Southeast Asia. *Geosci. Frontiers*, **6**, 817–823, doi:10.1016/j.gsf.2014.02.009.

Luo, J.-J., W. Sasaki, and Y. Masumoto, 2012: Indian Ocean warming modulates Pacific climate change. *Proc. Natl. Acad. Sci. USA,* **109**, 18701–18706, doi:10.1073/pnas. 1210239109.

Mateo, C. M., and Coauthors, 2014: Assessing the impacts of reservoir operation to floodplain inundation by combining hydrological, reservoir management, and hydrodynamic models. *Water Resour. Res.*, **50**, 7245–7266, doi:10.1002/2013 WR014845.

Molle, F., 2007: Scales and power in river basin management: The Chao Phraya River in Thailand. *Geogr. J.,* **173**, 358-375, doi:0.1111/j.1475–4959.2007.00255.x.

Muangsong, C., B. Cai, N. Pumijumnong, C. Hu, and H. Cheng, 2014: An annually laminated stalagmite record of the changes in Thailand monsoon rainfall over the past 387 years and its relationship to IOD and ENSO. *Quat. Int*., **394**, 90–97, doi:10.1016/ j.quaint.2014.08.037.

Nijssen, B., R. Schnur, and D. P. Lettenmaier, 2001: Global retrospective estimation of soil moisture using the variable infiltration capacity land surface model, 1980–93. *J. Climate*, **14**, 1790-1808, doi:10.1175/1520-0442(2001)014<1790:GREOSM>2.0. CO;2.

Rakwatin, P., T. Sansena, N. Marjang, and A. Rungsipanich, 2013: Using multi-temporal remote-sensing data to estimate 2011 flood area and volume over Chao Phraya River basin, Thailand. *Remote Sens. Lett*., **4**, 243–250, doi:10.1080/2150704X. 2012. 723833.

Singhrattna, N. B., K. Rajagopalan, K. Kumar, and M. Clark, 2005: Interannual and interdecadal variability of Thailand summer monsoon. *J. Climate,* **18**, 1697–1780, doi:10.1175/JCLI3364.1.

Sriwongsitanon, N., and W. Taesombat, 2011: Effects of land cover on runoff coefficient. *J. Hydrol*., **410**, 226–238, doi:10.1016/j.jhydrol.2011.09.021.

Tebakari, T., J. Yoshitani, and C. Suvanpimol, 2005: Time-space trend analysis in pan evaporation over kingdom of Thailand. *J. Hydrol. Eng*., **10**, 205–215, doi:10.1061/ (ASCE)1084-0699(2005) 10:3(205).

Thai Meteorological Department, 2011: Annual weather summary of Thailand in 2011. [Available online at: http://www.tmd.go.th/programs%5Cuploads%5Cyearly Summary %5 CAnnual2011_up.pdf].

——, 2012: The climate of Thailand. [Available online at: http://www.tmd.go.th/en/ archive/thailand_climate.pdf].

Tokinaga, H., S.-P. Xie, A. Timmermann, S. Mcgregor, T. Ogata, H. Kubota, and Y. M. Okumura, 2012: Regional patterns of tropical Indo-Pacific climate change: Evidence of the Walker circulation weakening. *J. Climate,* **25**, 1689–1710, doi:10.1175/JCLI-D-11-00263.1.

Trigg, M. A., K. Michaelides, J. C. Neal, and P. D. Bates, 2013: Surface water connectivity dynamics of a large scale extreme flood. *J. Hydrol.,* **505**, 138–149, doi:10.1016/ j.jhydrol.2013.09.035.

Trisirisatayawong, I., M. Naeije, W. Simons, and L. Fenoglio-Marc, 2011: Sea level change in the Gulf of Thailand from GPS-corrected tide gauge data and multi-

satellite altimetry. *Global Planet. Change,* **76**, 137–151, doi:10.1016/j.gloplacha.2010.12.010.

van den Dool, H., J. Huang, and Y. Fan, 2003: Performance and Analysis of the constructed analogue method applied to U.S. soil moisture applied over 1981–2001. *J. Geophys. Res.,* **108**, D16, 8617, doi:10.1029/2002JD003114.

van OldenBorgh, G. J., A. van Urk, and M. Allen, 2012: The absence of a role of climate change in the 2011 Thailand floods. *Bull. Amer. Meteor. Soc.,* **93**, 1407–1049, doi:10.1175/BAMS-D-11-00021.1.

Wang, S.-Y., and R. R. Gillies, 2013: Influence of the Pacific quasi-decadal oscillation on the monsoon precipitation in Nepal. *Climate Dyn*., **40**, 95–107, doi:10.1007/s00382-012-1376-2.

——, B. Buckley, J.-H. Yoon, and B. Fosu, 2013: Intensification of pre-monsoon tropical cyclones in the Bay of Bengal and its impacts on Myanmar. *J. Geophys Res.,* **118**, 4373–4384, doi:10.1002/jgrd.50396.

——, B. Fosu, R. R. Gillies, and P. M. Singh, 2015: The deadly Himalayan snowstorm of October 2014: synoptic conditions and associated trends [in "Explaining Extreme Events of 2014"]. *Bull. Amer. Meteor. Soc*., **96** (12), S89–S94, doi:10.1175/BAMS-D-15-001131.

Yatagai, A., K. Kamiguchi, O. Arakawa, A. Hamada, N. Yasutomi, and A. Kitoh, 2012: APHRODITE: Constructing a long-term daily gridded precipitation dataset for Asia based on a dense network of rain Gauges. *Bull. Amer. Meteor. Soc*., **93**, 1401–1415, doi:10.1175/BAMS-D-11-00122.1.

Yeh, S.-W., Y.-G. Ham, and J.-Y. Lee, 2012: Changes in the tropical pacific SST trend from CMIP3 to CMIP5 and its implication of ENSO. *J. Climate,* **25**, 7764–7771, doi:10.1175/JCLI-D-12-00304.1.

TABLES AND FIGURES

Table 2-1. CMIP5 specifics as used in this study.

Acronym	Model name	Organization, country	Ensemble member size
CanESM2	Second Generation Canadian Earth System Model	Canadian Centre for Climate Modelling and Analysis, Canada	5
CCSM4	Community Climate System Model, version 4	National Center for Atmospheric Research, USA	3
CNRM-CM5	Centre National de Recherches Météorologiques Coupled Global Climate Model, version 5	Centre National de Recherches Météorologiques /Centre Européen de Recherche et de Formation Avancées en Calcul Scientifique, France	6
GFDL CM3	Geophysical Fluid Dynamics Laboratory Climate Model, version 3	National Oceanic and Atmospheric Administration/ Geophysical Fluid Dynamics Laboratory, USA	3
GFDL-ESM2	Geophysical Fluid Dynamics Laboratory Earth System Model, version 2	National Oceanic and Atmospheric Administration/ Geophysical Fluid Dynamics Laboratory, USA	1
CSIRO Mk3.6.0	Commonwealth Scientific and Industrial Research Organisation Mark 3.6.0	Commonwealth Scientific and Industrial Research Organization/Queensland Climate Change Centre of Excellence, Australia	4
FGOALS	Flexible Global Ocean-Atmosphere-Land System Model	Institute of Atmospheric Physics, Chinese Academy of Sciences, China	1
GISS-E2	Goddard Institute for Space Studies Model E2	National Aeronautics and Space Administration Goddard Institute for Space Studies, USA	3
IPSL-CM5	L'Institut Pierre-Simon Laplace Coupled Model, version 5	L'Institut Pierre-Simon Laplace, France	3
NorESM1	Norwegian Earth System Model, version 1	Norwegian Climate Center, Norway	1

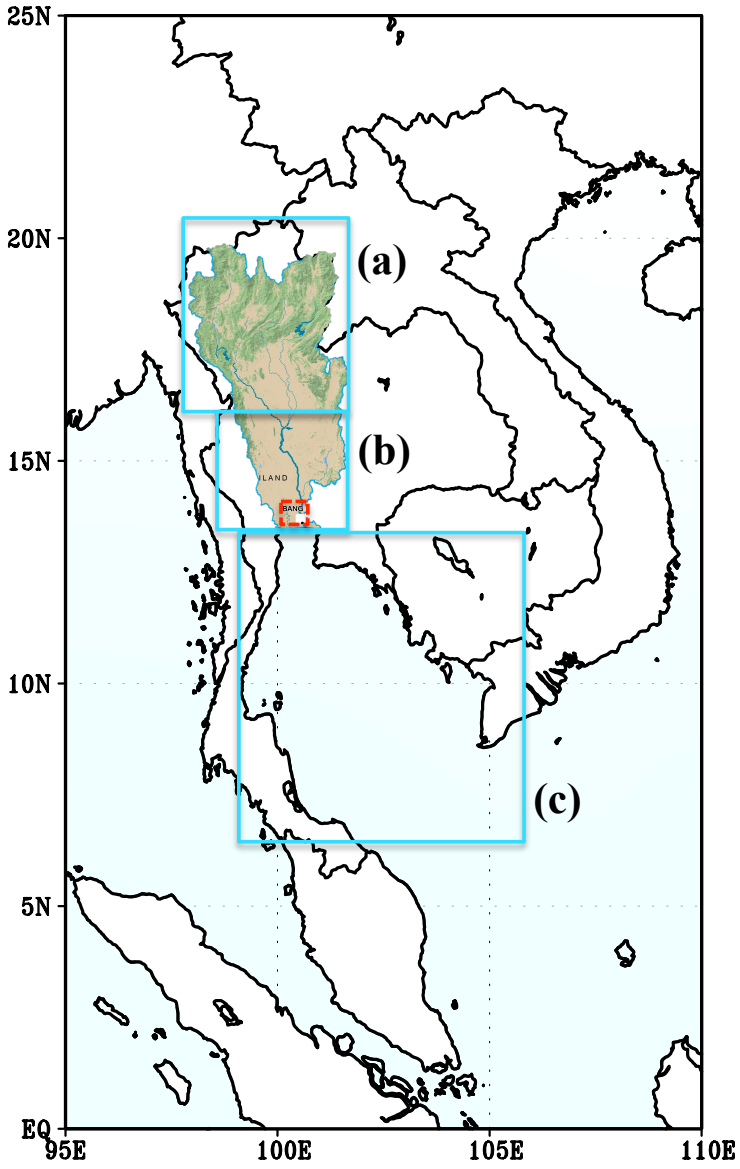

FIG. 2-1. Map of Thailand and the CPRB (shaded area of terrain) outlined with blue boxes highlighting northern Thailand or upper CPRB (indicated by “a”), central Thailand or lower CPRB (indecated by “b”), and the Gulf of Thailand (indicated by “c”). The red box marks the location of Bangkok.

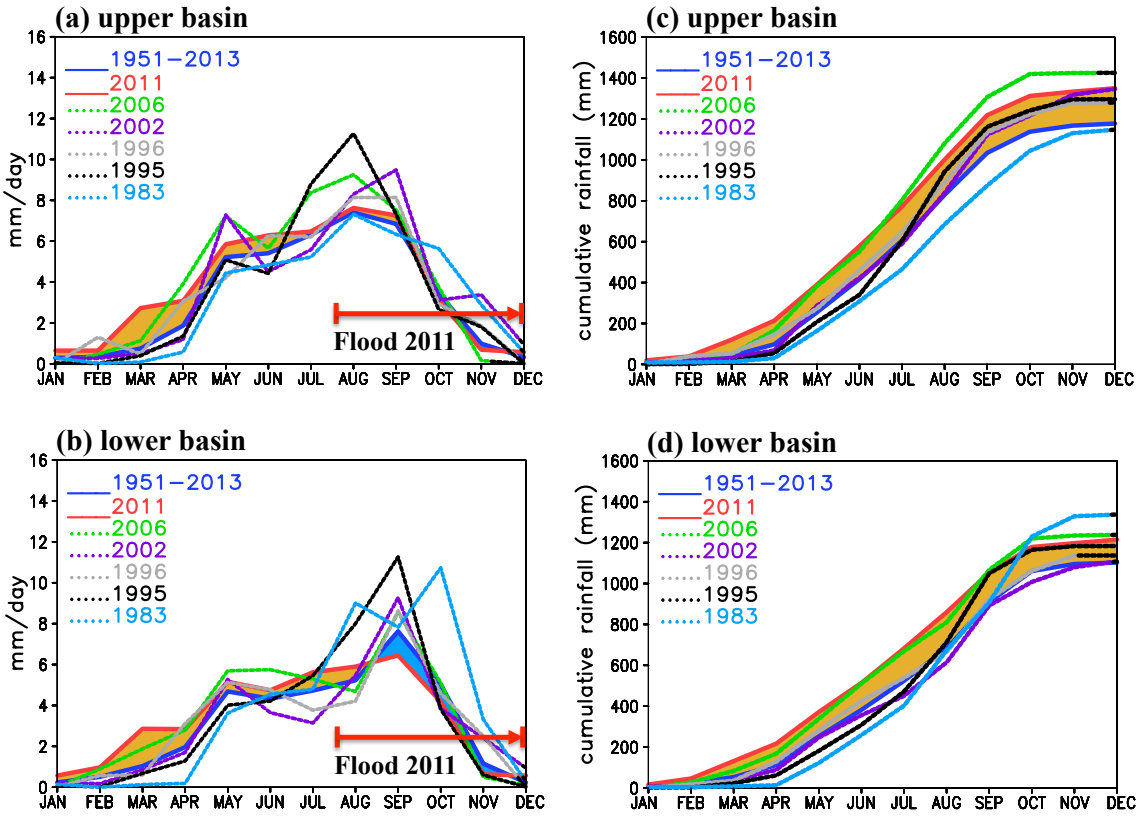

FIG. 2-2. (a),(b) The 63-yr average (1951–2013) monthly rainfall overlaid with the 6 flood years for the upper (top) and lower CPRB (bottom). (c),(d) Cumulative rainfall of each flood year and the 63-yr average for the upper (top) and lower (bottom). The above- and below-normal rainfall in 2011 is indicated by yellow- and blue-filled areas, respectively.

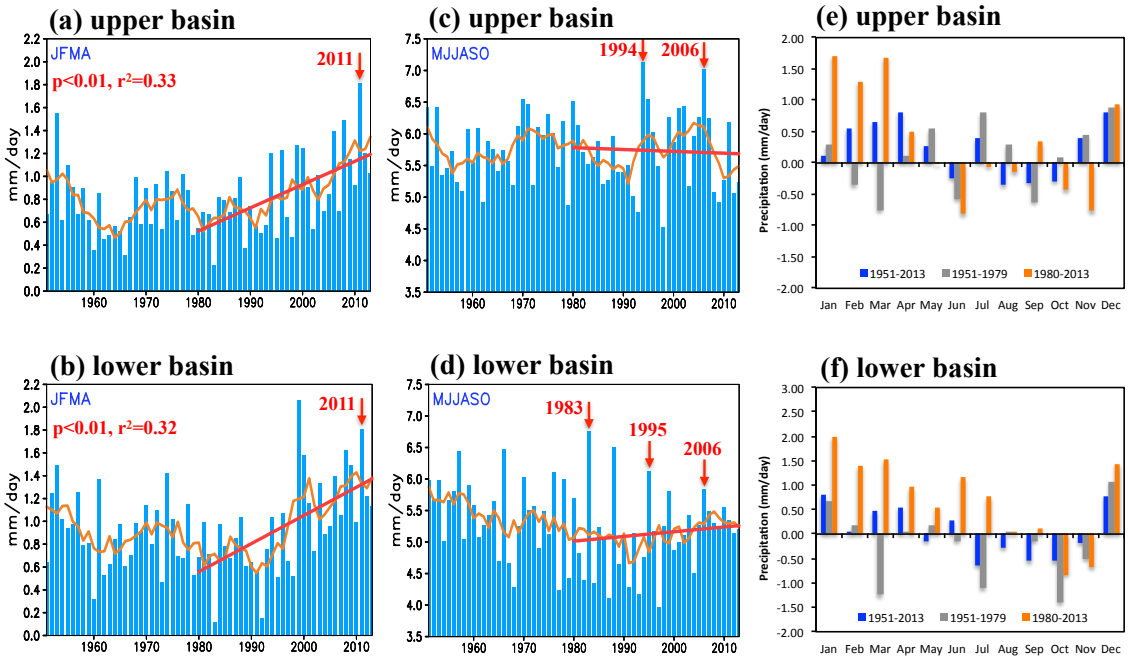

FIG. 2-3. Premonsoon (January–April) rainfall overlaid with the linear trend of the period 1980-2013 (red) and the 5-yr moving average (orange) for the upper CPRB. (b) As in (a), but for the lower CPRB. Linear trend slopes are highly significant with $r^2 = 0.33$ and 0.32, $p < 0.01$, for the upper and lower CPRB, respectively. (c),(d) As in (a),(b), but for the monsoon season (May–October). (e),(f) Linear trend slopes of monthly rainfall for the periods of 1951–2013, 1951–79, and 1980–2013 in the upper and lower CPRB, respectively.

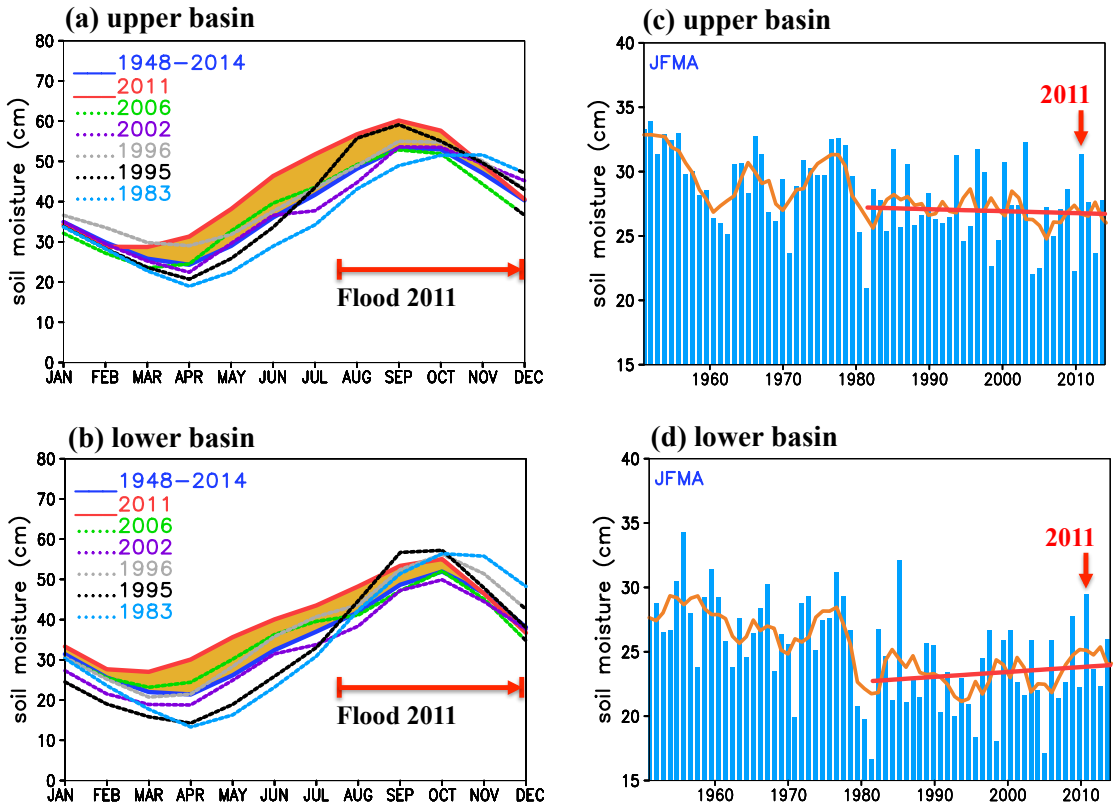

FIG. 2-4. Monthly distribution of soil moisture computed from the 1951–2014 average overlaid with 6 flood years in the (a) upper CPRB and (b) lower CPRB. The above-normal soil moisture content in 2011 is indicated by the yellow area. Pre-monsoon soil moisture for the (c) upper CPRB and (d) lower CPRB overlaid with the linear trend after 1980 (red) and the 5-year moving everage (orange).

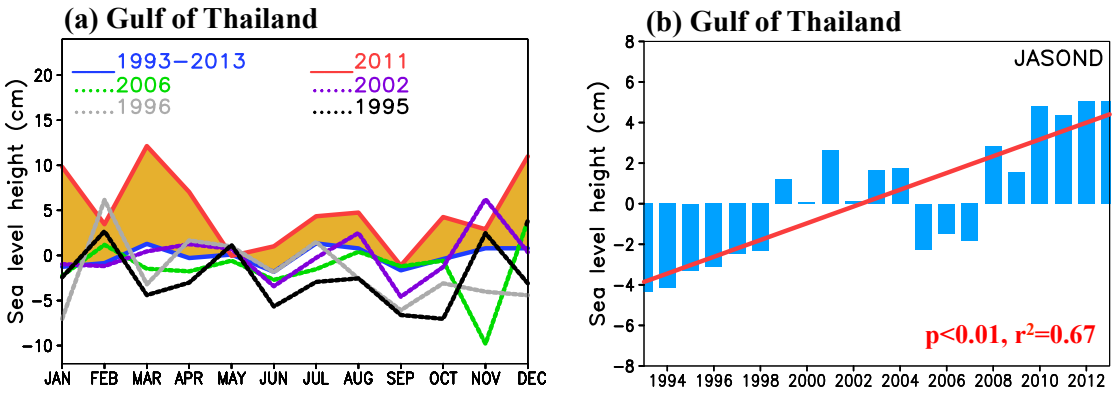

FIG. 2-5. (a) Monthly distribution of sea level hieght in the Gulf of Thailand from the long-term (1993–2013) average and overlaid with 6 flood years. The anomaly of 2011 sea level height from normal is indicated by the yellow area. (b) Flood-period sea level height (July–December) overlaid with the linear trend. The linear trend slope was highly significant with $r^2 = 0.67$ and $p < 0.01$.

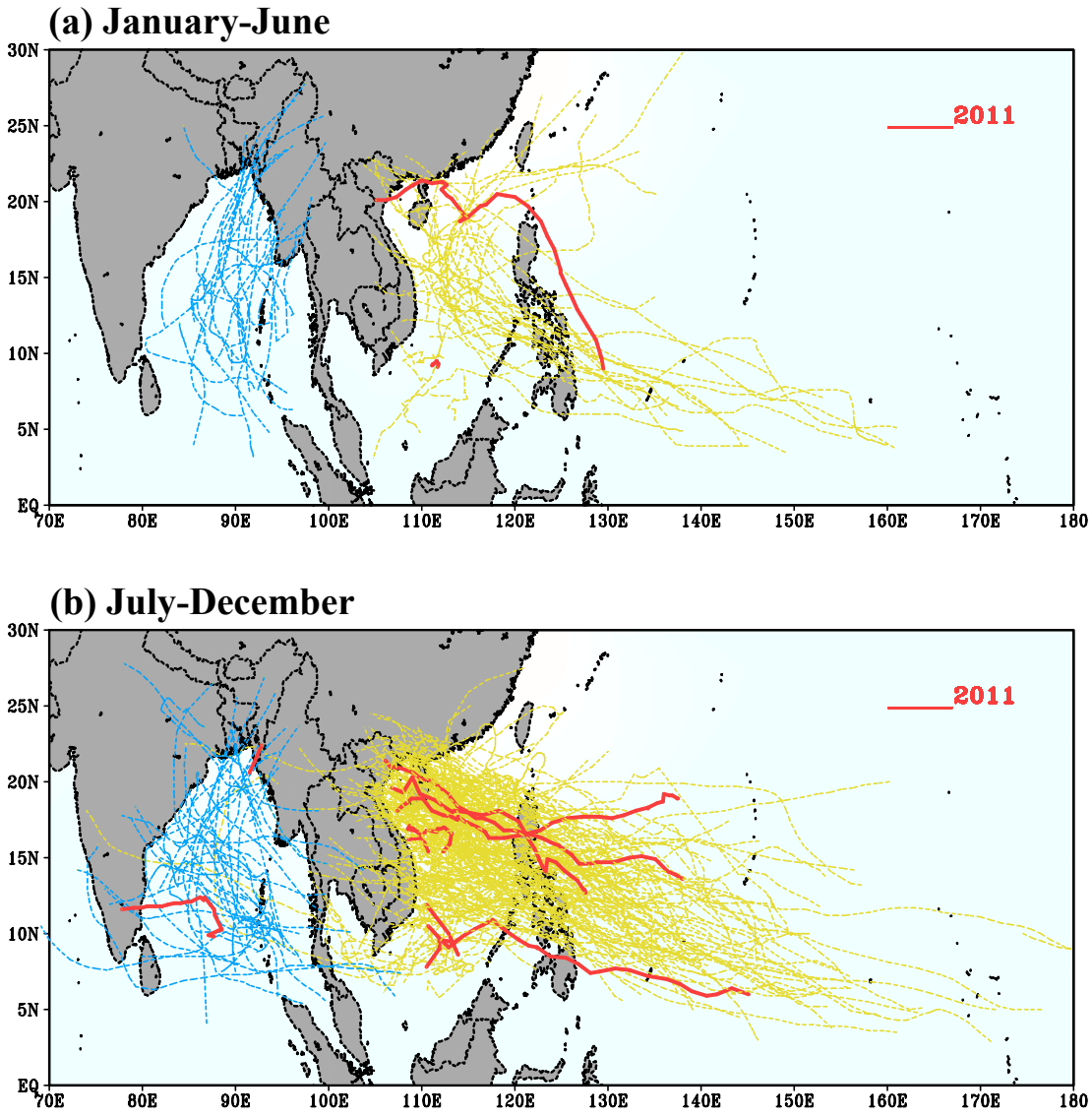

FIG. 2-6. Tropical cyclone tracks that could have affected Thailand from both the Bay of Bengal (blue) and western North Pacific (yellow) over the period 1975–2014 during (a) January–June and (b) July–December. Red lines indicate 2011 tropical cyclones.

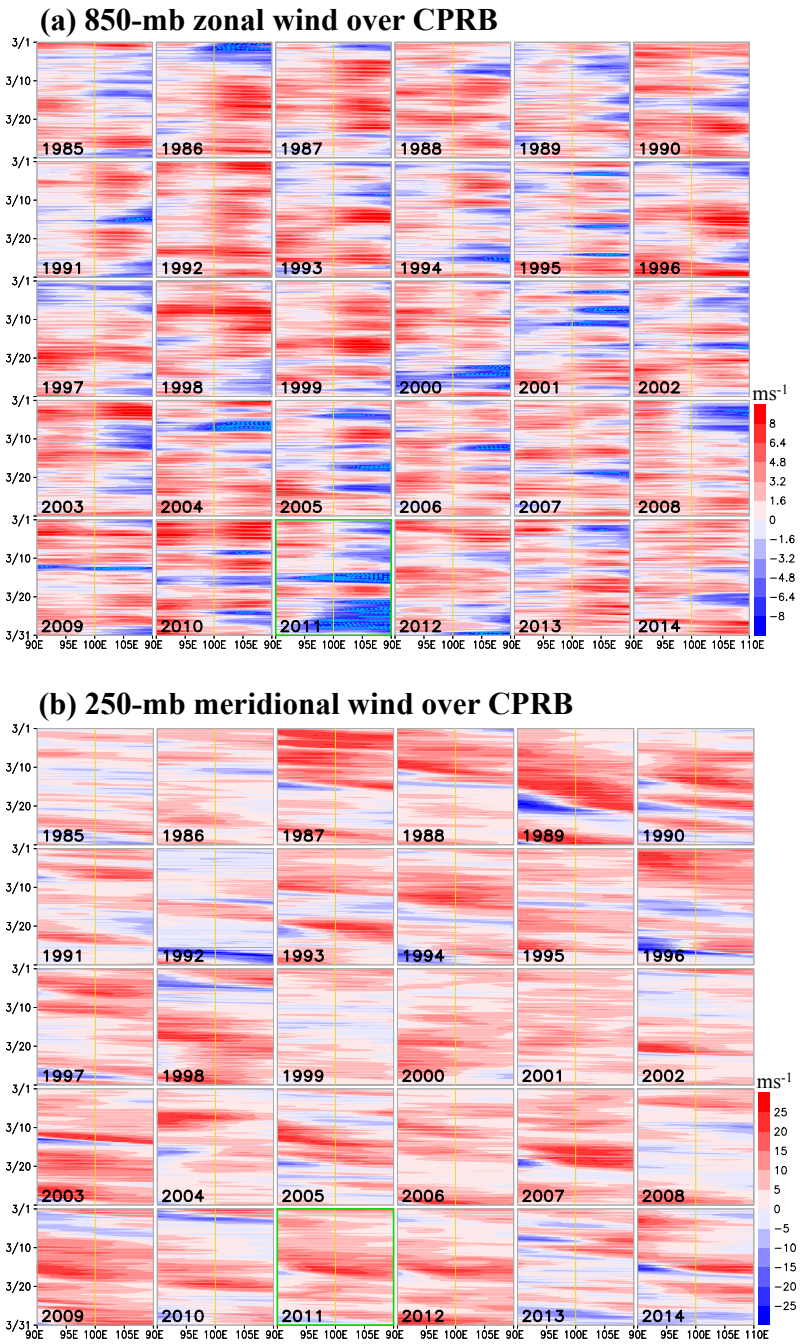

FIG. 2-7. (a) The 6-hourly *u* wind at 850 mb during 1–31 Mar for each year since 1985, averaged over 13°-20°N across the CPRB from 95° to 110°E (the light-blue dashed contours represent –8 ms^{-1}). (b) As in (a), but for the *v* wind at 250 mb.

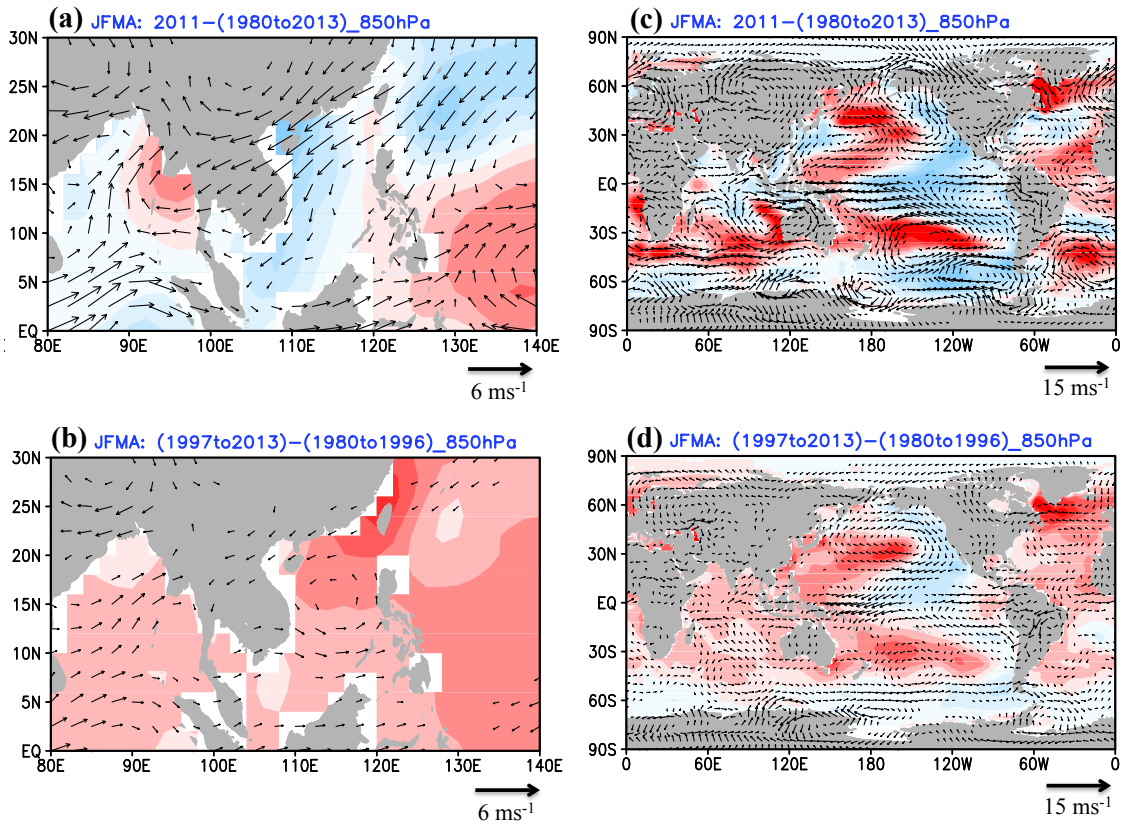

FIG. 2-8. The 850-mb wind (vectors) and SST anomalies (shading) computed from (a) 2011 and (b) epoch between the period of 1997–2013 and 1980–96 for Southeast Asia in the premonsoon season [January–April (JFMA)]. (c),(d) As in (a),(b), but for the global domain.

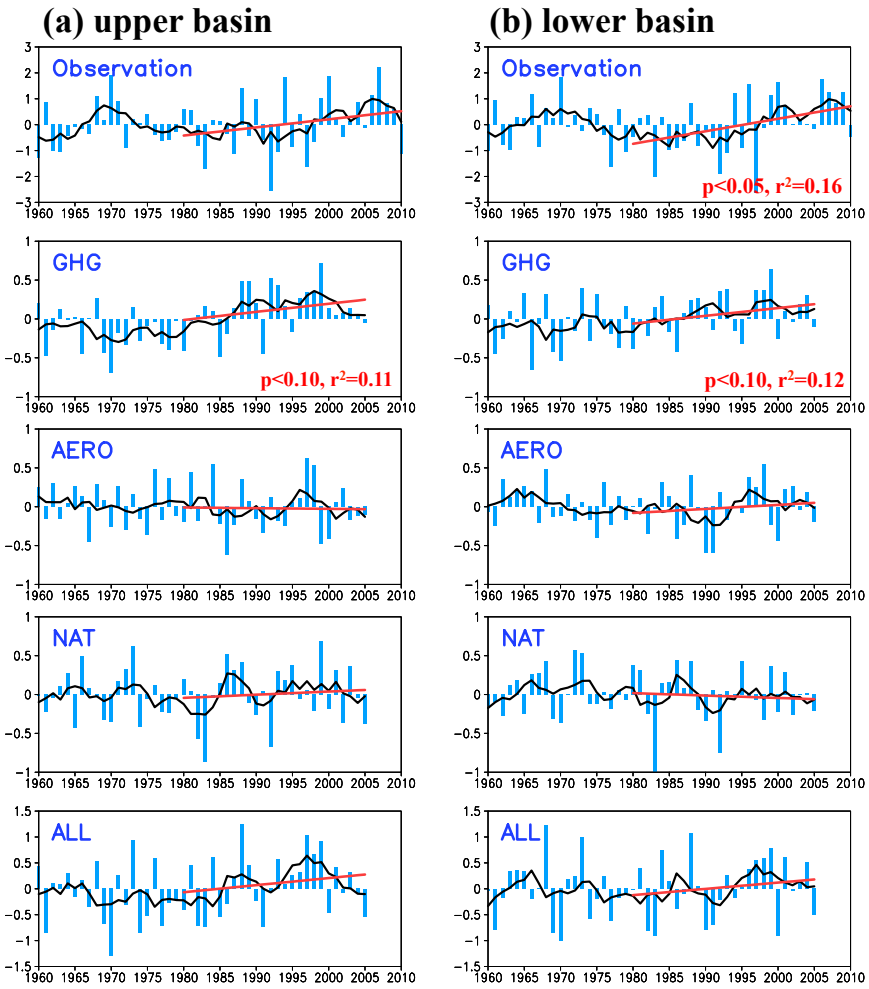

FIG. 2-9. Normalization of time series is given by [(value of variable x_i – sample mean μ)/sample std dev σ]. Annual mean is plotted against the overall mean as the zero line. The anomaly means above the overall mean are plotted as positive and anomaly means below the overall mean are plotted negative. The r^2 and p values are given for those that are significant.

CHAPTER 3

A SEASONAL PREDICTION FOR THE WET–COLD SPELLS LEADING TO WINTER CROP DAMAGE IN NORTHWESTERN TAIWAN WITH A COMBINED EMPIRICAL–DINAMICAL APPROACH[2]

ABSTRACT: Winter crop losses from extreme weather in Taiwan have increased in the recent decade, with those losses associated with pronounced wet-and-cold events (temperature <10 ºC and precipitation >5 mmd^{-1}). The regional and global patterns of atmospheric circulation and the sea surface temperature (SST) related to the extreme cold that damages fruits, vegetables, and paddy rice in northwest Taiwan were investigated. Cool SST anomalies in the western North Pacific (WNP) and warm SST in the central-eastern Pacific associated with the Pacific meridional mode (PMM) shared a significant role in the occurrence of wet-and-cold events in northwest Taiwan. The interactions of the WNP/PMM with the North Pacific Oscillation (NPO) and the Central Pacific type of El Niño led to a pronounced lead–lag relationship with the occurrence of wet-and-cold events. An empirical model was subsequently developed to predict the wet-and-cold event frequency using observed values of WNP, Niño-3.4, and Arctic Oscillation from year-1 and predicted indices of WNP and PMM derived from the Climate Forecast System Version 2 (CFSv2) outputs. The predictive skill of this hybrid empirical–dynamical model was statistically significant throughout the 6 months leading up to the

[2] *The material for this chapter was recently published as*: Promchote, P, Wang S-YS, Shen Y, Johnson PG, Yao M-H. 2018. A seasonal prediction for the wet-cold spells leading to winter crop damage in northwestern Taiwan with a combined empirical-dynamical approach. *Int. J. Climatol*. **38**: 578–583. http://doi.org/10.1002/joc.5194.

occurrence of wet-and–cold events.

KEY WORDS seasonal forecast; wet–cold spells; winter-crop damage; CFSv2; climate diagnosis; empirical–dynamical model; Taiwan

1. Introduction

Located in the subtropical Asia-Pacific region (Figure 3-1), Taiwan undergoes frequent extreme weather not only in the form of heavy precipitation and strong winds but also from cold air bursting out of inner Siberia during winter. High-value winter crops grown in Taiwan such as pears, strawberries, plums, peaches, and grapes are susceptible to both freeze/frost (below 0 ºC) and chilling temperatures (<12.5 ºC) (Snyder and de Melo-Abreu, 2005). The cold stress can cause biochemical and physical damage such as surface pitting, internal discoloration, water-soaked tissues, ripening failure, and increased susceptibility to decay organisms (Wang, 2010; Aguiar, 2012). The winter season of January–February coincides with the period when Asian pears are grafted followed by bloom. Critical low temperature for bud growth of pear is 23ºC, while temperatures below 15 and 1 ºC can kill buds with a 10% and 90% probability, respectively (Longstroth, 2012). Most winter fruits and vegetables are sensitive to rainfall, particularly strawberries that are susceptible to physical damage such as pitted fruit surface and cracking (Herrington *et al*., 2013). Thus, the combination of a cold front bringing in rainfall followed by sudden cooling can cause substantial damage to winter crops. Crop losses from cold damage in Taiwan have accounted for NT$ 5726 million

(~USD 180 millions) during 1991–2015. In January 2016 alone, enormous crop losses (NT$ 276 million and 5024 ha) occurred due to frosts and unprecedented snow cover (Council of Agriculture, 2016).

Taiwan's winter climate is influenced by the East Asian winter monsoon (EAWM) with cold air originating from the Siberian-Mongolian High (SMH) (Wang *et al*., 2000; Hsu *et al*., 2001; Chang *et al*., 2006). Cold surges with temperature dropping below 4 ^{o}C within 24–48 hours (Chen *et al*., 2002, 2004; Hong *et al*., 2008) are often accompanied by rainy days in the north and northeast of Taiwan (Chen and Huang, 1999; Chen and Chen, 2003). In January 2016, chilling temperature occurred throughout the country and below-freezing temperatures were observed in mountain areas as low as 300 m (Central Weather Bureau of Taiwan, 2016). These cold events embedded in the overall warming trend is likely not explained by the reported weakening of EAWM after 1980s (Hung and Kao, 2010) and associated nighttime warming trend (Shiu *et al*., 2009). Interannual variability of the EAWM and its effects on cold surges in Taiwan was linked to a number of climate modes including La Niña (Zhang *et al*., 1997; Wang *et al*., 2000; Cheung *et al*., 2012), negative phase of the North Atlantic Oscillation (NAO) (Hong *et al*., 2008), negative phase of the Arctic Oscillation (AO) (Cheung *et al*., 2012; Woo *et al*., 2012), and cooling sea surface temperature (SST) with high latent heat flux to the east of Taiwan (Hsu *et al*., 2001).

Despite its relatively small geographical area, Taiwan's climate is highly regionalized. Winter northeasterly flow interacts with the island's mountain range producing different rainfall regimes (Chen and Chen, 2003; Chien and Kuo, 2006). The phenomena promote

orographic precipitation over the northeast (windward side) and frontal rain in the northwestern Taiwan (Chen and Huang, 1999; Yen and Chen, 2000; Hung and Kao, 2010). The northwestern city of Miaoli, our study area, belongs to a spring–summer regime with a late-winter beginning of its rainy season.

The objectives of this study are to (1) explore the link of specific winter weather patterns with crop damage of fruits, vegetables and paddy rice, (2) understand the climate modes contributing to such weather patterns, and (3) develop an empirical and dynamical combination of prediction method for certain crop damaging weather patterns; this is, instead of predicting the local climate using direct climate model outputs. We derive multivariate regressions using selected climate indices from both observation and climate model forecasts as explanatory variables.

2. Methods and data sets

We selected a single location for this research to prevent complication from the aforementioned, highly variable weather pattern and geography of Taiwan. The analysis is specific to Miaoli County in northwestern Taiwan (Figure 3-1), which is an important area for the cultivation of high-value economic crops (i.e. strawberries, Asian pear, plums and grapes). Miaoli is one of the five cities (Hsinchu, Miaoli, Taichung, Chiayi, Ilan) with a high risk of crop damage from natural disaster and has been listed in a loss assessment and insurance plan of Taiwan (Wang, 2016). Among the five cities, Miaoli has had the highest amount of damage to these crops due to cold events during 1989–

2016, particularly in the months of January and February (Council of Agricultural (COA), 2016; http://eng.coa.gov.tw).

2.1. Crop damage and weather events

Our target season is January and February (JF) which is the high-risk period for cold stress. Statistics of crop losses from cold weather during 1989–2016 in Miaoli County were derived from official reports (while 2016 was used for this study, this year's reports had not yet received official status) from the COA website (http://eng.coa.gov.tw). Crop damage was quantified by damaged area (hectares), percent damaged, actual damaged area (damaged area multiplied by percent damaged), quantity (metric tons), and value (NT$1000). In order to describe the damage scale of different crops, each damage category was normalized by dividing its numbers with the maximum value, obtaining a scale from 0 to 1. The five damage categories were subsequently summed up to present the crop-damage intensity of all types with a cumulative scale from 0 to 5.

Daily minimum temperature and precipitation were recorded by Miaoli District Agricultural Research weather station (120.827831 ^{o}E, 24.494803 ^{o}N) with an elevation of 100 m (Figure 3-1). This station is referred to as Miaoli hereafter. The data were used to compute frequencies of six weather events, namely: cold, dry-cold (DC), wet-before-cold (WBC), wet-with-cold (WWC), wet-after-cold (WAC) and wet-cold (WC) as described in Table 3-1. Cold day was defined by chilling threshold at 10 ^{o}C instead of 12.5 ^{o}C (Snyder, and de Melo-Abreu, 2005) because some field crops such as rice seedlings can tolerate temperature as low as 10 ^{o}C (Krishnan *et al*., 2011). Wet days were

defined by rainfall of at least 5 mm in order to ensure the possible impacts on crops (rather than using 0.1 mm of the rain-day definition as used in Hung and Kao, 2010). All weather events were presented in normalized scales similar to that for crop-damage intensity. The independent occurrence and association magnitude of crop-damage intensity to each weather event were tested by Pearson's chi-squared (χ^2) and Phi and Cramér's V (Φ_c) (Corder and Foreman, 2014). The year that each weather event occurred is denoted as year 0, while year-1 indicates the previous year. The WC year 0, selected by WC frequency above 4.5 (normalized scale), includes 1990, 1992, 1993, 1996, 1997, 2004, 2005, 2010, 2011, 2012 and 2016. The years with the absence of WC event are DC year 0 (2001, 2002, 2006, 2007, 2009 and 2015).

2.2. Meteorological data and climate indices

Climate patterns in JF were analyzed by using three monthly datasets during the period of 1989–2016: (1) The NOAA Extended Reconstructed Sea Surface Temperature (SST) version 4 (ERSST.v4) with 2.0^o x 2.0^o resolution (Liu *et al*., 2014; Huang *et al*., 2015), provided by the NOAA/OAR/ESRL PSD (http://www.esrl.noaa.gov/psd/); (2) sea level pressure (SLP) and (3) wind fields at different pressure levels were obtained from the NCEP/NCAR reanalysis with a resolution of 2.5^o x 2.5^o (Kalnay *et al*., 1996). Composite maps of anomalous SST and SLP superimposed with 850-mb wind anomaly were constructed for WC, DC, and the difference between WC and DC (WC-DC) in two composited years (year 0 and year-1).

Six climate indices were analyzed: (1) the detrended Niño-3.4 index; (2) the western North Pacific (WNP) index which is average de-trended SST anomaly from 122°–132°E to 18°–28°N (Wang *et al*., 2012); (3) the North Pacific Oscillation (NPO) produced from covariance-based straight empirical orthogonal function (EOF) analysis of SLP anomaly (Linkin and Nigam, 2008); (4) the AO; (5) Pacific Decadal Oscillation (PDO) both obtained from the NOAA Climate Prediction Center (CPC) (http://www.cpc.ncep.noaa.gov/); (6) and the Pacific meridional mode (PMM) SST and wind indices (Chiang and Vimont, 2004) obtained from http://www.esrl.noaa.gov/psd/data/timeseries/monthly/PMM/.

2.3. CFSv2 reforecast

To assess the feasibility of applying dynamical seasonal prediction to cold damage, we adopted the NCEP Climate Forecast System Version 2 (CFSv2) (Saha *et al*., 2014). The model can predict the El Niño-Southern Oscillation (ENSO) and associated temperature signals up to 9 months ahead (Kim *et al*., 2012; Jiang *et al*., 2013; Lang *et al*., 2014). However, precipitation prediction skill is limited to less than 1 month (Yuan *et al*., 2011; Wang *et al*., 2013a) and the prediction is better over the oceans than over the land (Jiang *et al*., 2013). We used surface air temperature (*T*) data from both the CFSv2 Operational Forecasts (CFS-OF) and CFS Reforecast (CFS-R) 'First-Look' (Saha *et al*., 2014). The CFS-OF product is 6-hourly surface fluxes, which was derived for a 6-month forecast of JF 2012–2016. Data from the first date of the month (date 01) with 4-time steps (00Z, 06Z, 12Z, 18Z) were 31-day averaged for January and 28-day averaged for February to

represent the monthly *T*. The CFS-R product is 6-hourly time series from 9-month runs. The 6-month hindcast of the period 1989–2010 were computed by the same method as used with CFS-OF with a 5-day interval. The nearest date to the start of the month was selected as the starting date. The monthly *T* of CFS-OF and CFS-R were merged for covering the period of 1989–2016. The dataset was computed for the WNP index and PMM′ (explained further in section 3.3; see Table 3-S1, Supporting Information for lists of acronyms and abbreviations).

3. Results and discussion

3.1. Relation of crop damage and wet–cold events

Daily temperature, precipitation and crop damages of different types in Miaoli are presented in Figure 3-2 for each year during 1989–2016. The damage often occurred in January and February coinciding with chilling threshold temperatures (<10^{o}C with red shading) and precipitation higher than 5 mmd^{-1} (i.e. in 2005, 2010, 2014, 2016). The more crops that were damaged were likely associated with the stronger wet-and-cold weather events (hereafter “wet-cold”, e.g. 2016). Also noteworthy is the lack of crop damage (e.g. 2006, 2013, 2015) when only cold or wet spells are present, suggesting the importance of a combination wet–cold situation to cause crop damage.

From Taiwan’s COA records, most of the damaged crops are fruits (pears, strawberries, plums, peaches, wax apples, grapes and loquats) which grafting spikes and flower buds of pears were the most frequently destroyed. According to Roan and Chen

(2005), low temperature and high relative humidity (>85%) reduced pollen germination in pear, resulting in low pollination and fruit set. For other crops with different growth stages, 10°C critical temperature can generate abnormal metabolic processes (Wang, 2010) and cold rain (and snow) can accelerate injury and increase microorganism infection. Similarly, continuous rainfall of 10–30 mmd^{-1} for 2–3 days (as shown in Figure 3-2) is sufficient to cause direct damage (Herington *et al*., 2013).

Figure 3-3 shows the time series of (a) crop damage intensity and (b)–(g) frequencies of weather events during 1989–2016. The occurrence of crop damage generally corresponds to those of various wet and cold combination events. The χ^2 of 5.19 and Φ_c of 0.44 suggested that crop damage is most similar to and significantly associated with WWC. Other weather events (WBC, WAC, WC – see Section 2.1) could link to the damage if the comparison was made only for the 2004–2016 period. The absence of crop damage from 1989 to 2003, which apparently was not explained by wet–cold frequencies (i.e. JF in 1992), might be related to multiple factors such as the cold magnitude, cultivation practices or data collection. It will require a more extensive survey to examine this speculation. We note that the slight cooling trends (Figure 3-S1(d)), low-temperature anomaly (Figure 3-S1(e)), and the frequency of cold days (< 10°C) (Figure 3-S1(c)) in Miaoli coexisted with the increase in crop damage after 2003, suggesting a possible climate factor. Regarding the interannual variation, crop damage from wet-cold conditions was different in the strong El Niño years. Unprecedented wet–cold events with large crop damage occurred in 2016, a strong El Niño year, while the previous strong El

Niño event such as 1998 was warm and wet (Figure 3-2). We will explain this further in sections below.

3.2. Climate patterns associated with the wet–cold spells

The climate patterns associated with the cold days in Miaoli were first examined from regression maps (Figure 3-4). We observed a combination of patterns comprising a Central-Pacific (CP) El Niño type (Weng *et al*., 2009), a PMM in the subtropics (Chiang and Vimont, 2004) in the SST regression (Figure 3-4(a)), and a NPO-like pressure dipole (Linkin and Nigam, 2008) in the SLP regression (Figure 3-4(b)). Equatorial warm SST pool between the CP and the Philippine Sea is connected with the PMM signal of the subtropical SST band (Figure 3-4(a)). The frequency of cold days significantly correlates with cold SST in the vicinity of Taiwan as well as along the Western Pacific rim from tropic (~5^{o}N) to subtropics (~30^{o}N), eastern Japan, central subtropics, and eastern equator. The cool sea surface temperature anomaly (SSTA) near Taiwan and the accompanying warm tropical SSTA in Figure 3-4(a) resemble the WNP pattern that, according to Wang *et al*. (2012), can enhance surface pressure over southern East Asia. The observation that no correlation was found between the cold days and the Niño-3.4 SST confirms the results in section 2.1 that crop damage with wet–cold conditions were not associated with ENSO events, thereby negating the use of ENSO (year 0) as a predictor. The results also indicate the significant roles of WNP-SST on cold winter anomalies, echoing the findings of Wang *et al*. (2012) and others. For instance, Hsu *et al*.

(2001) suggested that the maximum heat flux was centered in the east of Taiwan and this heat flux variation was greater than those in the ENSO region.

The SST and SLP patterns associated with WC, DC and WC-DC year 0 are given in Figure 3-5. Consistent to the patterns in Figure 3-4, the WC year 0 situation is accompanied by warm SSTA in the CP and PMM regions (Figure 3-5(a)) and an intensified Siberian High and Aleutian low (Figure 3-5(d)). A seemingly opposite pattern appears in the DC year 0 (Figures 3-5(b) and (e)). To illustrate their difference, we plot the WC minus DC patterns in Figures 3-5(c) and (f). Anomalous cold temperatures surrounding Taiwan were indeed associated with relatively strong EAWM as indicated by the enhanced Siberian high. The wet–cold period also accompanied by the anomalous southwesterly winds over Taiwan colliding with the northerly flow over the WNP; this can increase the latent heat flux over the marine area, promoting precipitation. These results reflect the seasonal climate pattern modulating the frequency of WC and DC events rather than the mean of cold-surge days. Moreover, winter rainfall in Taiwan has increased over the past 80 years (Yu *et al*., 2006). According to Hung and Kao (2010), the increased rainfall was influenced by the increases in SST and moisture over the South China Sea associated with southwesterly flows. Figure 3-5(c) shows that, in the eastern Pacific, a cyclonic anomaly developed near the southern node of the NPO, a process that can reinforce the CP El Niño (Yu *et al*., 2012; Vimont, 2016).

Next, the composite analyses of year-1 for WC, DC, and WC-DC were constructed to illustrate climate patterns that are linked to the occurrence of WC events in year 0. The use of year-1 makes physical sense because most of the climate modes of interest exhibit

a broad spectrum of 3–6 years, meaning that it would take more than a year for those modes to completely transition from one phase to another. Comparing to year 0, WC year-1 had stronger negative SSTA in the WNP and weaker positive SSTA in the ENSO and PMM regions (Figure 3-6(a)). Similarly, more pronounced cold SSTA over the ENSO region and a strong warm band extended northeastward in DC year-1 (Figure 3-6(b)). These delineate the warm SSTA in WNP that can lead to the development of cold ENSO events in the following year (Wang *et al*., 2012, 2013b). Furthermore, DC year 0 tends to occur 1 year after an equatorial cold SSTA band similar to a La Niña event (Figures 3-5(b) and 3-6(b)). Positive PMM can trigger El Niño events with a 7- to 9-month lead (Larson and Kirtman, 2013), and the PMM-ENSO interaction was found to strengthen the CP ENSO (Lin *et al*., 2015). Yu *et al*. (2012) indicated that the occurrence of CP El Niño have increased after 1990. Regarding SLP anomalies, the NPO and Mongolian High coexisted in WC year-1 (Figure 3-6(d)), while a low pressure covers Mongolia 1 year prior to increased DC cases (Figure 3-6(e)). Although the signals in Figures 3-5 and 3-6 can be explained with 80% of confidence interval, which is only marginally significant, the impacts of these circulation patterns on Miaoli's winter climate are nonetheless measurable.

3.3. Predictive skill evaluation

The findings presented thus far have indicated significant and persistent connections with certain climate modes. Their physical processes linking to WC events in northeastern Taiwan require further research through climate diagnostics. Moreover, the immediate

implication for coping with crop losses lies in the predictability of these aforementioned climate modes (the goal of this paper). As shown in Table 3-2, the correlation coefficients (r) provided that WNP, PMM-wind, PMM-SST and NPO were the potential predictors to estimate cold and DC events at year 0. None of these indices correlated with the WC events. Thus, the regression models to predict WC occurrences during the JF season were constructed for different combinations of the climate indices from year 0 and year-1. The potential models were chosen based on overall fit by considering the adjusted-coefficient of multiple determination (R^2_{adj}) and the statistic significance of coefficient ($\widehat{\beta_s}$) (Kutner *et al*., 2004). After evaluation, two potential models were selected:

$$\widehat{WC} = \widehat{\beta_0} + \widehat{\beta_1}\ \text{Niño} - 3.4\ (\text{JF}_{\text{year-1}}) + \widehat{\beta_2}\ \text{WNP}\ (\text{JF}_{\text{year-1}}) + \widehat{\beta_3}\ \text{WNP}\ (\text{JF}_{\text{year 0}})\ \text{PMM} - \text{SST}\ (\text{JF}_{\text{year 0}}) \quad (1)$$

$$\widehat{WC} = \widehat{\beta_0} + \widehat{\beta_1}\ \text{Niño} - 3.4\ (\text{JF}_{\text{year-1}}) + \widehat{\beta_2}\ \text{WNP}\ (\text{JF}_{\text{year-1}}) + \widehat{\beta_3}\ \text{WNP}\ (\text{JF}_{\text{year 0}})\ \text{PMM} - \text{SST}\ (\text{JF}_{\text{year 0}}) + \widehat{\beta_4}\ \text{AO}\ (\text{J}_{\text{year-1}}) \quad (2)$$

Model 1 was significant with p-value of 0.0061 and R^2_{adj} of 0.35 whereas the model 2 was slightly higher fit with p-value of 0.0031 and R^2_{adj} of 0.42. Though adding January AO of year-1 improved the estimation skill for model 2, model 1 contains fewer variables with the same level of significant confidence (99%). The estimated WC days (WC_{est}) from the two models and the observed WC days (WC_{obs}) were significantly correlated with analogous patterns (Figure 3-7(e)). The large difference between WC_{est} and WC_{obs} was visible in the years with anomaly high or low WC events. Note here for the PMM-SST, we used an alternative methodology that simplifies the calculation of PMM-SST

instead of deriving it from the maximum covariance analysis (MCA) (Chiang and Vimont, 2004); this led to a PMM-SST proxy, denoted as PMM′ (which has a 0.94 correlation coefficient with the PMM-SST; Figure 3-S2). The computation of PMM′ was based on regression map between JF-SST and a time-series of cold events during 1989–2016 that was constructed over 32°N–21°S to 175°E–95°W (white box in Figure 3-4(a) following Chiang and Vimont, 2014). Each year's PMM′ is represented by an anomaly detrended value of the difference between averaged SST in the areas of positive (red-shaded area) and areas of negative (blue-shaded area) regression coefficients (details are given in the caption of Figure 3-S3). Thereafter, the models were tested by replacing PMM-SST with PMM′ as computed from observed SST. The results in Figure 3-7(d) indicated that the PMM′ index acted closely with the PMM-SST (Figure 3-7(e)).

The WNP and PMM′ indices in January (J), February (F) and average JF were estimated from CFSv2 outputs for 0 to 6 lead months (e.g. a forecast for JF made in July–August; JA signified as a 6 lead month). These are referred to as CFS-WNP and CFS-PMM′. Figures 3-8(a)–(c) illustrate the correlation coefficients (*r*) of WNP derived from observed SST (WNP) and CFS-WNP, whereas the *r* values of PMM-SST and CFS-PMM′ are given in Figures 3-8(d)–(f). The CFSv2 performance for CFS-WNP and CFS-PMM′ in JF was limited to 1 and 2 months, respectively. This relatively low predictive skill might result from a cold bias in the equatorial Pacific and a warm bias in the North Pacific as reported by the previous studies (i.e. Kim *et al*., 2012; Barnston and Tippett, 2013).

Next, the models were tested by using CFS-WNP for WNP($JF_{year\ 0}$) and CFS-PMM′ for PMM′ ($JF_{year\ 0}$) derived from CFSv2 outputs for 0 to 6 lead months. The correlation coefficients of observed and predicted JF-WC days computed from the model 1 and model 2 in different lead times are shown in Figures 3-8(g) and (h), respectively. Both observed and predicted patterns of the JF-WC are clearly illustrated in Figure 7. Figures 3-7(a)–(c) (left) and Figure 3-8(g) showed that model 1 could predict WC days up to 5 months in advance with moderated correlation to WC_{obs} (r = 0.54). Slightly superior skill was obtained from model 2, in which the WC days can be predicted for 6 months with r = 0.59 (Figures 3-7(a)–(c), right) and Figure 3-8(h)).

A diagram outlining the 'path' in which the unstandardized (ordinary) and standardized regression coefficients (Bondari, 1990; Kline, 2016) of Equation (2) connects with the various climate modes/indices with the WC events is shown in Figure 3-9. Here, the direct effects of each climate index on the WC events and interrelationship among climate indices were compared by the standardized coefficients (path coefficients) (Wright, 1921, 1934; Carey, 1998). An unstandardized coefficient, estimated from the original scale of each climate index variable in a multiple regression model, indicates the number change in WC days associated with a 1-unit change of climate index. A standardized coefficient, estimated from the transformed climate variable into the standardized variable with means of 0 and standard deviation of 1.0 (see caption of Figure 3-9), suggests a relative change in standard deviations between WC days and a climate index. As the standardized coefficients of all climate indices in the regression model were estimated from a common scale, the coefficient magnitudes can be

compared. Figure 3-9 suggested that the WNP index in year-1 contributed the largest negative ($\widehat{\beta_2}$ = –3.58, –0.47) and WNP*PMM′ in year 0 contributed the largest positive ($\widehat{\beta_3}$ = 1.03, 0.50) effects on WC events. Conversely, interrelated effects among climate indices were insignificant. It is feasible that the regression models can predict WC days in 6-month advance provided that a near-term forecast of the WNP and PMM′ is achievable. Of note, positive SSTA of Niño-3.4 and negative phase of AO from year-1 also influenced the WC days. The dominant negative AO and ENSO proceeding a stronger EAWM and associated cold surges have been documented (i.e. Cheung *et al*., 2012; Chang and Lu, 2012; Woo *et al*., 2012; He *et al*., 2017) and this lends support to our finding. Conversely, the connection of climate indices from year-1 to WNP*PMM′ in year 0 was not well depicted.

3.4. Discussion

The upshot of this combined empirical–dynamical approach is that it overcomes the limitation that individual WNP or PMM′ index alone could not predict the WC frequency, yet their interactions or combined effects could. The role of WNP*PMM′ in modulating weather in Taiwan appears to vary in different ENSO years. For example, during the weak El Niño event of 2004, the highest WC events persisted with anomalously cold WNP (–0.23) and warm PMM-SST (0.67). Intensified negative PMM-SST (–7.33) coupled with positive WNP (0.56) in the 1998 El Niño was favorable for warm-wet conditions. Weak negative PMM-SST (–2.21) counteracted the warm WNP (0.44) that directed to cold-wet events such as in 2016. These results depict the function

of WNP-PMM teleconnection on the occurrences of wet-cold events. The negligible role of NPO in the regression models echoed its reported diminishing role as an ENSO precursor since the mid-20th century (i.e. Chang *et al*., 2007; Wang *et al*., 2013b). Further analysis is needed to disclose the physical process linking each climate mode to another in terms of impacts on northwest Taiwan's winter weather.

4. Concluding remarks

The observed increase in winter crop losses from extreme weather in Taiwan have led to a national concern. Given the significance of crop damage, crop insurance for natural disasters including cold damage of pear grafts has been promoted since November 2015 (Wang, 2016). However, operational and trustworthy seasonal outlooks for such cold damage are lacking. The previously known climate indicators (i.e. EAWM, ENSO events) and climate forecasts could not depict the unprecedented extreme weather and crop losses such as was experienced in 2016. This study identified the climate patterns related to the winter crop damage in Miaoli (northwestern Taiwan) and developed a combined empirical–dynamical prediction method for those key patterns based on multivariate regression and the CFSv2 forecast outputs. During the 1989–2016 period, winter crop damage in Miaoli was mainly caused by the concurrence of cold and wet (WC) conditions. Either the cold or wet days alone, such as chilling threshold temperature below 10^{o}C (cold) or precipitation above 5 mmd^{-1} (wet), did not necessarily lead to significant losses.

We found that the cold frequency was associated by the teleconnection patterns of anomalously cold SST in WNP, warm PMM, negative NPO and CP El Niño; the former three together comprise the optimal ENSO precursor. Consistently, the aforementioned climate factors coupled with a pronounced Siberian High and enhanced Aleutian low were dominant in the WC year. The analysis pointed out that an intensified WNP index in year-1 preceded the appearance of ENSO in year 0, a finding that is consistent with Wang *et al*. (2012). This suggested the demonstrated usage of the WNP index (year-1) in the prediction model for WC events (given that negative WNP is a precursor of El Niño). This finding adds value to the current challenge that arises from the lack of correlation between the cold/WC frequencies and the ENSO events. Subsequently, we built a model to predict WC frequency by utilizing the interaction of WNP and PMM′ indices in year0 (derived from the CFSv2) with historical WNP, El Niño, and AO. Among the climate patterns, the most significant factors impacting WC events were WNP in year-1 and WNP*PMM′ in year 0. This links Taiwan's winter climate variation to the developing stage (rather than the maturing phase) of ENSO. The capability of CFSv2 to predict the WNP and PMM′ were limited to less than 2 months, yet the regression model outperforms CFSv2 by 4 more months for the WC prediction.

The ongoing climate change adaptation plan of Taiwan (Council of Agriculture, 2016) has already highlighted the importance of establishing a monitoring and early-warning system for agriculture meteorology in order to stabilize domestic food and feed supply as well as price. Predictions of winter temperature and precipitation in Asia by climate models have seen steady improvements, but their capability in forecasting the highly

variable subtropical-marine climate of Taiwan is lacking. Currently, climate forecasts have not yet shown any skill in handling the occurrence of critical low temperatures and rain-induced chill damage on crops, as the model resolution is too coarse to reflect the complex topography of Taiwan. Given the proof of concept in this study, further development of a similar hybrid model for the prediction of crop losses would be beneficial. Additional evaluation of the multi-model ensemble (MME) approach of seasonal prediction, which has shown a superior forecast skill compared to a single model likes the CFSv2 (Barnston *et al*., 2003; Kirtman *et al*., 2014), may assist in forecasting the occurrence of WC days that can lead to crop damage.

Regardless, the preliminary prediction results of this study could be used to guide the farmers either to protect their crops from the WC events, such as the use of shelter systems (Lim *et al*., 2014), or by shifting time of cold sensitive management practices, such as grafting pear after February (Roan and Chen, 2005). Adding the prediction monitoring of damaging conditions will benefit farmers by helping retain income and reduce compensation payments from the government following crop damage.

Acknowledgements

This research was supported by the Utah State University Agricultural Experiment Station, Royal Thai Government PhD scholarship and Central Weather Bureau of Taiwan.

Supporting information

Supporting information (Figure 3-S1, Figure 3-S2, and Figure 3-S3) is provided in APPENDIX A.

References

Aguiar JL. 2012. *Symptoms of Frost, Freezing and Chilling Injury on Vegetables*. Western Farm Press: Penton, New York. http://westernfarmpress.com/vegetables/ symptoms- frost- freezing- and- chilling-injury-vegetables (accessed 22 November 2016).

Barnston AG, Tippett MK. 2013. Predictions of Nino 3.4 SST in CFSv1 and CFSv2: a diagnostic comparison. *Clim. Dyn.* **41**(5): 1615–1633. https://doi.org/10.1007/s00382 - 013- 1845- 2.

Barnston AG, Mason SJ, Goddard L, DeWitt DG, Zebiak SE. 2003. Multimodel ensembling in seasonal climate forecasting at IRI. *Bull. Am. Meteorol. Soc.* **84**(12): 1783–1796. https://doi.org/10.1175/BAMS- 84- 12- 1783.

Bondari K. 1990. Path Analysis in Agricultural Research. In *2nd Annual Conference Proceedings on Applied Statistics in Agriculture*. New Prairie Press: Kansas. http://newprairiepress.org/cgi/viewcontent.cgi?article=1439&context=agstatconferenc e (accessed 11 January 2017).

Carey G. 1998. *Multiple regression and path analysis*. http://psych.colorado.edu/˜carey/ Courses/PSYC7291/handouts/pathanal2.pdf (accessed 11 January 2017).

Central Weather Bureau of Taiwan. 2016. http://www.cwb.gov.tw/eng/ (accessed 22 November 2016).

Chang C-P, Lu M-M. 2012. Intraseasonal predictability of Siberian high and East Asia winter monsoon and its interdecadal variability. *J. Clim.* **22**: 1773–1778. https://doi.org/10.1175/JCLI-D-11-00500.1.

Chang C-P, Wang Z, Hendon H. 2006. 3. The Asian winter monsoon. In *The Asian Monsoon*, Wang B (ed). Praxis, Springer: Berlin Heidelberg, 89–127.

Chang P, Zhang L, Saravanan R, Vimont DJ, Chiang JCH, Ji L, Seidel H, Tippett MK. 2007. Pacific meridional mode and El Niño-Southern Oscillation. *Geogr. Res. Lett.* **34**: L16608. https://doi.org/10.1029/ 2007GL030302.

Chen C-S, Chen Y-L. 2003. The rainfall characteristics of Taiwan. *Mon. Weather Rev.* **131**: 1323–1341. https://doi.org/10.1175/1520- 0493(2003)131<1323:TRCOT >2.0.CO;2.

Chen C-S, Huang J-M. 1999. A numerical study of precipitation characteristics over Taiwan Island during the winter season. *Meteorol. Atmos. Phys.* **70**: 167–183. https://doi.org/10.1007/s007030050032.

Chen T-C, Yen M-C, Huang W-R, Gallus WA. 2002. An East Asian cold surge: case study. *Mon. Weather Rev.* **130**: 2271–2290. https://doi.org/ 10.1175/1520- 0493 (2002)130<2271:AEACSC>2.0.CO;2.

Chen T-C, Huang W-R, Yoon J-H. 2004. Interannual variation of the East Asian cold surge activity. *J. Clim.* **17**: 401–413. https://doi.org/ 10.1175/1520- 0442(2004)017 <0401:IVOTEA>2.0.CO;2.

Cheung HN, Zhou W, Mok HY, Wu MC. 2012. Relationship between Ural-Siberian blocking and the East Asian winter monsoon in relation to the Arctic Oscillation and the El Niño-Southern Oscillation. *J. Clim.* **25**: 4242–4256. https://doi.org/10.1175/JCLI-D-11-00225.1.

Chiang J, Vimont D. 2004. Analogous Pacific and Atlantic meridional modes of tropical atmosphere–ocean variability. *J. Clim.* **17**: 4143–4158. https://doi.org/10.1175/JCLI 4953.1.

Chien F-C, Kuo Y-H. 2006. Topographic effects on a wintertime cold front in Taiwan. *Mon. Weather Rev.* **134**: 3297–3316. https://doi.org/10.1175/MWR3255.1.

Corder GW, Foreman DI. 2014. *Nonparametric Statistics: A Step-by-Step Approach*, 2nd edn. John Wiley & Sons, Inc.: Hoboken, NJ, 267 pp.

Council of Agriculture (COA). 2016. *Adaptation strategy in response to climate change influence on agriculture*. http://eng.coa.gov.tw/content_view.php?catid=2505303&hot_new=2503505 (accessed 28 November 2016).

He S, Gao Y, Li F, Wang H, He Y. 2017. Impact of Arctic Oscillation on the East Asian climate: a review. *Earth-Sci. Rev.* **164**: 48–62. https:// doi.org/10.1016/j.earscirev. 2016.10.014.

Herrington ME, Hardner C, Wegener M, Woolcock LL. 2013. Rain damage on three strawberry cultivars grown in subtropical Queensland. *Int. J. Fruit Sci.* **13**: 52–59. https://doi.org/10.1080/15538362.2012 .696982.

Hong CC, Hsu H-H, Chia H-H, Wu C-Y. 2008. Decadal relationship between the North Atlantic Oscillation and cold surge frequency in Taiwan. *Geophys. Res. Lett.* **35**: L24707. https://doi.org/10.1029/ 2008GL034766.

Hsu H-H, Chen Y-L, Kau W-S. 2001. Effects of atmosphere-ocean interaction on the interannual variability of winter temperature in Taiwan and East Asia. *Clim. Dyn.* **17**: 305–316. https://doi.org/10 .1007/s003820000116.

Huang B, Banzon VF, Freeman E, Lawrimore J, Liu W, Peterson TC, Smith TM, Thorne PW, Woodruff SD, Zhang H-M. 2015. Extended reconstructed sea surface temperature version 4 (ERSST.v4): I. Upgrades and intercomparisons. *J. Clim.* **28**: 911–930. https://doi .org/10.1175/JCLI- D- 14- 00006.1.

Hung C-W, Kao P-K. 2010. Weakening of the winter monsoon and abrupt increase of winter rainfalls over northern Taiwan and Southern China in the early 1980s. *J. Clim.* **23**: 2357–2367. https://doi.org/10.1175/2009JCLI3182.1.

Jiang X, Yang S, Li Y, Kumar A, Wang W, Gao Z. 2013. Dynamical prediction of the East Asian winter monsoon by the NCEP Climate Forecast System. *J. Geophys. Res. Atmos.* **118**: 1312–1328. https://doi.org/10.1002/jgrd.50193.

Kalnay E, Kanamitsu M, Kistler R, Collins W, Deaven D, Gandin L, Iredell M, Saha S, White G, Woollen J, Zhu Y, Leetmaa A, Reynolds R. 1996. The NCEP/NCAR 40-year reanalysis project. *Bull. Am. Meteorol. Soc.* **77**: 437–471. https://doi.org/10.1175 /1520- 0477(1996)077, 0437:TNYRP.2.0.CO;2.

Kim H-M, Webster PJ, Curry JA. 2012. Seasonal prediction skill of ECMWF system 4 and NCEP CFSv2 retrospective forecast for the northern hemisphere winter. *Clim. Dyn.* **39**: 2957–2973. https://doi .org/10.1007/s00382- 012- 1364- 6.

Kirtman BP, Min D, Infanti JM, Kinter JL III, Paolino DA, Zhang Q, van den Dool H, Saha S, Mendez MP, Becker E, Peng P, Tripp P, Huang J, DeWitt DG, Tippett MK, Barnston AG, Li S, Rosati A, Schubert SD, Rienecker M, Suarez M, Li ZE, Marshak J, Lim Y-K, Tribbia J, Pegion K, Merryfield WJ, Denis B, Wood EF. 2014. The North American multimodel ensemble: phase-1 seasonal-to-interannual prediction; phase-2 toward developing intraseasonal prediction. *Bull. Am. Meteorol. Soc.* **95**(4): 586–601. https://doi.org/10.1175/BAMS- D- 12- 00050.1.

Kline RB. 2016. *Methodology in the Social Sciences: Principles and Practices of Structural Equation Modeling*, 4th edn. The Guilford Press: New York, NY, 534 pp.

Krishnan P, Ramakrishnan B, Reddy KR, Reddy VR. 2011. High temperature effects on rice growth, yield and grain quality. In *Advances in Agronomy*, Vol. **111**, Sparks DL (ed). Academic Press: Burlington, Canada, 87–206.

Kutner MH, Nachtsheim CJ, Neter J. 2004. *Applied Linear Regression Models*, 4th edn. McGraw-Hill: Irwin, NY, 701 pp.

Lang Y, Ye A, Gong W, Miao C, Di Z, Xu J, Liu Y. 2014. Evaluating skill of seasonal precipitation and temperature predictions of NCEP CFSv2 forecasts over 17 hydroclimatic regions in China. *J. Hydrometeorol.* **15**: 1546–1559. https://doi.org/ 10.1175/JHM-D-13-0208.1.

Larson S, Kirtman B. 2013. The Pacific Meridional mode as a trigger for ENSO in a high-resolution coupled model. *Geophy. Res. Lett.* **40**: 3189–3194. https://doi.org/ 10.1002/grl.50571.

Lim K-H, Gu M, Song J-H, Cho Y-S, Kim W-S, Kim B-S, Jung S-K, Choi H-S. 2014. Growth, fruit production, and disease occurrence of rain-sheltered Asian pear trees. *Sci. Hort.* **177**: 37–42. https://doi.org/ 10.1016/j.scienta.2014.07.030.

Lin C-Y, Yu JY, Hsu H-H. 2015. CMIP5 model simulations of Pacific meridional mode and its connection to the two types of ENSO. *Int. J. Climatol.* **35**: 2352–2358. https://doi.org/10.1002/joc.4130.

Linkin ME, Nigam S. 2008. The North Pacific Oscillation-West Pacific teleconnection pattern: mature-phase structure and winter impacts. *J. Clim.* **21**: 1979–1997. https://doi.org/10.1175/2007JCLI2048.1.

Liu W, Huang B, Thorne PW, Banzon VF, Zhang H-M, Freeman E, Lawrimore J, Peterson TC, Smith TM, Woodruff SD. 2014. Extended Reconstructed Sea surface temperature version 4 (ERSST.v4): II. Parametric and structural uncertainty estimations. *J. Clim.* **28**: 931–951. https://doi.org/10.1175/JCLI-D-14-00007.1.

Longstroth M. 2012. *Freeze Damage Depends on Tree Fruit Stage of Development*. Michigan State University Extension. http://msue.anr .msu.edu/news/freeze_damage _depends_on_tree_fruit_stage_of_ development

Roan S-F, Chen I-Z. 2005. Improving fruit setting in top-grafted pear production. *Pear Cultivation and Management Technology Proceed- ing*, pp. 223-241 (in Chinese).

Saha S, Moorthi S, Wu X, Wang J, Nadiga S, Tripp P, Behringer D, Hou Y-T, H-y C, Iredeli M, Ek M, Meng J, Yang R, Mendez MP, van den Dool H, Zhang Q, Wang W, Chen M, Becker E. 2014. The NCEP climate forecast system version 2. *J. Clim.* **27**: 2185–2208. https://doi .org/10.1175/JCLI- D- 12- 00823.1.

Shiu C-J, Liu CL, Chen J-P. 2009. Diurnally asymmetric trends of temperature, humidity, and precipitation in Taiwan. *J. Clim.* **22**: 5635–5649. https://doi.org/10.1175/2009 JCLI2514.1.

Snyder RL, de Melo-Abreu JP. 2005. *Frost Protection: Fundamentals, Practice and Economics*, Vol. **1**. Food and Agriculture Organization of the United Nations: Rome. http://www.fao.org/docrep/008/y7223e/y7223e0a.htm.

Vimont D. 2016. *Your Eight-minute Speed Date with the Pacific Meridional Mode*. https://www.climate.gov/news- features/blogs/enso/ your- eight- minute- speed- date- pacific- meridional- mode (accessed 28 November 2016).

Wang CY. 2010. Alleviation of chilling injury in tropical and subtropical fruits. In Proceedings of IIIrd IS on Tropical and Subtropical Fruits, Souza M, Drew R (eds). Acta Horticulture 864*,* ISHS. 267–273. http:// ucce.ucdavis.edu/files/datastore/234-2405.pdf (accessed 11 Novem- ber 2016).

Wang D-L. 2016. *The Policy and Pilot Plan: Top-Grafting Pears for Crop Natural Disaster Insurance in Taiwan, R.O.C.* http://ap.fftc.agnet.org/ ap_db.php?id=653.

Wang B, Wu R, Fu X. 2000. Pacific-east Asian teleconnection: how does ENSO affect east Asian climate? *J. Clim.* **13**: 1517–1536. https://doi .org/10.1175/1520-0442(2000)013<1517:PEATHD>2.0.CO;2.

Wang S-Y, L'Heureux M, Chia H-H. 2012. ENSO prediction one year in advance uing western North Pacific sea surface temperatures. *Geophys. Res. Lett.* **39**: L05702. https://doi.org/10.1029/2012GL05 0909.

Wang S-Y, Chia H-H, Gillies RR, Jiang X. 2013a. Quasi-biweekly mode and its modulation on the diurnal rainfall in Taiwan forecasted by the CFS. *Weather Forecast.* **28**: 981–993. https://doi.org/10.1175/WAF- D- 12- 00120.1.

Wang S-Y, L'Heureux M, Yoon J-H. 2013b. Are greenhouse gases changing ENSO precursors in the western North Pacific? *J. Clim.* **26**: 6309–6322. https://doi.org/ 10.1175/JCLI-D-12-00360.1.

Weng H, Behera SK, Yamagata T. 2009. Anomalous winter climate conditions in the Pacific rim during recent El Niño Modoki and El Niño events. *Clim. Dyn.* **32**: 663–674. https://doi.org/10.1007/ s00382- 008- 0394- 6.

Woo SH, Kim BM, Jeong J-H, Kim SJ, Lim GH. 2012. Decadal changes in surface air temperature variability and cold surge characteristics over northeast Asia and their relation with the Arctic Oscillation for the past three decades (1979-2011). *J. Geophys. Res.* **117**: D18117. https://doi.org/10.1029/2011JD016929.

Wright S. 1921. Correlation and causation. *J. Agric. Res.* **20**: 557 – 587.

Wright S. 1934. The method of path coefficients. *Ann. Math. Stat.* **5**(3): 161 – 215.

Yen M-C, Chen T-C. 2000. Short communication seasonal variation of the rainfall over Taiwan. *Int. J. Climatol.* **20**: 803–809. https://doi .org/10.1002/1097- 0088 (20000615) 20:7<803::AID- JOC525>3 .0.CO;2- 4.

Yu PS, Yang T-C, Kuo CC. 2006. Evaluating long-term trends in annual and seasonal precipitation in Taiwan. *Water Resour. Manage.* **20**: 1007–1023. https://doi.org/ 10.1007/s11269-006-9020-8.

Yu J-Y, Lu MM, Kim ST. 2012. A change in relationship between tropical central Pacific SST variability and the extratropical atmosphere around 1990. *Environ. Res. Lett.* **7**: 034025. https://doi.org/10.1088/ 1748- 9326/7/3/034025.

Yuan X, Wood EF, Luo L, Pan M. 2011. A fist look at Climate Forecast System version 2 (CFSv2) for hydrological seasonal prediction. *Geophys. Res. Lett.* **38**: L13403. https://doi.org/10.1029/2011GL0 47792.

Zhang Y, Sperber KR, Boyle JS. 1997. Climatology and internannual variation of the East Asian Winter monsoon: results from the 1979-95 NCEP/NCAR reanalysis. *Mon. Weather Rev.* **125**: 2605–2619 https:// doi.org/10.1175/1520- 0493(1997)125<2605: CAIVOT>2.0 .CO;2.

Tables and Figures

Table 3-1. Abbreviations used to categorize weather events.

Weather event (Abbreviation)	Description
Cold	Temperature < 10 ^{o}C
Dry-cold (DC)	Temperature < 10 ^{o}C with no precipitation (0 mm) before, during, and after the cold day
Wet-before-cold (WBC)	Temperature < 10 ^{o}C with precipitation ≥ 5 mm in the previous day only
Wet-with-cold (WWC)	Temperature < 10 ^{o}C and precipitation ≥ 5 mm on same day only.
Wet-after-cold (WAC)	Temperature < 10 ^{o}C with precipitation ≥ 5 mm on the following day only
Wet-cold (WC)	Temperature < 10 ^{o}C with precipitation ≥ 5 mm either before, during, or after the cold day

Table 3-2. Correlation coefficients (*r*) between each JF-mean of weather event and climate index.

Index Event	Nino3.4	WNP	PMM-SST	PMM-Wind	AO	NPO	PDO
Cold	-0.10	-0.58**	0.40**	0.47**	-0.01	-0.34*	0.17
DC	-0.15	-0.52**	0.39**	0.38*	-0.07	-0.36*	0.21
WBC	0.16	-0.15	0.06	0.32	-0.17	-0.03	-0.06
WWC	0.12	-0.16	0.04	0.24	-0.23	0.00	-0.01
WAC	-0.10	-0.29	0.10	0.20	-0.20	-0.14	-0.02
WC	0.08	-0.25	0.10	0.31	-0.18	-0.04	-0.03

r with ** and * are significant at 99% and 95% confidence interval, respectively.

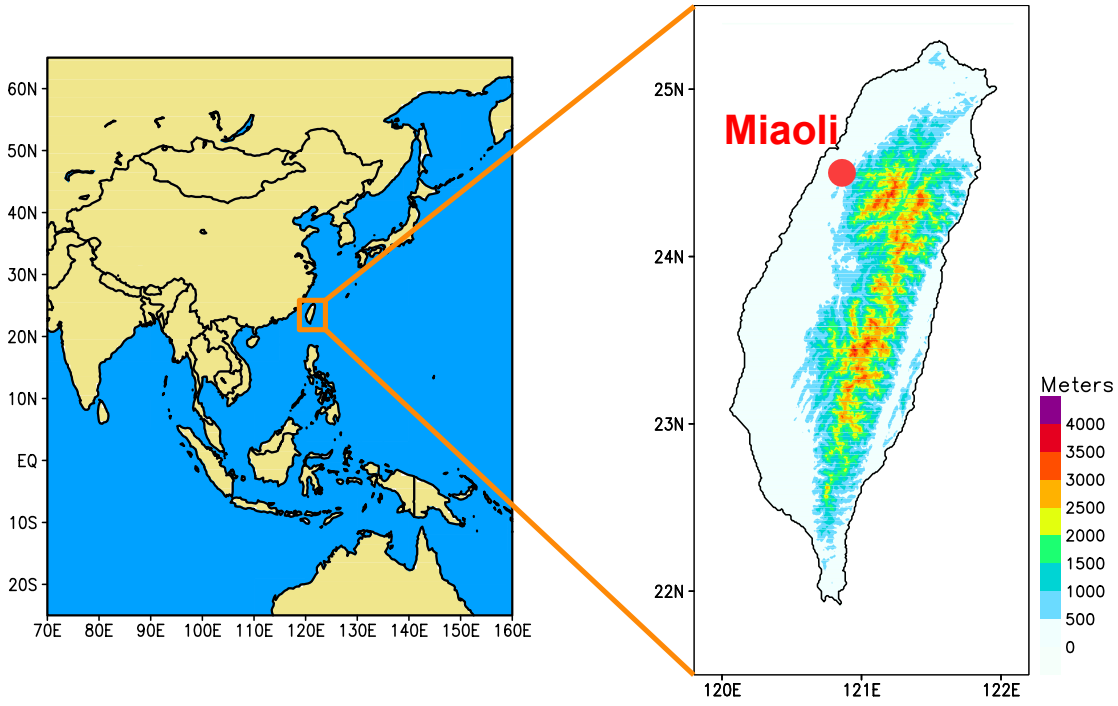

Figure 3-1. Map of Taiwan with terrain elevation above mean sea level and location of Miaoli city.

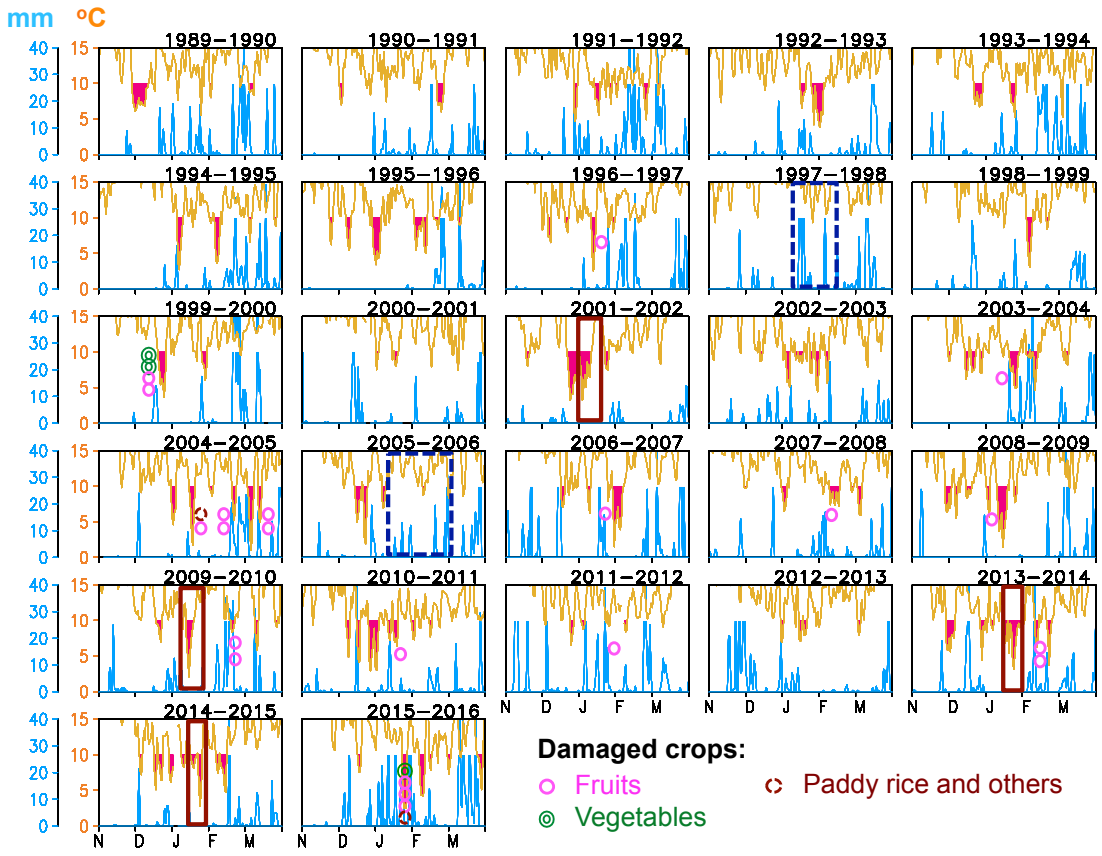

Figure 3-2. Daily temperature (yellow lines-top side), precipitation (blue lines-bottom side), and damaged crops (opened-circles) in November–March 1989–2016. Blue-dashed line boxes indicate wet spells and red-solid line boxes indicate cold spells.

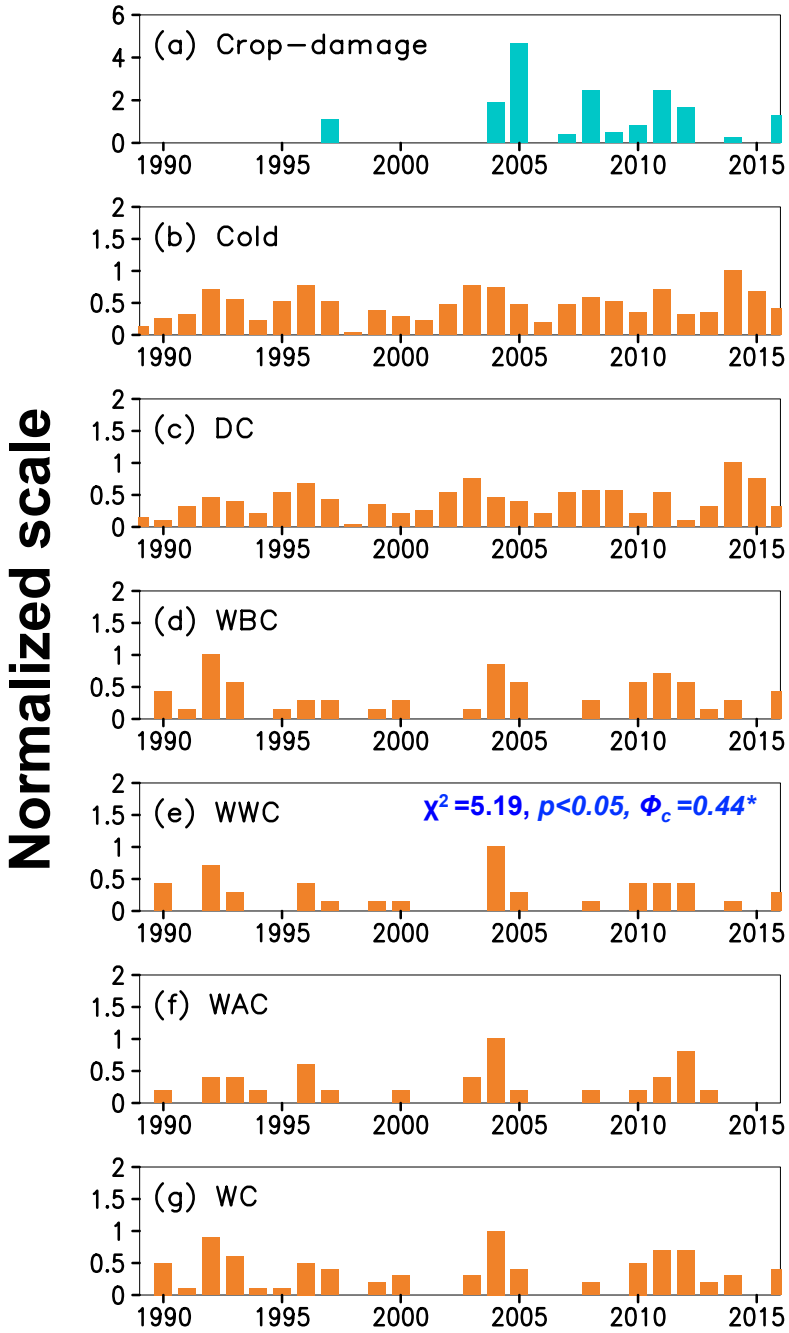

Figure 3-3. Crop damage intensity (a) and (b)–(g) frequency of weather events in January–February 1989–2016 (χ^2 is derived from Pearson's chi-squared test; Φ_c is Phi and Cramér's V).

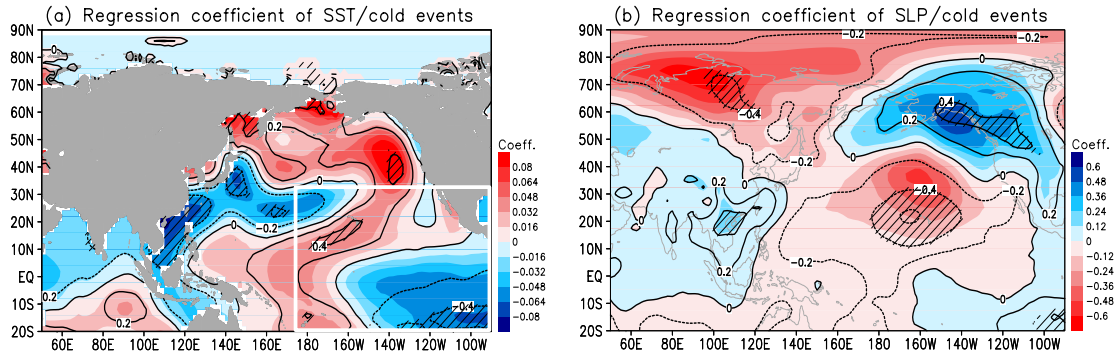

Figure 3-4. Regression coefficient (shading) and correlation coefficient (contours) of (a) SST and (b) SLP computed against a time-series of cold days in January–February 1990–2016. Hatched areas indicate the significance of correlation coefficients exceeding 95% confidence interval. White box in (a) denotes the areas for PMM' computation.

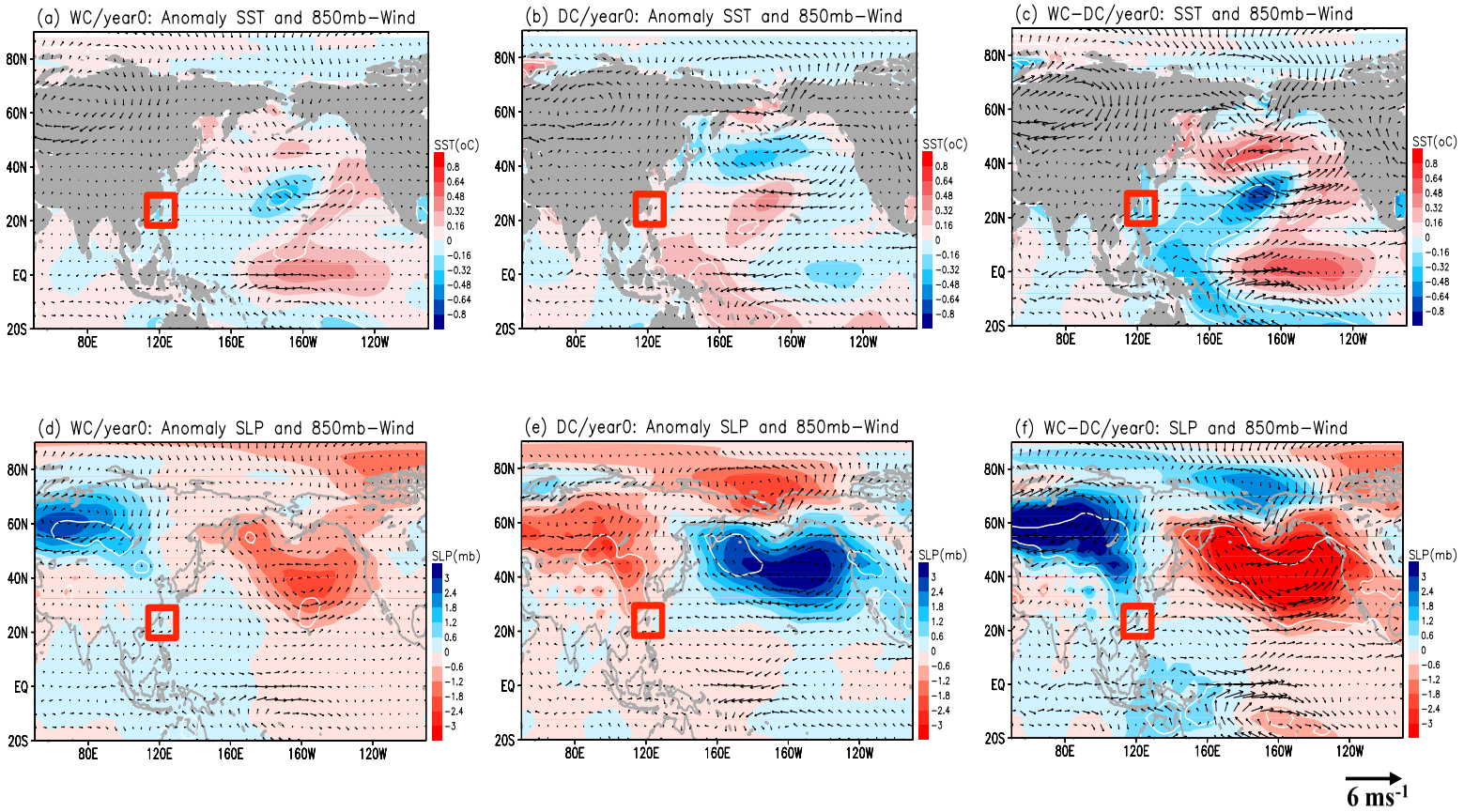

Figure 3-5. Composite analysis for year 0 with (a) wet-cold event, (b) dry-cold event, and (c) difference between wet-cold and dry-cold events computed for the 850-mb wind (vector) with SST anomalies (shading) in January–February. (d) through (f) are the same as (a) through (b), but computed for SLP (shading). White contours indicate statistical significance exceeding 80% confidence interval as determined by a two-tailed Student' s *t* test. Red boxes indicate the location of Taiwan.

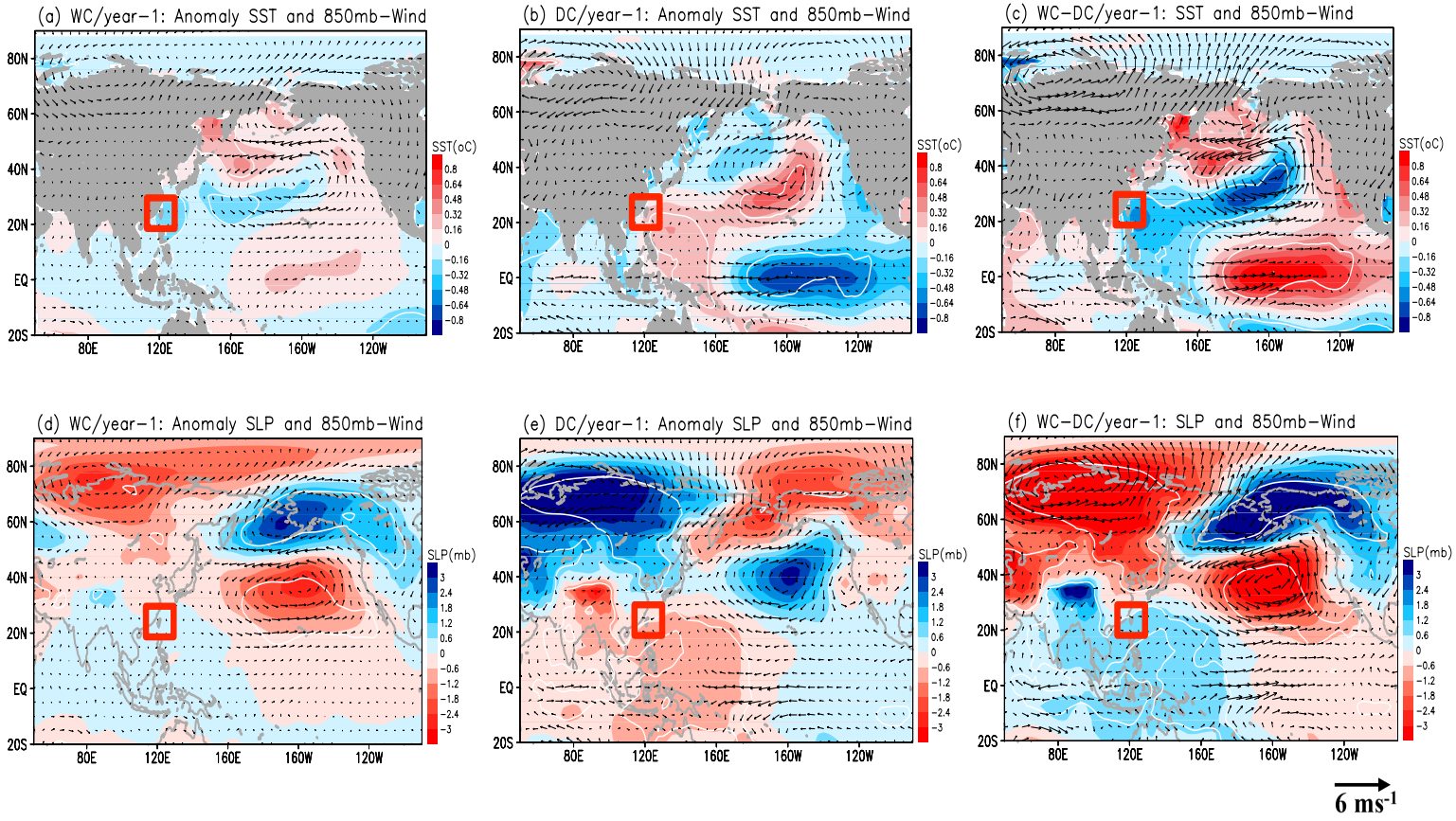

Figure 3-6. Composite analysis for year-1 with (a) wet-cold event, (b) dry-cold event, and (c) difference between wet-cold and dry-cold events computed for the 850-mb wind (vector) with SST anomalies (shading) in January–February. (d) through (f) are the same as (a) through (b), but computed for SLP (shading). White contours indicate statistical significance exceeding 80% confidence interval as determined by a two-tailed Student’ s *t* test. Red boxes indicate the location of Taiwan.

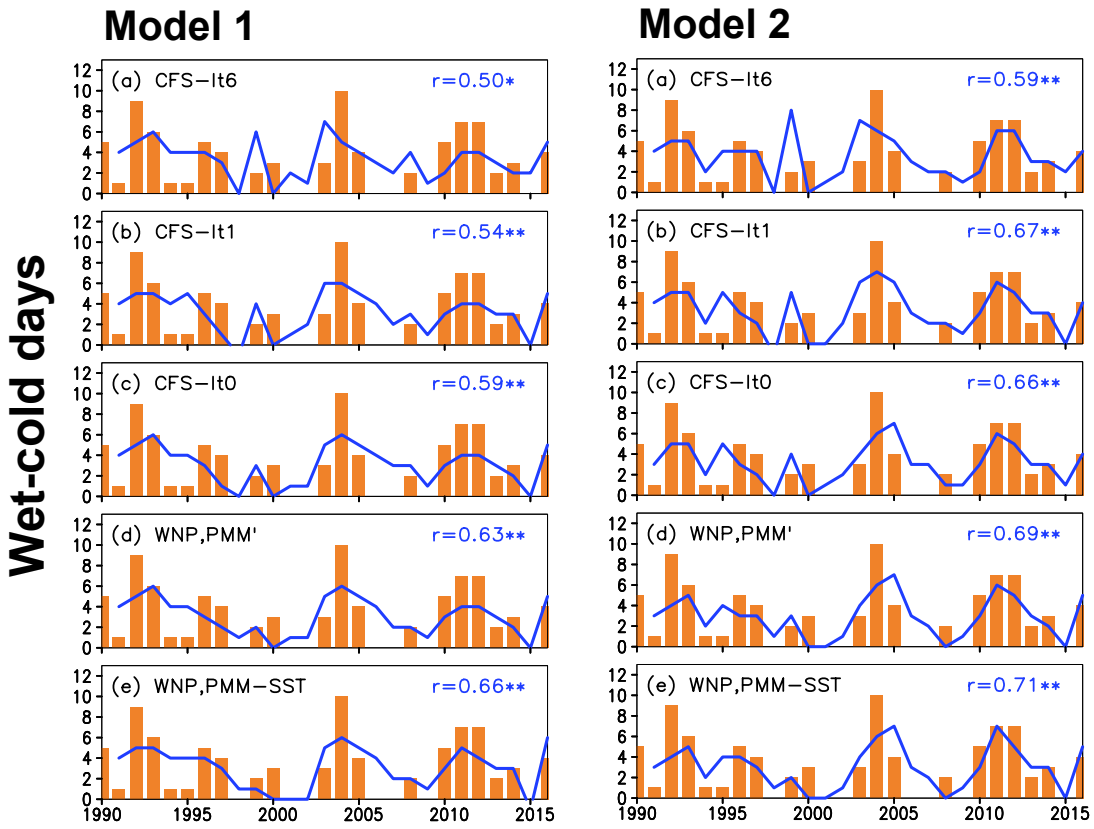

Figure 3-7. Observed wet and cold (WC) days (bars) in January–February and the estimated WC days (lines) derived from two regression models by using historical data (WNP, Niño 3.4, AO) and data in year 0; (a) CFS-WNP with CFS-PMM′ derived from CFSv2-lead month 6, (b) CFS-WNP with CFS-PMM′ derived from CFSv2-lead month 1, (c) CFS-WNP with CFS-PMM′ derived from CFSv2-lead month 0, (d) WNP with PMM′, and (e) WNP with PMM-SST. Correlation coefficients (*r*) with ** are significant, exceeding 99% confidence interval.

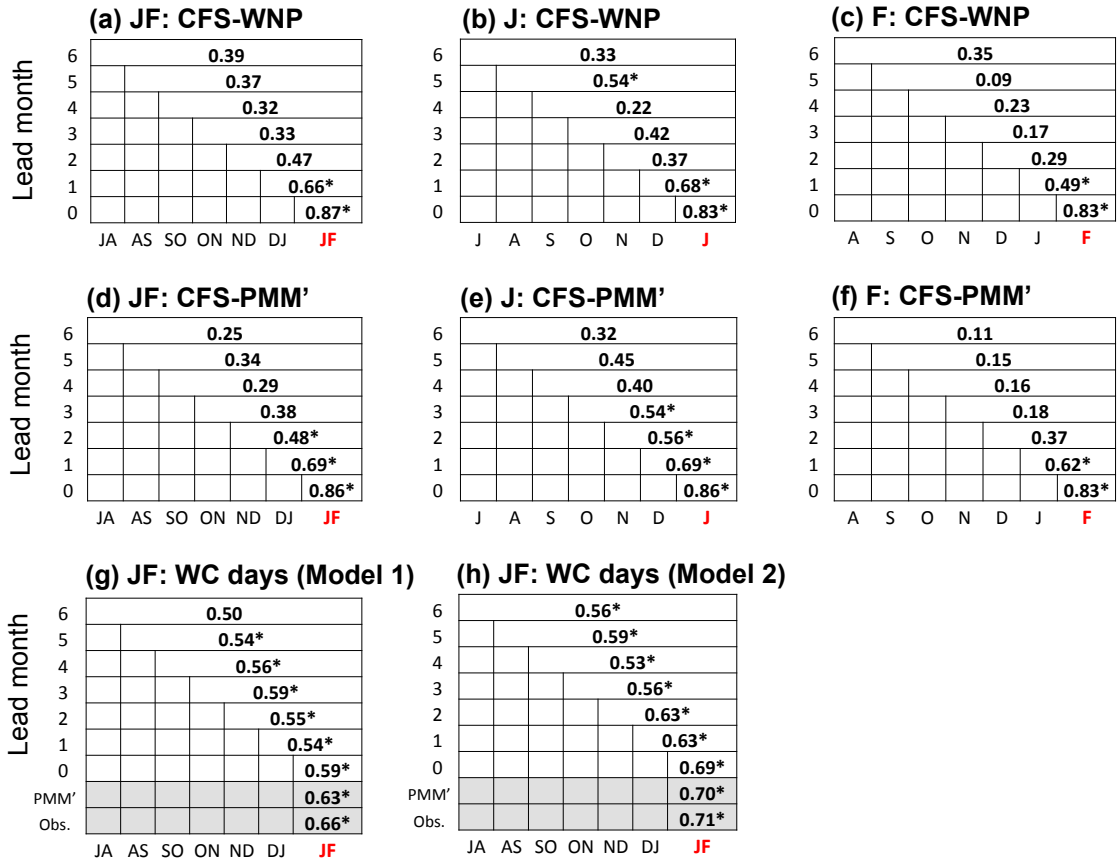

Figure 3-8. (a) through (c) show correlation coefficients (*r*) between WNP and CFS-WNP (lead month 0–6) in January–February (JF), January (J), and February (F). (d) through (f) are the same as (a) through (c) but computed for PMM-SST and CFS-PMM′. (g) shows *r*-values between observed-WC days and estimated-WC days derived from regression model 1 by using WNP with PMM-SST (Obs.), WNP with PMM′ (PMM′), and CFS-WNP with CFS-PMM′ (0-6). (h) is the same as (g) but derived the estimation from model 2. Correlation coefficients (*r*) with * are significant exceeding 99% confidence interval.

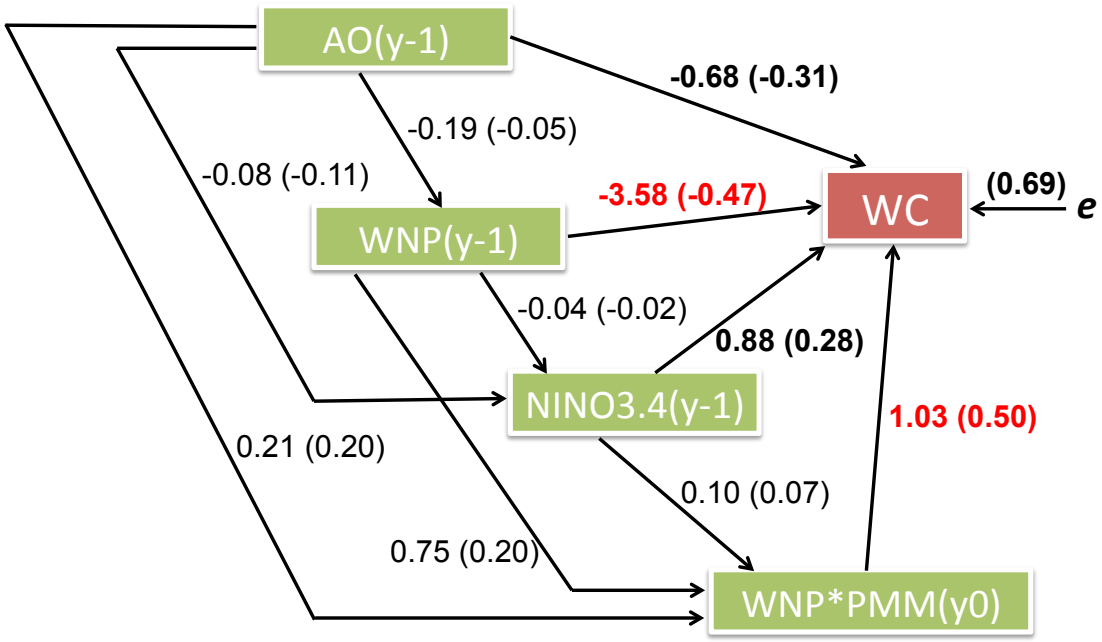

Figure 3-9. Unstandardized and standardized (numbers in parentheses) regression coefficients among climate indices determined the wet-cold (WC) days using regression model 2. Unstandardized coefficients were estimated from the original scores of each climate index in the regression model, while standardized coefficients (path coefficients) were estimated from the standard scores (z-scores). The z -scores of each climate index are given by [(raw score x_i – population mean μ) / population standard deviation σ]. The error variance of the model is given as e.

CHAPTER 4

PROJECTED RICE GROWTH AND YIELD IN TAIWAN UNDER CHANGING COLD SEASON

ABSTRACT

Rice cultivation in Taiwan is most productive during the dry season (January–June) but is sensitive to cold temperature and global warming driven variability in the winter monsoon season. To enable prediction and planning for future rice production under these more variable conditions, we used the common rice model, ORYZA(v3), to assess the influence of predicted future climate on the potential growth and yield of japonica rice (*Oryza sativa* subsp. *japonica)* in three distinct agro-climatological regions of Taiwan during the dry season. Simulations were constructed for three planting dates (15 January, 30 January, and 14 February) and three different periods (1986–2005, 2006–2025, and 2026–2045) using the high-emission (RCP 8.5) scenarios from the latest climate projection data of the Coordinated Regional Climate Downscaling Experiment (CORDEX). We found that increased temperature during the early part of the growing season significantly shortens the rice vegetative phase and lowers future yields. Compared to 1986, by 2045 rice maturation is projected to be 6–9 days and 7–11 days earlier for the central-west and the north-east regions, respectively. Despite the effects of increasing CO_2, modelled yields indicate significant reductions (3.3–10%) during 2026–2045. Increased CO_2 in the future can enhance yield by 8.5–18%, which is more beneficial to the early planting date and at the north-eastern part of Taiwan. Yield

variability will increase leading to extreme low and high yields and is most important in predicting future yields.

Keywords: Rice yield, Phenology, Climate change, CORDEX, ORYZA(v3), Taiwan

1. Introduction

Rice (*Oryza sativa* L.) is sensitive to low-temperature such that its growth and development are severely damaged at temperatures below 15ºC (Krishnan et al., 2011). Taiwan is a major rice producing country and is situated in an area affected by East Asia winter monsoon. As a result, Taiwan's first crop rice, cultivated from January–June, is exposed to chilling stress during the seedling stage (Council of Agriculture, 2018). Reproductive phases, especially anthesis, flowering, and grain filling periods are most susceptible to low (<18 ºC) or high (> 32 ºC) temperature and unfavorable environments (Krishnan et al., 2011; Lee, 2001; Ghadirnezhad and Fallah, 2014). Taiwan's climate has seen changes in both the mean and variability of precipitation, temperature, and atmospheric CO_2 concentration (Hsu and Chen, 2002; Hsu et al., 2011). Since 1980, mean temperature in Taiwan has increased by 0.29 ºC per decade, with the highest warming occurring in winter and the northern region (Hsu et al., 2011). This trend is accompanied by an increasing number of hot days (> 30 ºC) and decreasing cold days (<13 ºC) (Hsu and Chen, 2002; Hsu et al., 2011), and a reduction in winter precipitation. An increase in winter temperature may reduce cold injury, however warm spring temperatures may increase spikelet sterility.

Several studies have evaluated the impacts of climate change on rice yield in Taiwan applying crop models (Matthews et al., 1997) and statistical models (Change, 2002; Chen and Change, 2005; Chiuen et al., 2013; Wu et al., 2015). Those studies focused on the mean yield change considering the whole island of Taiwan, whereas growth and yield variability with respect to rice varieties in different climatological areas and for specific seasons have been less studied. The study with crop models predicted reductions in rice yield of approximately 7.4% for 1^{o}C of temperature increase (Matthews et al., 1997). Likewise, statistical models found that the impacts of climate change on rice yield resulted in changes of various magnitudes and differed per farm management (e.g. Change, 2002). A benefit of rising CO_2 in favor of future rice yield for mid- to high-latitudes was argued (e.g. Rosenzweig et al., 2014; Li et al., 2015; Zhang et al., 2015; Pugh et al., 2016). According to Matthews et al. (1997), larger concentrations of CO_2, e.g. up to 600 ppm can increase simulated rice yield in Asia by 24-36%, but the advantage of CO_2 reduces with increasing temperature. Taiwan's rice yield was projected to increase from 2 to 28 % depending on the crop models and scenarios of General Circulation Models (Matthews et al., 1997). Yet, few recent studies have modelled the effects of rising CO_2 on rice yield in Taiwan.

This study aims to (1) validate and test the rice model, ORYZA(v3), for Taiwan's unique climate and rice production practices, and (2) evaluate the influence of future climate conditions during the winter–spring season on the change in mean and variability of rice growth and yield for different regions in Taiwan. The study areas, data collection, and simulation framework are described in Section 2. Section 3 presents simulation

outputs that consist of model calibration and validation (3.1), responses of rice to temperature (3.2–3.3), and potential rice yield with/without CO_2 effects (3.4–3.5). Section 4 presents discussion and section 5 provides some conclusions.

2. Material and methods

2.1. Study areas

Our study was conducted for the cities of Taichung, Chaiyi, and Illan in Taiwan (Fig. 4-1a) which represent primary cultivated areas of rice production during the dry season (January–June). Illan is located in the north-east, while Taichung and Chaiyi are located in the central-western part of the island (Fig. 4-1a inset). Climatology patterns of these three locations are different (Figs. 4-1b1–b3). During the early-mid period of rice cultivation (January–March), Illan is wet and cold with low radiation; Taichung is dry and cold with moderate radiation; Chaiyi is dry and cold with high radiation. The peak of the rainy season is in late spring for Taichung, in summer for Chaiyi, and in fall–winter for Ilan (Figs. 4-1b1–b3; Yen and Chen, 2000). Thus, irrigation is required for rice cultivation during the dry season. Average temperatures of 16–30 ^{o}C are required for rice growth. The seasonal temperature of Illan (21.30 ^{o}C) is slightly lower than both Taichung (22.51 ^{o}C) and Chaiyi (22.47 ^{o}C). The rice crop can be at risk of low temperature injury in January–February for all three locations when minimum temperature drops below 10 ^{o}C. During the growing period, Chaiyi, Taichung, and Ilan receive approximately radiation of 14.7, 11.5, and 9.6 MJ m^{-2} d^{-1}, respectively.

2.2. Data collection

2.2.1. Observed rice data

Growth and yield data of Tainung 71 (TN71) (*Oryza sativa* subsp. *Japonica*) were obtained from field experiments during the dry season (January–June) from 2009 to 2016. The experiments were conducted at the Taiwan Agricultural Research Institute, Taichung (24.031°N, 120.688 °E,). Major phenological stages were recorded and plant samples were collected weekly to measure leaf area index (LAI) and biomass of different plant parts. Grain yield at harvest was reported at a moisture content of 14%.

2.2.2. Observed weather data

We obtained the observed daily precipitation (*P*), maximum temperature (T_{max}), minimum temperature (T_{min}), mean temperature (*T*), short-wave radiation (*RAD*), average wind speed (*WS*), and relative humidity (*RH*) from weather stations located in Taichung (24.031 °N, 120.688 °E), Chaiyi (23.496 °N, 120.433 °E) and Illan (24.764 °N, 121.757 °E) for the period 1987-2016 for Chaiyi and Illan (1990–2016 for Taichung). We calculated saturated vapor pressure (*Es*, kPa) using *T* and actual vapor pressure (*Ea*, kPa) using *Es* and *RH* (Eqs. 2, 3 in Table 4-S1). Observed data of monthly CO_2 concentrations in Taiwan were obtained from the NOAA website (ftp://aftp.cmdl.noaa.gov/data/trace_ gases/).

2.2.3. Projected climate data

We used historical climate data (1986–2005) from the historical experiment and future climate data (2006–2045) from the RCP 8.5 emission scenario. The datasets were

outputs from three running models with 0.44° (~50 km) spatial resolution for East-Asia domain (EAS-44) of Coordinated Regional Climate Downscaling Experiment (CORDEX) (https://esgf-index1.ceda.ac.uk/search/cordex-ceda/) (see model names in Table S1). Daily data on T_{max}, T_{min}, *P-flux*, surface downwelling *RAD* flux, near-surface *RH*, and near-surface *WS* were extracted on the grid points nearby the weather stations in Taichung, Chaiyi, and Illan. We used calculated *Ea* as described in 2.2.2. The datasets were statistically downscaled before incorporating into the rice model (see 2.3.2). The data of annual CO_2 concentrations were outputs of RCP 8.5 experiment from General Circulation Model.

2.3. Simulation framework

We used the ORYZA(v3) (Li et al., 2017), the newest version of the ORYZA2000 rice model (Bouman et al., 2001), that can predict rice growth and yield in an irrigated lowland ecosystem (e.g. Li et al., 2013; Zhang and Tao, 2013; Li et al., 2017). The simulation of yield potential, obtained under no stress from water, nutrients, pests, disease, and weeds (Evans and Fisher, 1993) can depict the impacts of temperature, solar radiation and CO_2. Since rice cultivation in the dry season in Taiwan is under irrigation, water supply from precipitation is not included. We conducted the simulation following three steps as described in Fig. 4-2:

2.3.1. Step (A): ORYZA(v3) calibration, validation, and evaluation

We used a crop dataset from field experiments in 2009 for calibration and later datasets in 2010–2016 for validation (Fig. 4-2, Step A). Calibration is done for important

crop-parameters under potential production by using observed weather parameters and observed rice data (Fig. 4-2, Step A1). We parameterized rates of four development stages (DVS) and used these rates (Table 4-S2) for further calibration of the maximum value of relative leaf growth rate, partitioning factors for crop organs, rate of leaf death, and fraction of stem reserves. The calibrated values that provide a good fit between observation and simulation in biomass and phenological dates were used for the validation (Fig. 4-2, Step A2) and described as in the next paragraph.

Performance of the model in the calibration and validation processes was evaluated by comparing simulated outputs with observation (Fig. 4-2, Step A3). We determined the slope (α), intercept (β), coefficient of determination (R^2) and significance of the linear regression model by Student's *t*-test [$P(t)_1$]. Additionally, Student's paired *t*-test of means with unequal variance [$P(t)_2$] and absolute root of mean square error (RMSE) were measured (Eq. 3 in Table 4-S1). The model provides best simulation results when α is 1, β is 0, $P(t)_1$ is smaller than 0.05 (significance of regression), $P(t)_2$ is larger than 0.05 (simulated and observed means are not different) and the RMSE is similar or lower to the standard deviation (SD) of observation.

2.3.2. Step (B): downscaling of outputs from climate model

Figure 4-2 step B describes CORDEX datasets (steps B1 and B2, section 2.2.3) and downscaling process (steps B3 and B4). Each weather parameter of each model was adjusted to have its mean and variation close to the observed by using bias correction (Hawkins et al., 2013; Navarro-Racines and Tarapues-Montenero, 2015). The adjusted

CORDEX using monthly mean and RMSE of 1990–2005 was applied to the daily data (Eq. 4 in Table 4-S1).

2.3.3. Step (C): simulation of potential rice growth and yield

The ORYZA model was run to simulate rice growth and yield from 1986 to 2045 by using the adjusted-CORDEX data and two schemes of CO_2, with and without rising-CO_2 concentration (Fig. 4-2, Step C). We used fixed CO_2 at 385 ppm for the simulations (Fig. 4-2, Step C1) since that concentration was measured at the end of historical period (2005) for rice growing season. The simulation with CO_2 effects was run using projected CO_2 data of 1986–2045 (Fig. 4-2, Step C2). The simulation for both with and without rising CO_2 was done for three periods (1986–2005, 2006–2025, and 2026–2045) and considering three planting dates based on the day of year (DOY); 15 DOY (15 January), 30 DOY (30 January), and 45 DOY (14 February). The percent change of mean yields from future years were calculated and compared to those from historical yield (1986–2005). Probability density functions were constructed (following Parzen, 1961; Cimbala, 2010) with a bin size of 0.5 tones ha^{-1} to illustrate yield distribution and variation for the three periods.

3. Results

3.1. ORYZAv3 performance

The model parameterization results in a good fit ($R^2 > 0.93$; Table 4-S3) between simulated values and observations for the above ground biomass (Fig. 4-3a) and LAI

(Fig. 4-3b). In the validation process, the $P(t)_2$ values for flowering (0.91) and maturity (0.93) dates indicate no-statistical difference between the simulation values and observation (Table 4-S4). The simulation of phenological dates is validated by a significant R^2 (0.98 and 0.79; $P(t)_1 < 0.01$) in the linear regression (Table 4-S4). Simulated yield and total above ground biomass (TAGB) are also indifferent to the observations during 2009–2016, in which the $P(t)_2$ of yield and TAGB are 0.51 and 0.59 (Table 4-S4), respectively. The simulation results arrived at a RMSE of 1.433 tons ha^{-1} for yield and 1.538 tons ha^{-1} for TAGB; which are higher than the standard deviation (SD) of the observations (1.240 and 1.362 tons ha^{-1}). The large RMSE values are because of high simulated bias in 2011, 2014 and 2015 (Figs. 4-4a and 4-4b) (discuss in 4.3). If those 3-year outliers are excluded, the correlation between simulation and observation is close to the one–one line with a significant R^2 of 0.79 and 0.69 (Fig. 4-4c; Table 4-S4). The new RMSE for yield (0.551 tons ha^{-1}) and TAGB (1.043 tons ha^{-1}) positively compares to the observed SD (0.892 and 1.479 tones ha^{-1}) (Table 4-S4). All results suggest that ORYZA(v3) adequately simulates rice growth and yield for the TN67 rice variety.

3.2. Response of rice phenology on warming trend

Mean temperature, projected by CORDEX, illustrates a warming trend during the rice growing season and increasing at rates of 0.030, 0.025, and 0.031 $^oC\ year^{-1}$ at Taichung, Chaiyi, and Ilan, respectively (Fig. 4-S1). The change is from 22 ± 0.4 ^oC in the historical

period (1986–2005) to 23 ± 0.4 ºC by 2045 for Taichung and Chaiyi. The largest increase of mean temperature occurs at Ilan which is from 21 ± 0.3 ºC to 23 ± 0.6 ºC.

Rice phenological stages are responsive to rising temperature and simulated results show the stages being shorter, as presented in Figure 4-5. Compared to 1986, rice maturation at Taichung, Chaiyi and Illan will be faster 7–9, 6–8, and 7–11day respectively by 2045. The change rates of the vegetative phase and maturity dates are greater at Ilan (1.2–1.4 and 1.2–1.8 day decade^{-1}) than the rates at Taichung (1.0–1.1 and 1.1–1.5 day decade^{-1}) and Chaiyi (0.8–1.0 and 1.1–1.4 day decade^{-1}). The earlier planting date results in a shorter duration of crop growth. The vegetative phase is more responsive to increases in GDD than the reproductive stage both with and without CO_2 effects. This simulation suggests a most likely significant change of temperature in winter months (January–February). We highlight that the decreasing trend of maturity date significantly correlates to yield reduction in three locations and three planting dates throughout 1986–2045 (Fig. 4-6).

3.3. Spikelet sterility because of temperature

Excessively high or low temperatures during flowering stage can cause spikelet sterility, which is caused by reduced pollen germination on the stigma during anthesis (Matsui et al., 1997; Zeng et al., 2017). The simulation determines spikelet sterility by using 21ºC and 36.5 ºC as a critical low and high temperatures, respectively (Eqs. 5, 6, 7 in Table 4-S1). We report the spikelet sterility factors because of low temperature (SF1; 1=low sterility, 0=high sterility) and high temperature (SF2; 1= high fertility, 0 = low

fertility). Rice production in the three cities has low risk (SF1>0.95) from cold caused sterility (or cold sterility) whereas heat caused sterility (or heat sterility) tends to increase under the simulation conducted both with (data not shown) and without rising CO_2 (Fig. 4-7). The heat sterility is low (SF2 >0.95) for early planted rice while an increasing trend of heat sterility is observed (SF2 <0.95) for the later planting dates (30DOY and 45DOY). The increase in heat sterility for planting on 30DOY at Taichung and Ilan significantly correlates to low yields (Figs. 4-7a and 4-7c).

3.4. Potential change of rice yield in the future without rising CO_2

A reduction of average yield in the future is predicted for all studied locations with the later planting date being more vulnerable to the changing climate. The simulated yields at Taichung during 2006–2025 and 2026–2045 reduced by 1.6–2.5% and 8.5–10 % in comparison to the historical yields (6.46–6.96 tons ha^{-1}), respectively (Fig. 4-8a). Among the three cities, Chaiyi provides the highest simulated yield, which responds to its suitable climate pattern for rice growth (see 2.1). Its future yields are reduced 1.4–3.9 % by 2025 and 5.6–7.1 % by 2045 in comparison to the historical yields (8.63–9.40 ton ha^{-1}) (Fig. 4-8b). Ilan has the lowest rice productivity, with its historical yields at 5.89–6.10 tons ha^{-1}. Simulated yields for Ilan are different than the other two cities, with an increase of 4.1–6.2 % during 2006–2025 and a later decrease of 3.3–9.1 % by 2045 (Fig. 4-8c). Increased temperatures during 2006–2025 may provide fewer cold days or a mean temperature shift to near optimum for rice growth. Later, the temperature may be too high

or close to the critical threshold. High GDD inducing the short vegetative growth period and low radiation may also lead to the yield reduction (Figs. 4-S3 and 4-S4).

The simulated yields for the three locations not only change in their means, but their variability tends to increase in the future. We present the probability density of yield to clearly exhibit yield distribution and variability (Fig. 4-9). The distribution curves show a shift in mean yield that is lower for all locations and planting dates, with the latest planting date providing the lowest yield. Yield variability changed slightly during 2006–2025, while a large increase occurs during 2026–2045, particularly at Ilan. An increase of yield variability expands the probability of low yield to 2–4, 4–6, and 0–2 tons ha^{-1}, that is comparable to a 40–70%, 34–56%, and 67–100% reduction from the historical average-yield for Taichung, Chaiyi, and Ilan, respectively. This suggests the increase in variability has potentially more impact on rice production than the average yield change. The increase of yield variability is possibly caused by increased variability of total GDD and radiation during the growing period (Figs. 4-S3 and 4-S4).

3.5. Effects of rising CO_2 on rice yield

Atmospheric CO_2 during 1986–2045 is projected to increase 2.75 ppm $year^{-1}$ and will reach 513 ppm by 2045 (Fig. 4-S2). The ORYZA(v3) quantifies CO_2 effects on plant growth and yield through photosynthesis (Eq. 8 in Table 4-S1). The simulation suggests rising CO_2 concentration enhances rice yield in all locations and for all planting dates (Fig. 4-8, shaded box). The simulated yield at Taichung increased by 6.3–6.9 % during 2006–2025 and 8.5–10% during 2026–2045 (Fig. 4-8a). The yield increases more if

planting on 15DOY than for the later planting dates. Similarly, the simulated yield at Chaiyi increase by 3.9–6.4% during 2006–2025 and 10–12% during 2026–2045 and the largest result is when planting on 30DOY (Fig. 4-8b). The greatest benefit of rising CO_2 occurs at Ilan where the future yields increase by 14–16% during 2006v2025 and 11–18% during 2026–2045. The early-planted crop tends to adapt to the increase in temperature and CO_2 better than the later planted crop (Fig. 4-8c).

Rice yield potential under a CO_2-rich climate also results in high variability. The probability density of yield depicts the change in both mean and variability for the three cities (Fig. 4-10). The highest yield in the future could reach 10–11 tons ha^{-1} for Taichung and 12–14 tons ha^{-1} at Chaiyi, whereas the lowest yield density is likely similar to historical levels (Figs. 4-10a and 4-10b). Yield variability at Ilan is higher than for the other two cities, and experiences changes both at the lowest (0–2 tons ha^{-1}) and at the highest yields (10–12 tons ha^{-1}) (Fig. 4-10c).

4. Discussion

4.1. Effects of temperature

Shortened phenological stages of rice growth under the warming trends are expected and in line with many previous studies (e.g. Shimono, 2011; Zhang and Tao, 2013; Zhang et al., 2015; Wang et al., 2017; van OORT and Zwart, 2018). The decrease in growing period stimulates development rate and an earlier transition to the reproductive phase, which limits the time for biomass production and results in low yield (van Heemst, 1986). Nonetheless, a shortened vegetative growth period does not increase susceptibility to cold

damage at the reproductive stage, since sterility due to cold temperature did not increase in our study. This is different from Shimono (2011) where, in Japan, the earlier rice phenological stage increases cold damage during the heading stage. Because of this, we hypothesized that the ORYZA model performance at low temperatures was limited in some locations (Devkota et al., 2013; van Oort et al., 2015; Espe et al., 2016). Our simulation without CO_2 effects also presents a low correlation between cold/heat spikelet sterility and yield. It is possible that (1) low risk exists from extreme temperatures during the flowering stage, (2) the rice model underestimates or overestimates the sterility factors (SF1 and SF2), or (3) there is low sensitivity of the rice model to quantify temperature effects on yields.

The SF1 may be underestimated because the model calculates cooling degree days from daily T rather than using T_{min} or cooling degree hours. Inaccurate SF2 could be caused by using too high of a critical heat threshold (36.5 ^{o}C) for the japonica rice, which some studies suggested is 33 ^{o}C (Jagadish et al., 2007; Bheemanahalli et al., 2016). Additionally, the SF2 could be affected by ignoring the flowering time and other factors such as wind velocity and relative humidity (Matsui et al., 1997). The observed sterility might be different from the simulation because only 1-hour exposure to low/high temperature of rice anthesis can cause spikelet sterility (Jagadish et al., 2007; Nguyen et al., 2014; Bheemanahalli et al., 2016), whereas the model considers a daily average temperature. The model was run using daily T, which may be a poor estimate to evaluate impacts of T_{min} and/or T_{max} anomaly on crop growth and yield. Additionally, the

simulated yield is more responsive to radiation (Table 4-S6, Fig. 4-S5a) than to temperature via GDD (Table 4-S5, Fig. 4-S5b) or sterility factors.

4.2. Effects of CO_2

Increases of modelled rice yield resulting from high CO_2 concentration is consistent to the previous studies (e.g. White et al., 2011; Rosenzweig et al., 2014; Li et al., 2015; Pugh et al., 2016; van Oort and Zwart, 2018). Notably, the actual results of CO_2 effects may be different than those obtained from our simulation, if the production is limited by growth factors such as nitrogen (N) fertilizer (Rosenzweig et al., 2014), high temperature (Li et al., 2015), and water supply (van OORT and Zwart, 2018; Yang et al., 2018). Additionally, uncertainty of crop models that evaluate effects of CO_2-fertilization may make these effects vary depending on the model structure, the CO_2 concentration and its interaction to other factors such as temperature (Li et al., 2015). At normal growth conditions, the elevated CO_2 may enhance photosynthesis and water use efficiency, but plants may be at risk of water deficit and high canopy temperature because of stomatal control (Haworth et al., 2016). Under high-CO_2 conditions and low N supply, nitrogen use efficiency can be reduced and a loss of Rubisco-enzyme content during the photosynthesis (Leakey et al., 2009). Likewise, diffusion of CO_2 into leaves will decrease when stomates close to avoid excessive water loss under high temperature and/or low water supply (Leakey et al., 2009; DaMatta et al., 2010).

4.3. Simulation bias in validation

The pronounced difference between simulated and observed yields (bias) in 2011, 2014, and 2015 are interesting cases (Fig. 4a). The simulated yields are responsive to radiation and GDD but the observed yields in the three years likely respond to low precipitation during a vegetative phase (Figs. 4-4a, 4-S5a, 4-S5b, and 4-S5c). This weather condition is different from that of the other validated years, which may be influenced by field experiment outputs or the simulation performance. A dry-warm climate with a high vapor pressure deficit in 2015 may cause lower observed yields than the simulation (Fig. 4-S5c). Leaf stomata will close in response to high transpiration, in order to control its conductance and will reduce CO_2 diffusion and growth, even under non-limited soil water (Parent et al., 2010). A dry-cold winter in 2011 and 2014 may be favorable for early stage growth compared to a wet-cold environment; resulted in higher observed yield than the simulation. Rice leaves have a thin layer of epicuticular wax (O'Toole et al., 1979) resulting in high wettability (Wang et al., 2015), which may create a sensitivity to stomatal blockage by a film of water, resulting in reduced CO_2 assimilation rates as observed in bean (*Phaselous vulgaris)* (Hanba et al., 2004). Thus, the negative effects of leaf wetness on photosynthesis in the dry-cold years is possible low but cannot be measured by the rice model. The simulation bias in the three years may be associated with climate phenomena (Fig. 4-S5d). The underestimated yields in 2011 and 2014 occurred during a cool phase of the western North Pacific while the overestimated yield in 2015 occurred during a warm phase of the Pacific meridional

mode – sea surface temperature (Wang et al., 2012; Promchote et al., 2018). More study may be required to explain the simulation bias.

5. Conclusions

The study presents projects changes in the cold season in Taiwan and its impacts on rice growth and yield potential made until 2045. Duration of rice growth will be shortened (6–11 days) with a lower mean yield (3.3–10%) under a warming trend (~0.03 ^{o}C year^{-1}). The yield reduction is projected to be offset by rising CO_2 concentrations (2.8 ppm year^{-1}), which can increase yield by 8.5–18%, particularly for rice planted early in the north-east region. The actual benefit from rising CO_2 will be limited by other stresses such as insufficient nitrogen fertilizer (Rosenzweig et al., 2014) and water supply (van OORT and Zwart, 2018; Yang et al., 2018). Additionally, the simulation projected increases in yield variability, where a large yield reduction (>67%) plausibly occurs under high CO_2 and non-limiting growth conditions. Our study suggests that future rice production may be more vulnerable due to the yield variability than from the mean yield change. We suggest further study to predict yield anomalies caused by extreme climate and prominent climate events. Multiple climate-models and crop-models should be used to reduce uncertainty of the simulation under extremely warm or cold environment (Zhang and Tao, 2013; Li et al., 2015).

Supporting information

Supporting information (Table 4-S1 to Table 4-S6 and Fig. 4-S1 to Fig. 4-S5) is provided in APPENDIX B.

References

Bheemanahalli, R., Sathishraj, R., Tack, J., Nalley, L.L., Muthurajan R., Jagadish K.S.V., 2016. Temperature thresholds for spikelets sterility and associated warming impacts for sub-tropical rice. Agric. For. Meteorol. 221, 122–130.

Bouman, B.A.M., Kropff, M.J., Tuong, T.P., Wopereis, M.C.S., ten Berge, H.F.M., van Larr, H.H., 2001. ORYZA2000: Modeling Lowland Rice. International Rice Research Institute, Metro Manila, Philippines.

Chang, C.-C, 2002. The potential impact of climate change on Taiwan's agriculture. Agric. Econ. 27, 51–64.

Chen, C.-C., Chang, C.-C., 2005. The impact of weather on crop yield distribution in Taiwan: some new evidence from panel data models and implications for crop insurance. Agric. Econ. 33(supplement), 503–511.

Chiuen, Y.-W, Huang, C.C., Tan, C.H., 2013. Modeling the rice-climate indices in Taiwan. Clim. Change Econ. 4(3), 1350012.

Cimbala, J.M., 2010. Probability Density Function, https://www.mne.psu.edu/cimbala/me345/Lectures/Probability_density_functions.pdf (accessed July 2018).

Council of Agriculture, 2018. Yearly Report of Taiwan's Agriculture: Agricultural Production, https://eng.coa.gov.tw (accessed December 2018).

DaMatta, F.M., Grandis, A., Arenque, B.C., Buckeridge, M.S., 2010. Impacts of climate change on crop physiology and food quality. Food Res. Int. 43, 1814–1823.

Devkota, K.P., Manschadi, A.M., Devkota, M., Lamers, J.P.A., Ruzibaev, E., Egamberdiev, O., Amiri, E., Vlek, P.L.G., 2013. Simulating the impact of climate change on rice phenology and grain yield in irrigated drylands of central Asia. J. Appl. Meteorol. Climatol. 52, 2033–2050.

Espe, M.B., Yang, H., Cassman, K.G., Guilpart, N., Sharifi, H., Linquist, B.A., 2016. Estimating yield potential in temperate high-yielding, direct-seeded US rice production systems. Field Crops Res. 193, 123–132.

Ghadirnezhad, R., Fallah A., 2014. Temperature effect on yield and yield components of different rice cultivars in flowering stage. Int. J. Agron., 846707.

Hanba, Y.T., Moriya, A., Kimura, K., 2015. Effect of leaf surface wetness and wettability on photosynthesis in bean and pea. Plant, Cell Environ. 27, 413–421.

Hawkins, E., Osborne, T.M., Ho, C.K., Challinor, A.J., 2013. Calibration and bias correction of climate projections for crop modelling: An idealized case study over Europe. Agric. For. Meteorol. 170, 19–31.

Haworth, M., Killi, D., Materassi, A., Raschi, A., Centritto, M., 2016. Impaired stomatal control is associated with reduced photosynthetic physiology in crop species grown at elevated [CO_2]. Front. Plant Sci. 7, 1568.

Hsu, H.-H., Chen, C.T., 2002. Observed and projected climate change in Taiwan. Meteorol. Atmos. Phys. 79, 87–104.

Hsu, H.-H., Chou, C., Wu, Y.-C., Lu, M.-M., Chen, C.-T., Chen, Y.M., 2011. Climate Change in Taiwan: Scientific Report 2011 (Summary). National Science Council, Taipei, Taiwan, ROC.

Jagadish, S.V.K., Craufurd, P.Q., Wheeler, T.R., 2007. High temperature stress and spikelet fertility in rice (*Oryza sativa* L.). J. Exp. Bot. 58(7), 1627–1635.

Krishnan, P.B., Ramakrishnan, K.R., Reddy, V.R., 2011. High temperature effects on rice growth, yield and grain quality, in: Sparks, D.L. (ed.), Advances in Agronomy, vol. 111. Academic Press, Burlington, pp 87–206.

Leakey, A.D., Ainsworth, E.A., Bernacchi, C.J., Rogers, A., Long, S.P., Ort, D.R., 2009. Elevated CO_2 effects on plant carbon, nitrogen, and water relations: six important lessons from FACE. J. Exp. Bot. 60(10), 2859–2876.

Lee, M.H., 2001. Low temperature tolerance in rice: The Korean experience increased lowland rice production in the Mekong Region, in: Fukai, S., Basnayake, J. (eds.), ACIAR Proceeding 101, Australian Centre for International Agricultural Research, Canberra ACT, pp. 109–117.

Li, T., Raman, A.K., Marcaida III, M., Kumar, A., Angeles, O., Radanielson, A.M., 2013. Simulation of genotype performances across a larger number of environments for rice breeding using ORYZA2000. Field Crops Res. 149, 312–321.

Li, T., Hasegawa, T., Yin, X., Zhu, Y., Boote, K., Adam, M., Bregaglio, S., Buis, S., Confalonieri, R., Fumoto, T., Gaydon, D., Marcaida M.3rd, Nakagawa, H., Oriol, P., Ruane, A.C., Ruget, F., Singh, B., Singh, U., Tang, L., Tao, F., Wilkens, P., Yoshida, H., Zhang, Z., Bouman, B., 2015. Uncertainties in predicting rice yield by

current crop models under a wide range of climate conditions. Glob. Change Biol. 21(3), 1328–1341.

Li, T., Angeles, O., Marcaida III, M., Manalo, E., Manalili, M.P., Radanielson, A., Mohanty, S., 2017. From ORYZA2000 to ORYZA (v3): An improved simulation model for rice in drought and nitrogen-deficient environments. Agric. For. Meteorol. 237–238, 246–256.

Matsui, T.M., Omasa, K., Horie, T., 1997. High temperature-induced spikelet sterility of Japonica rice at flowering in relation to air temperature, humidity and wind velocity conditions. Jpn. J. Crop Sci. 66(3), 449–455.

Matthews, R.B., Kropff, M.J., Horie, T., Bachelet, D., 1997. Simulating the impact of climate change on rice production in Asia and evaluating options for adaptation. Agric. Syst. 54(3), 399–425.

Navarro-Racines, C.E., Tarapues-Montenero, J.E., 2015. Bias-correction in the CCAFS-climate portal: a description of methodologies, http://ccafs-climate.org/downloads/docs/BC_methods_explaining_v2_jrv.pdf (accessed August 2018).

Nguyen, D.-N., Lee, K.J., Kim, D.-I, Anh, N.T., Lee, B.W., 2014. Modeling and validation of high-temperature induced spikelet sterility in rice. Field Crops Res. 156, 293–302.

O'Toole, J.C., Cruz, R.T., Seiber, J.N., 1979. Epicuticular wax and cuticular resistance in rice. Physiol Plant., 47, 239–244.

Parent, B., Suard, B., Serraj, R., Tardieu, F., 2010. Rice leaf growth and water potential are resilient to evaporative demand and soil water deficit once the effects of root system are neutralized. Plant, Cell and Environ., 33, 1256–1267.

Parzen, E., 1961. On Estimation of a probability density function and mode. Technical Report No.40. Applied Mathematics and Statistics Laboratories, Stanford University, Stanford, California.

Promchote, P., Wang, S.-Y.S., Shen, Y., Johnson, P.G. and Yao, M.-H., 2018. A seasonal prediction for the wet-cold spells leading to winter crop damage in northwestern Taiwan with a combined empirical-dynamical approach. Int. J. Climatol. 38, 571–583.

Pugh, T.A.M., Müller, C., Elliott, J., Deryng, D., Folberth, C., Olin, S., Schmid, E., Arneth, A., 2016. Climate change analogues suggest limited potential for intensification of production on current croplands under climate change. Nat. Commun. 7, 12608.

Rosenzweig, C., Elliott, J., Deryng, D., Ruane, A.C., Müller, C., Arneth, A., Boote, K.J., Folberth, C., Blotter, M., Khabarov, N., Neumann, K., Piontek, F., Pugh, T.A.M., Schmid, E., Stehfest, E., Yang, H., Jones, J.W., 2014. Assessing agricultural risks of climate change in the 21st century in a global gridded crop model intercomparison. PNAS 111(9), 3268–3273.

Shimono, H., 2011. Earlier rice phenology as a result of climate change can increase the risk of cold damage during reproductive growth in northern Japan. Agric. Ecosyst. Environ. 144, 201–207.

van Heemst, H.D.J., 1986. Crop phenology and dry matter distribution, in: van Keulen, H., Wolf, J. (eds.), Modelling of agricultural production: soil, weather and crops, Wageningen, pp. 13–60.

van Oort, P.A.J., Zwart, S.J., 2018. Impacts of climate change on rice production in Africa and causes of simulated yield changes. Glob. Chang. Biol., 24, 1029–1045.

van Oort, P.A.J., de Vries, M.E., Yoshida, H., Saito, K., 2015. Improved climate risk simulations for rice in arid environments. PLoS ONE 10(3), e0118114.

Wang, H., Shi, H., Wang, Y., 2015. The wetting of leaf surfaces and its ecological significances, Chapter 1. INTECH 295–321.

Wang S.-Y., L'Heureux, M., Chia, H.-H., 2012. ENSO prediction one year in advance using western North Pacific sea surface temperatures. Geophys. Res. Lett. 39: L05702.

Wang, X., Ciais, P., Li, L., Ruget, F., Vuichard, N., Viovy, N., Zhou, F., Chang, J., Wu, X., Zhao, H., Piao, S., 2017. Management outweighs climate change on affecting length of rice growing period for early rice and single rice in China during 1991-2012. Agric. For. Meteorol. 233, 1–11.

White, J.W., Hoogenboom, G., Kimball, B.A., Wall, G.W., 2011. Methodologies for simulating impacts of climate change on crop production. Field Crops Res. 124, 357–368.

Wu, S.J., Chiueh, Y.-W., Lien, H.-C., Hsu, C.T., 2015. Modeling risk analysis for rice production due to agro-climate change in Taiwan. Paddy Water Environ. 13, 391–404.

Yang, M., Xiao, W., Zhao, Y., Li, X., Huang, Y., Lu, F., Hao, B., Li, B., 2018. Assessment of potential climate change effects on the rice yield and water footprint in the Nanliujiang catchment, China. Sustainability 10, 242.

Yen, M.-C., Chen, T.C., 2000. Short communication seasonal variation of the rainfall over Taiwan. Int. J. Climatol. 20, 803–809.

Zeng, Y., Zhang, Y., Xiang, J., Uphoff, N.T., Pan, X., Zhu, D., 2017. Effects of low temperature stress on spikelet-related parameters during anthesis in Indica-Japonica hybrid rice. Plant Sci. 8, 1350.

Zhang, J., Feng, L., Zou, H., Liu, D.L., 2015. Using ORYZA2000 to model cold rice yield response to climate change in the Heilongjiang province, China. Crop J. 3, 317–327.

Zhang, S., Tao, F., 2013. Modeling the response of rice phenology to climate change and variability in different climatic zones: Comparisons of five models. Eur. J. Agron. 45, 165–176.

Figures

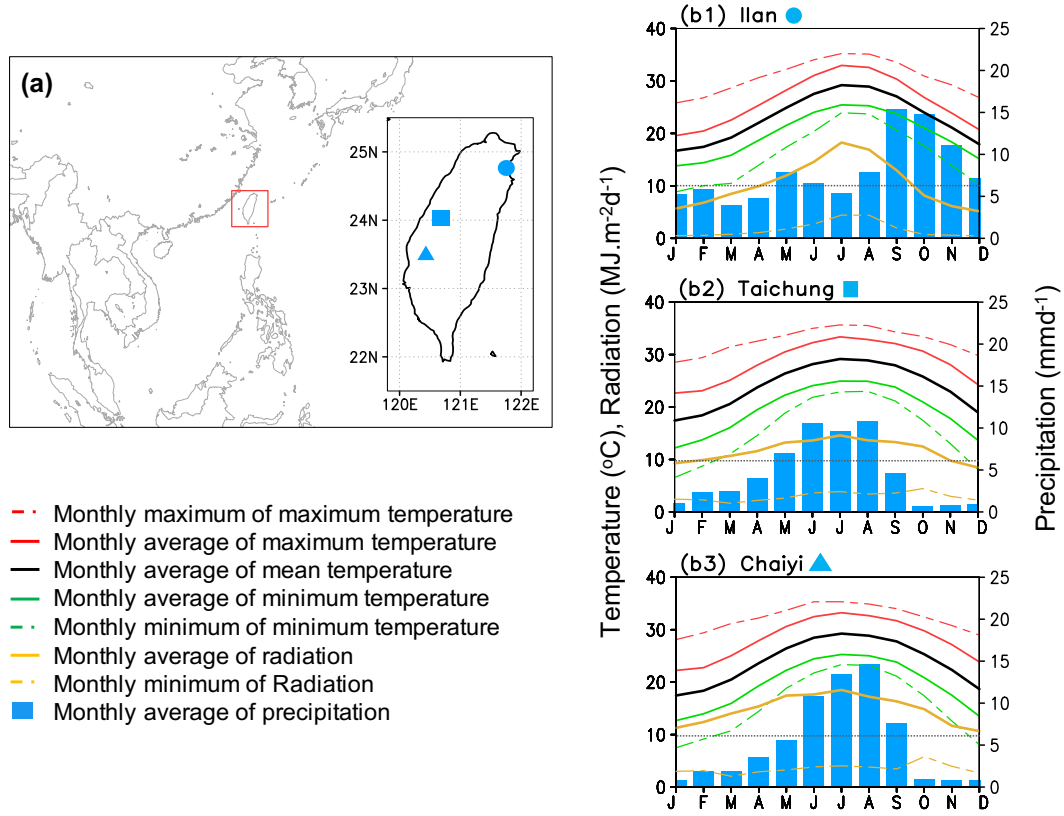

Fig. 4-1. Panel (a) show location of Taiwan (red box) and study areas; Ilan (circle), Taichung (square), and Chaiyi (triangular), and panels (b1)–(b3) present climatology patterns of the three areas.

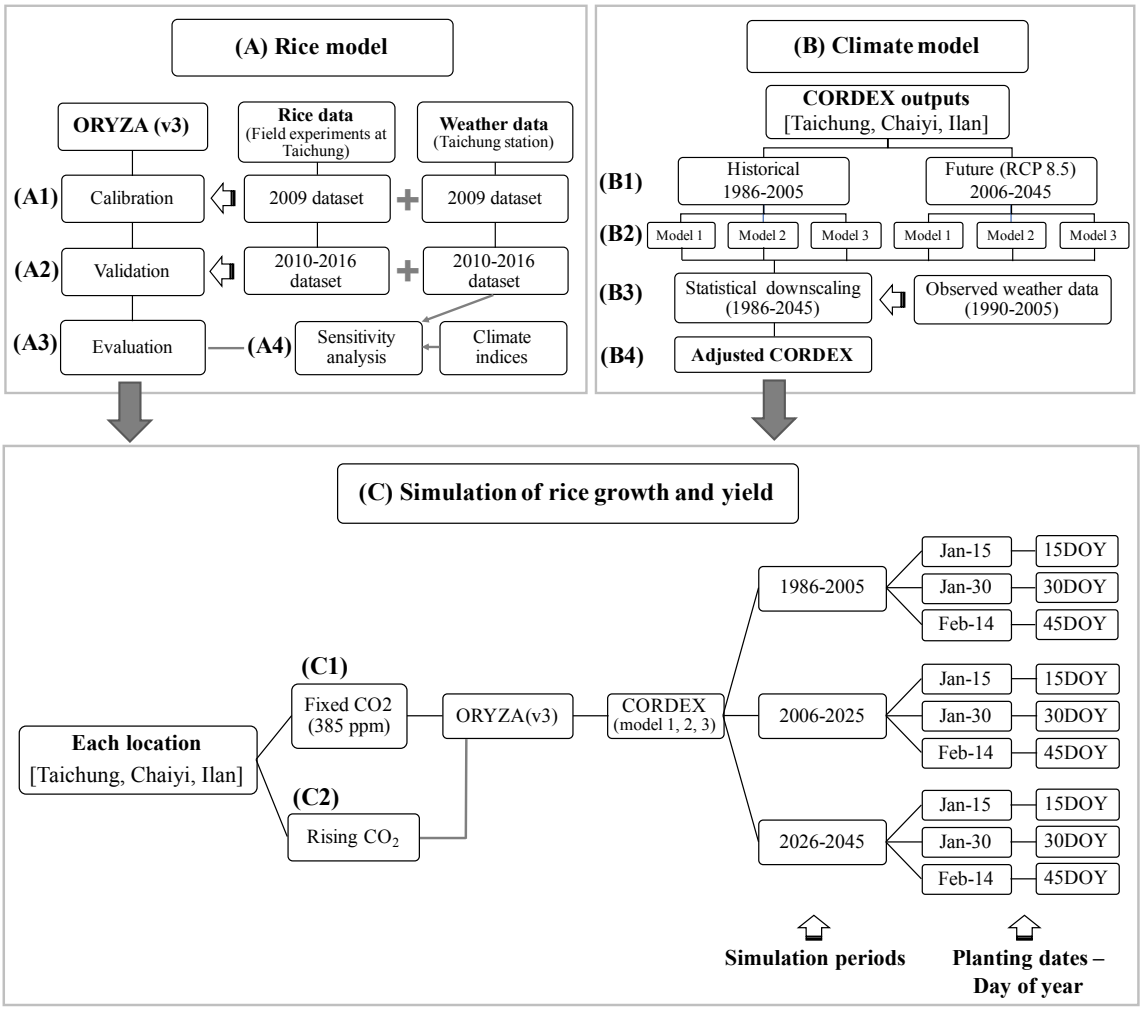

Fig. 4-2. Diagrams of methodological approaches to simulate rice growth and yield by using ORYZA(v3) rice model and outputs from CORDEX.

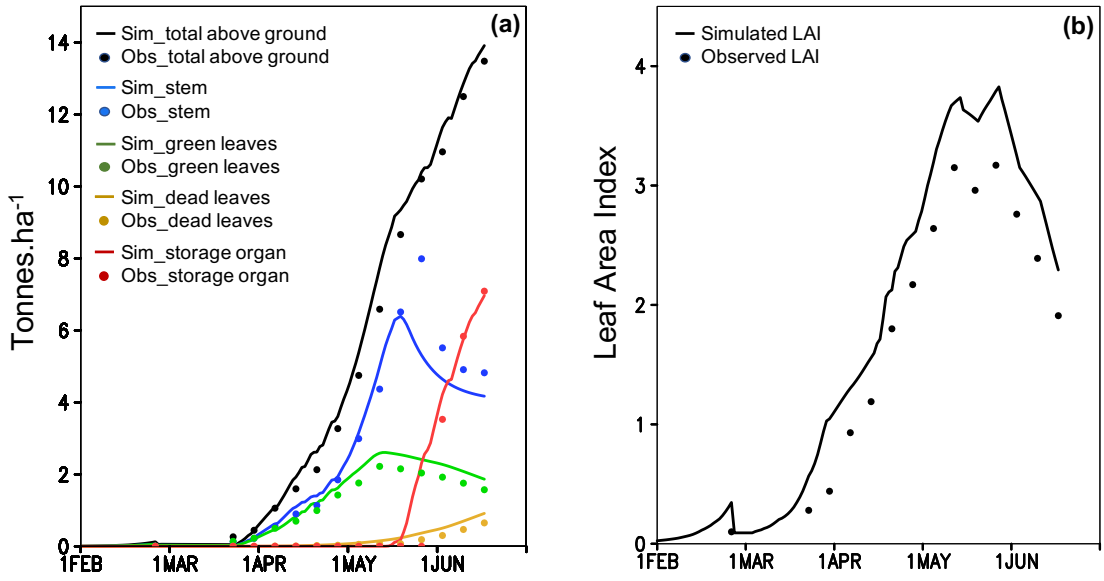

Fig. 4-3. ORYZA(v3) model calibration by using experimental data from 2009; observed (Obs) and simulated (Sim) (a) biomass, and (b) Leaf Area Index (LAI).

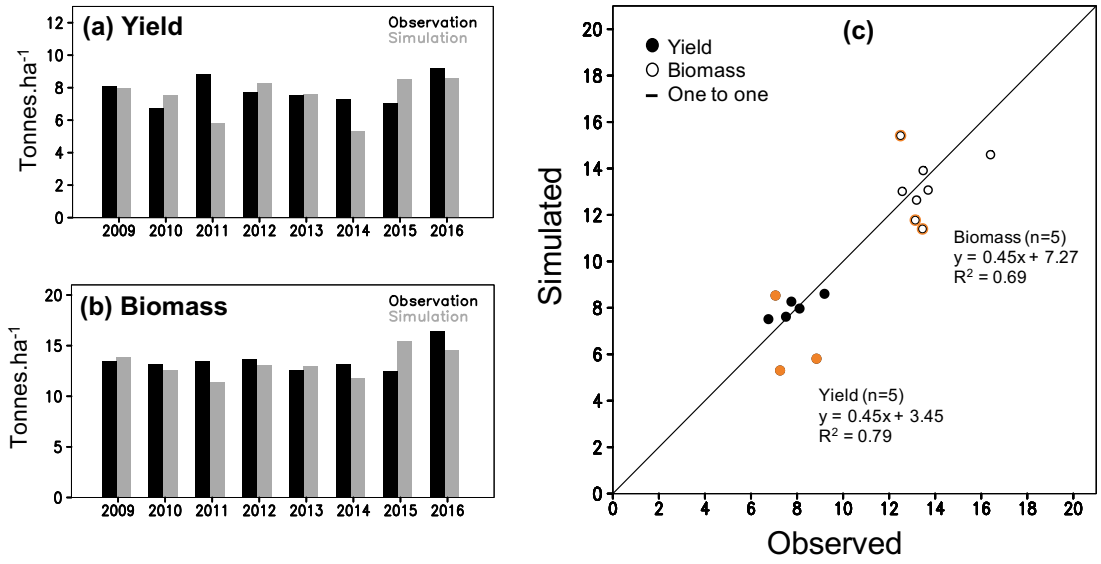

Fig. 4-4. ORYZA(v3) model validation by using experiment data from 2009–2016; observed and simulated (a) yield, and (b) total above ground biomass; panel (c) shows scatter plots for yield and biomass (orange-circle marks are 2011, 2014 and 2015).

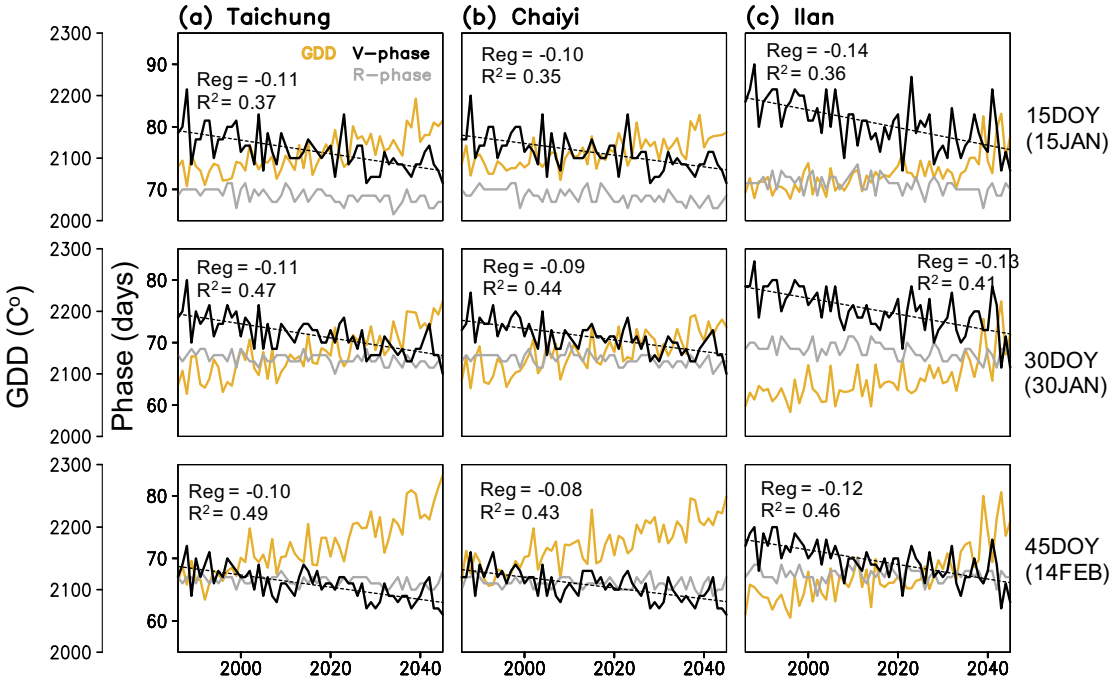

Fig. 4-5. Time series of simulated growing degree days (GDD), lengths of vegetative (V-phase) and reproductive (R-phase) stages for three planting dates (15, 30, 45 day of year) constructed for (a) Taichung, (b) Chaiyi, and (c) Ilan; linear regression coefficients (Reg) and coefficient of determination (R^2) between year and V-phase present in each panel.

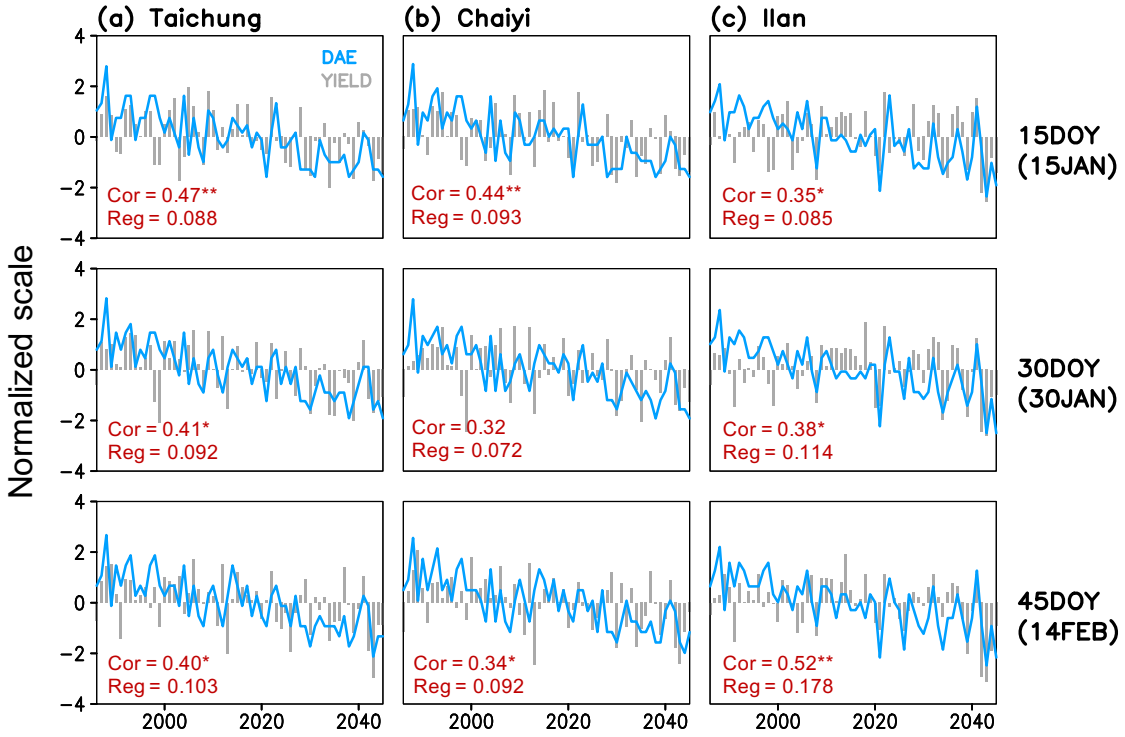

Figs. 4-6. Time series of simulated maturity date (day after emergence; DAE) and yield for three planting dates (15, 30, 45 day of year) constructed for (a) Taichung, (b) Chaiyi, and (c) Ilan; correlation coefficients (Cor) and linear regression coefficients (Reg) between maturity date and yield present in each panel (*, ** indicate significance of the coefficients exceeding 99% and 99.9% confidence interval).

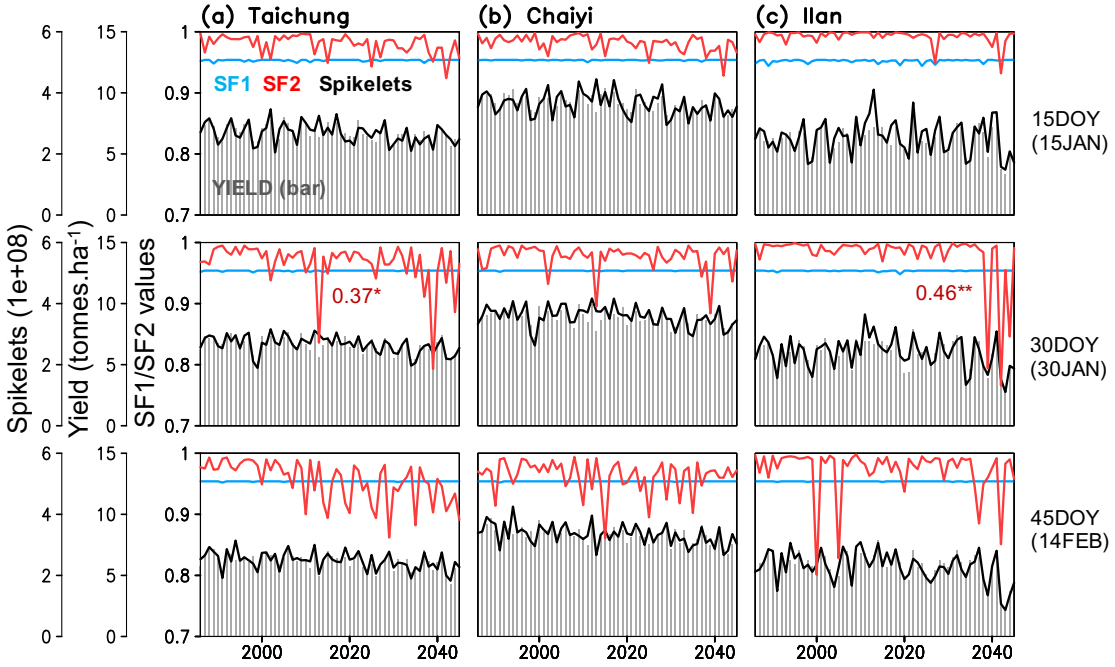

Fig. 4-7. Time series of simulated yield, number of spikelets, spikelet sterility factor because of low temperature (SF1) and spikelet fertility factor because of high temperature (SF2) for three planting dates (15, 30, 45 day of year) constructed for (a) Taichung, (b) Chaiyi, and (c) Ilan; numbers indicate significant correlation coefficients (exceeding 99% confidence interval) of SF2 and yield.

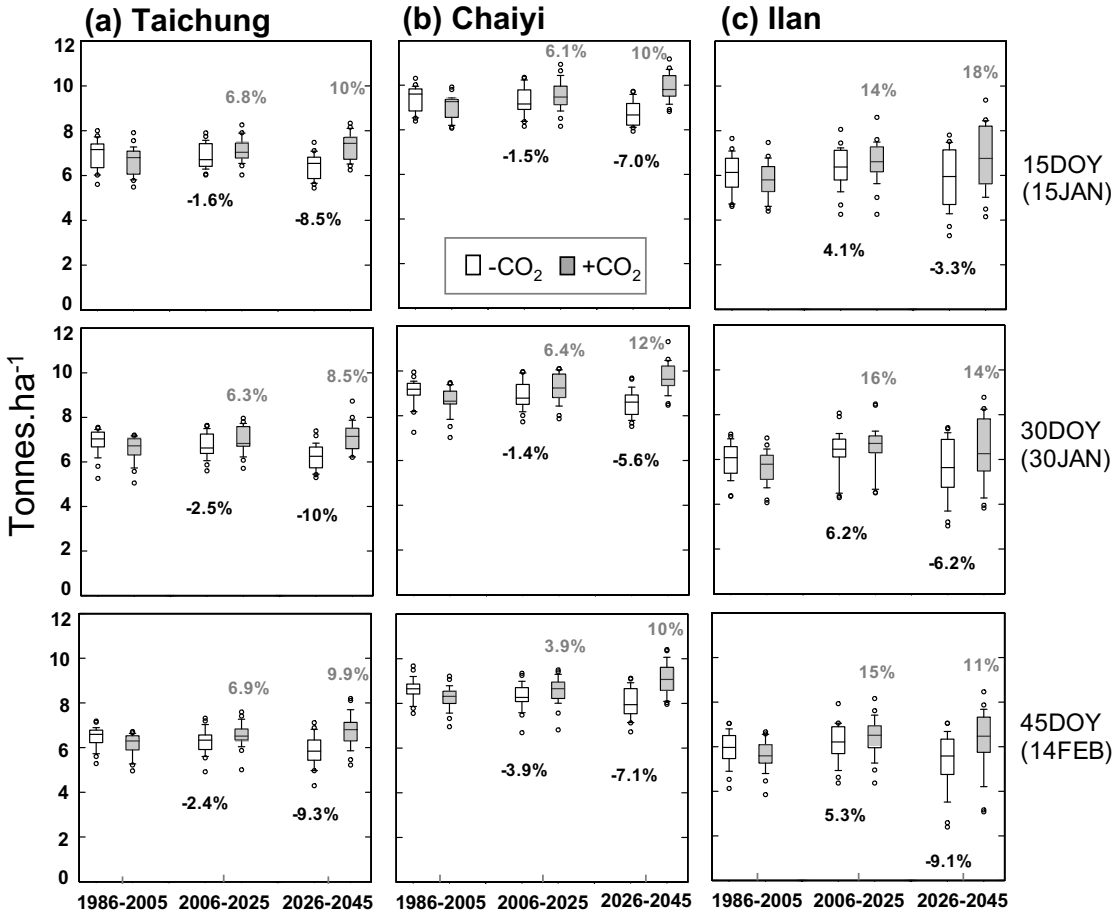

Fig. 4-8. Simulated yield (with and without CO_2 effects) for three planting dates (15, 30, 45 day of year) and three periods (1986–2005, 2006–2025, 2026–2045) constructed for (a) Taichung, (b) Chaiyi and (c) Ilan; numbers indicate percentage of averaged-yield change compares to historical period (1986–2005).

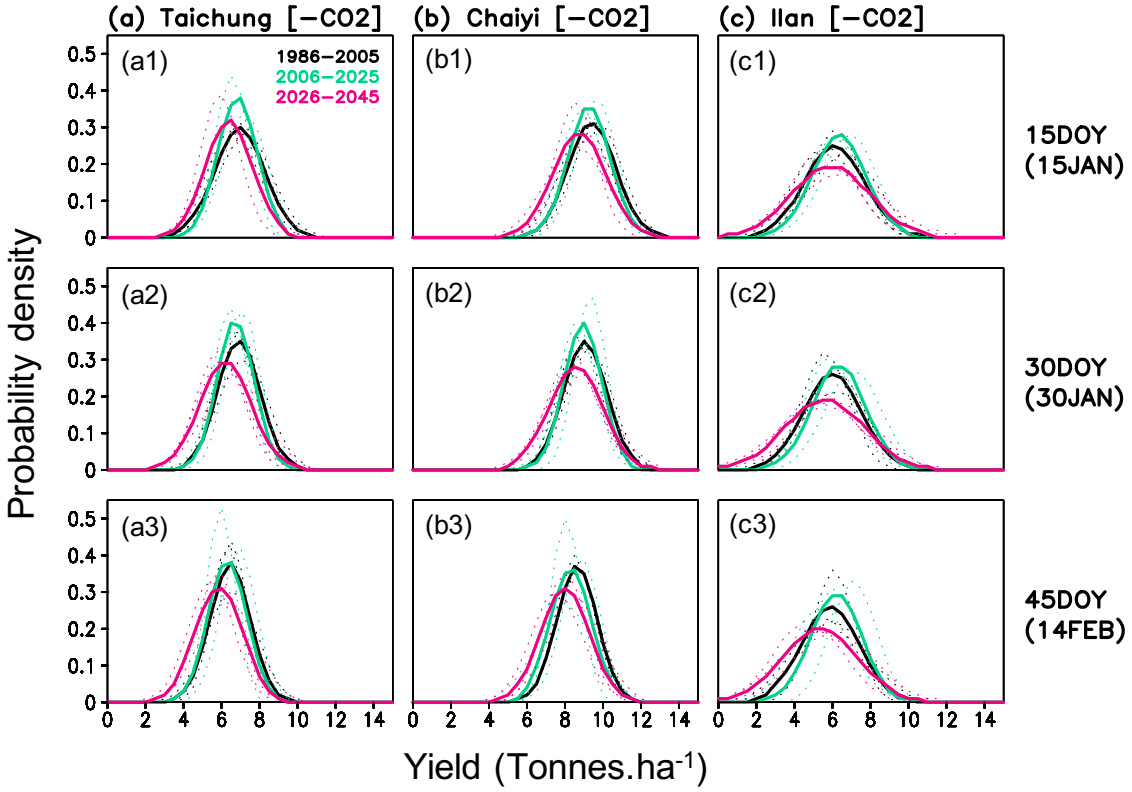

Fig. 4-9. Probability density function of simulated yield (without CO_2 effects) for three planting dates (15, 30, 45 day of year) and three periods (1986–2005, 2006–2025, 2026–2045) constructed for (a) Taichung, (b) Chaiyi and (c) Ilan; solid lines are averaged values from 3 models and dotted line are values of each model.

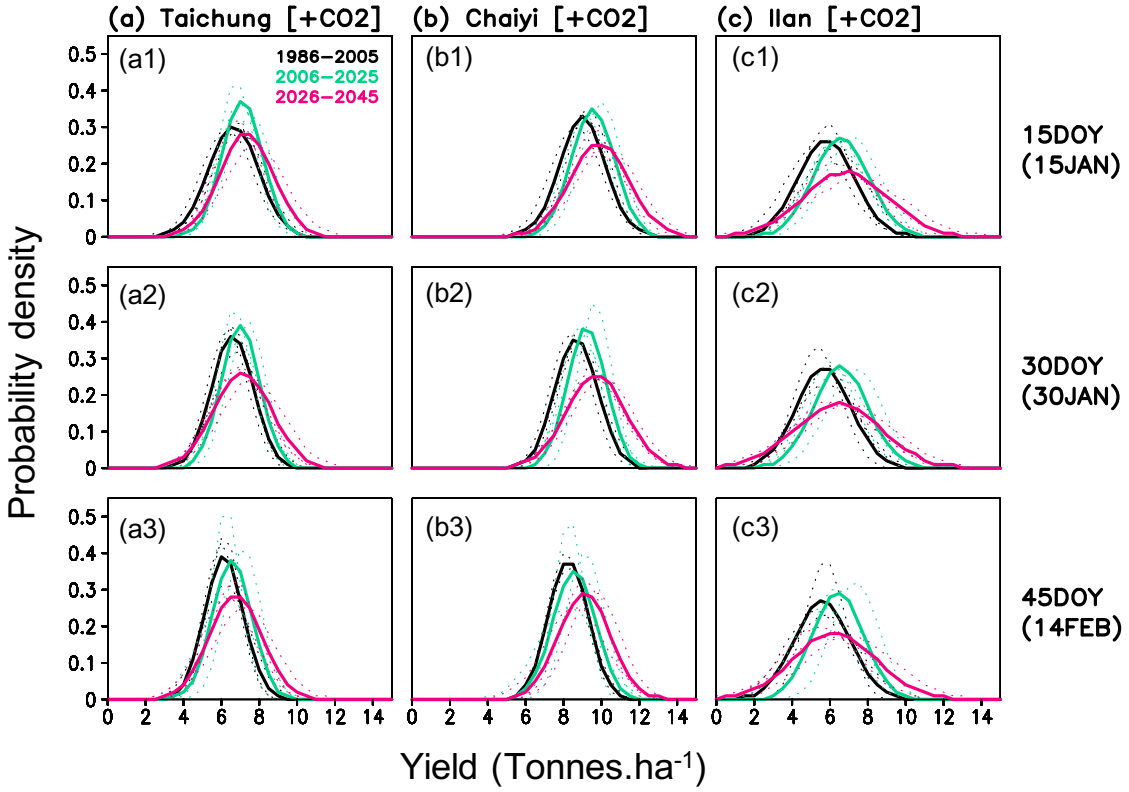

Fig. 4-10. Probability density function of simulated yield (with CO_2 effects) for three planting dates (15, 30, 45 day of year) and three periods (1986–2005, 2006–2025, 2026–2045) constructed for (a) Taichung, (b) Chaiyi and (c) Ilan; solid lines are averaged values from 3 models and dotted line are values of each model.

CHAPTER 5

CONCLUSIONS

The dissertation describes the application of climate diagnostic to understand nature and causes of extreme events associated by low temperature anomalies and their impacts on crop production in Taiwan and Thailand. The subsequently prediction based on the diagnostic results was developed in order to provide information and methodologies to manage risks and adapt to climate variability and change. Unexpected factors to cause extreme events and new understanding were disclosed from the case analysis both for the 2011 great flood in Thailand and 2016 anomalous cold in Taiwan.

The 2011 flood is distinguished from the other floods not only by monsoon rainfall but also from premonsoon rainfall in winter-spring seasons, other environmental factors such as soil moisture and sea level height, as well as poor drainage management. The main external forcing of climate change such as GHGs over the Chao Phraya River basin and strengthened northeasterly winds in La Niña year attributed to the premonsoon increase. The diagnostics suggest to monitoring premonsoon rainfall, low temperature anomaly, and sea level height adding from the common focus on monsoon rainfall that may help to alleviate the future flood and prevent total crop loss.

The succeeded application of climate diagnostic extended to evaluated wet and cold (WC) events leading to crop damage in Taiwan. The findings explicit the WC associated with the teleconnection patterns of cold SST anomaly in the WNP, warm PMM, negative NPO and CP El Niño which is different from previously known indicator such as EAWM. Understanding the driven factors for the WC events facilitates to

develop prediction models which combined outputs of climate parameters from CFSv2 model into statistical equations. The models can predict the WC events 6 month in advance while their performance is limited by the capacity of CFSv2 to predict WNP and PMM′. Further evaluate climate outputs from the multi-model ensemble (MME) may help to improve the prediction models for the WC events.

The study in WC events represents the seasonal prediction. Thus, the last study was expanded to evaluate long-term prediction for rice growth and yield in Taiwan. The results clearly present the negative effects of warming trend and benefit from elevated CO_2, which based RCP 8.5 scenarios, on the change in average yield. Yield variability projected to enlarge in the future which possibly relates to increase probability of climate extreme. The explanation of cold impacts on the rice growth and yield is restricted. That may be because of the capability of the single crop model to evaluate the temperature anomaly. Adding the determination by using multi crop-model ensembles as well as climate scenarios from MME would reduce uncertainty from the prediction. It is also challenge to apply combined empirical-dynamical approach for the long-term prediction.

Even though there are some limitation in the prediction, the three case studies reflect the strengths of climate diagnostics and the combination of these results into the prediction. Our models such as from the second study shows a better performance to predict the WC event than those only from climate model. Therefore, our methodologies would be an alternative way to make progress in prediction for crop production, that can be applied in other locations with a similar agro-climatological environment.

APPENDICES

APPENDIX A

SUPPORTING INFORMATION FOR CHAPTER 3

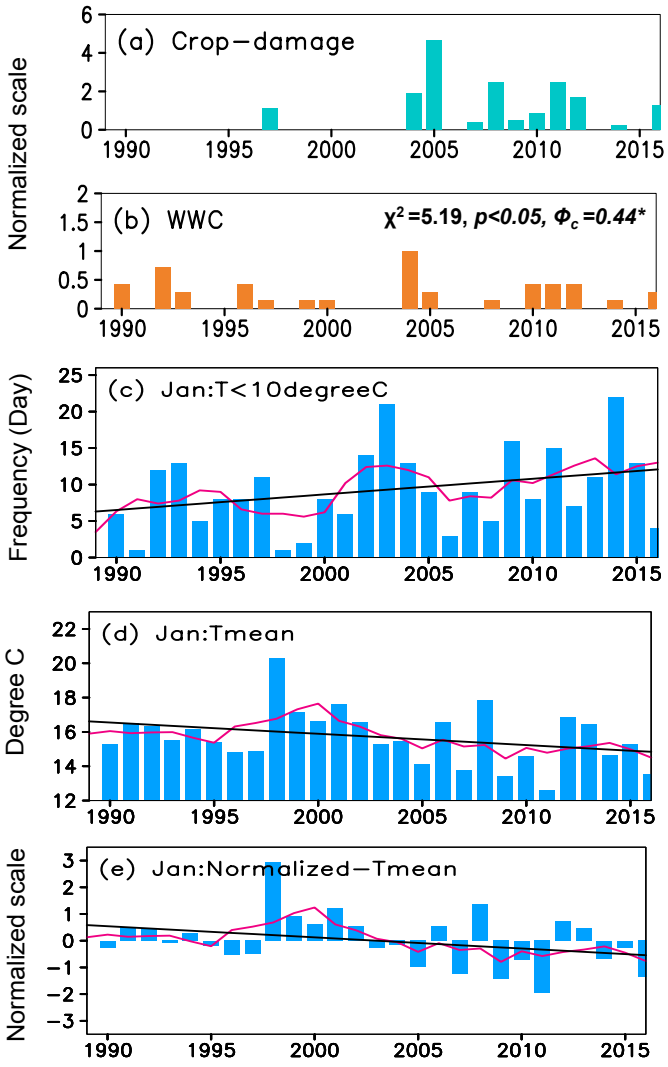

Figure 3-S1. (a) Crop-damage intensity and (b) wet with cold event in January-February, which are the same as Figure 3. (c) Number of days with temperature below 10 °C and (d) mean temperature (T_{mean}) in January overlaid with the 5-year moving average (red lines) and linear trend (black). (e) Normalization of T_{mean} in January, which indicates anomaly means, is derived from [(value of T_{mean} x_i – sample mean μ)/sample standard deviation σ].

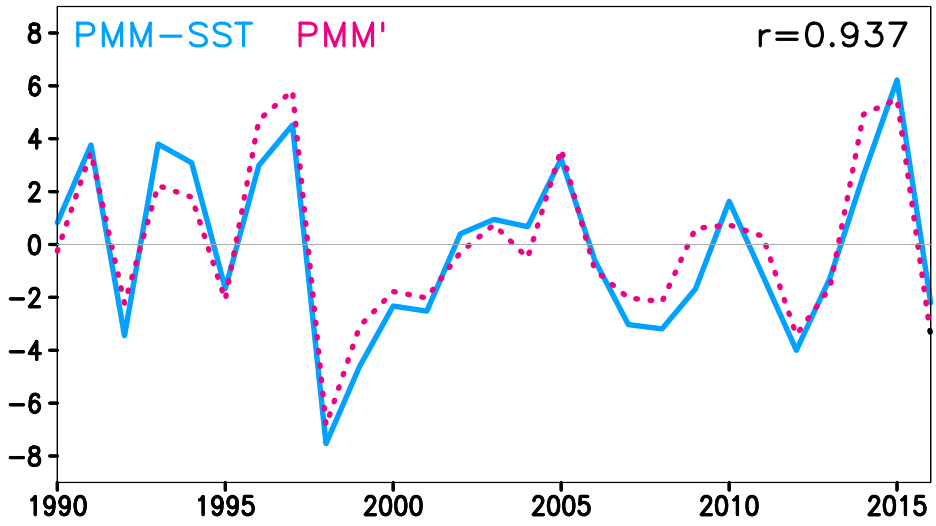

Figure 3-S2. Time series of PMM-SST and PMM′ (PMM-SST proxy) indicate that PMM′ has a high correlation coefficient (r = 0.937) with PMM-SST.

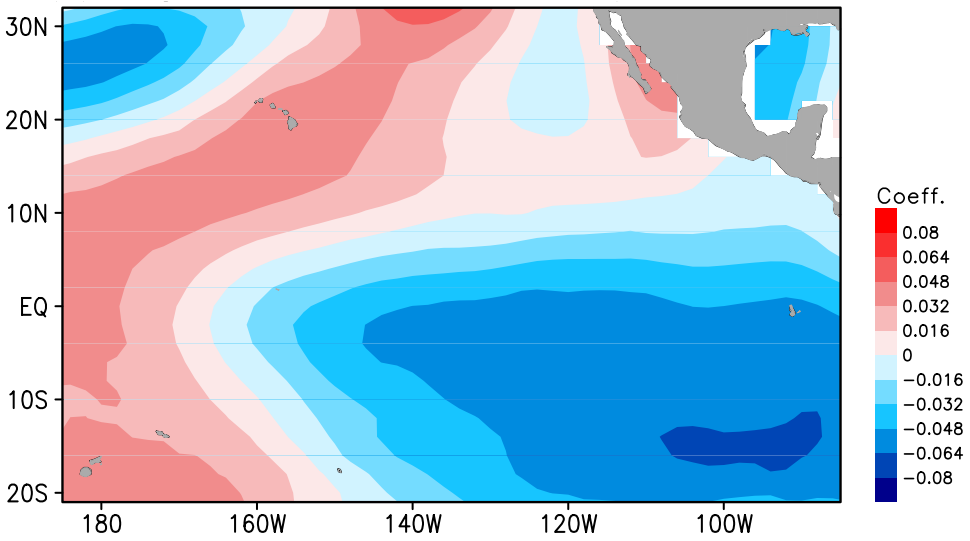

Figure 3-S3. Regression coefficient (shading) of SST computed against a time-series of cold days in January-February 1990–2016 constructed over 32°N–21°S to 175°E–95°W and used as reference areas for PMM′. Computation. PMM′ is PMM-SST proxy, which derived from JF-mean SST of the Pacific Ocean as the following steps: (1) In each year from 1990 to 2016, separately averaged SST from the area with positive (red-shaded area) and negative (blue-shaded area) coefficients; denoted those values as 'positive1' and 'negative1', respectively. (2) Annually derived a difference for the two values of averaged SST by subtracting 'positive1' with 'negative1' and denoted those values as 'diff'. (3) Calculated long-term means of SST from 'positive1' and 'negative 1' over a period of 1990-2016; denoted those values as 'ltm-positive1' and 'ltm-negative1'. (4) Derived a difference between 'ltm-positive1' and 'ltm-negative1' and denoted this value as 'ltm-diff'. (5) Annually computed anomaly value of 'diff' by subtracting 'diff' with 'ltm-diff' and denoted those values as 'anomaly'. (6) Computed coefficient or slope of linear trend from 'anomaly' and denoted this value as 'trn'. (7) De-trended anomaly value by subtracting 'anomaly' of each year with 'trn' to obtain PMM′ value.

APPENDIX B

SUPPORTING INFORMATION FOR CHAPTER 4

Table 4-S1
Lists of equations and names of CORDEX models used in this study.

Lists	Eq.	Descriptions
A. Equations		
$Es = 0.6108 \times 10^{\frac{7.5T}{237.7+T}}$	(1)	Es (kPa) is saturated vapor pressure *T* is mean temperature
$Ea = Es^{\frac{RH}{100}}$	(2)	Ea (kPa) is actual vapor pressure *RH* is relative humidity
$RMSE = \frac{\sqrt{\sum_{i=1}^{n} + (S_i - O_i)^2}}{n}$	(3)	S_i and O_i are simulated and observed values
$CDX_{adj} = \overline{OBS} + \frac{RMSE_{OBS}}{RMSE_{CDX}} \times (CDX - \overline{CDX})$	(4)	CDX_{adj} is adjusted-CORDEX parameter $\overline{OBS}$ is mean of observed parameter (OBS) $\overline{CDX}$ is mean of original-CORDEX parameter (CDX) $RMSE_{OBS}$ and $RMSE_{CDX}$ are root mean square errors of OBS and CDX
$SQ_t = \sum (22 - T_d)$ (Bouman et al., 2001)[1]	(5)	SQ_t (°Cd) is sum of cooling degree-day during the sensitivity period of rice panicles (DVS^2 = 0.75 to DVS = 1.2) Td is average temperature
$S_c = 1 - \frac{(4.6 + 0.054\ x\ SQ_t^{1.56})}{100}$	(6)	S_c or SF1 is the spikelet sterility factor due to low temperature
$S_h = \frac{1}{(1 + \exp(0.853(T_{m,a} - 36.6)))}$ (Bouman et al., 2001)	(7)	Sh or SF2 is the spikelet fertility factor due to high temperature $T_{m,a}$ is average daily T_{max} during the flowering period (DVS = 0.96 to DVS = 1.22)
$\varepsilon = \varepsilon_{340}\left(\frac{1 - \exp(-0.00305\ x\ CO_2 - 0.222)}{1 - \exp(-0.00305\ x\ 340 - 0.222)}\right)$ (Bouman et al., 2001)	(8)	ε is the coefficient of CO_2 effect ε_{340} is ε at a reference level of CO_2 concentration (340 ppm) CO_2 is the ambient CO_2 concentration for the simulation

Lists	Eq.	Descriptions
A. CORDEX models		
Model 1: ICHEC-EC-EARTH (r3i1p1) + DMI-HIRHAM5		Driving model: ICHEC-EC-EARTH RCM[3]: DMI-HIRHAM5
Model 2: ICHEC-EC-EARTH (r12i1p1) + CLMcom-CCLM5-0-2		Driving model: ICHEC-EC-EARTH RCM: CLMcom-CCLM5-0-2
Model 3: MPI-M-MPI-ESM-LR (r1i1p1) + CLMcom-CCLM5-0-2		Driving model: MPI-M-MPI-ESM-LR RCM: CLMcom-CCLM5-0-2

[1]Bouman, B.A.M., Kropff, M.J., Tuong, T.P., Wopereis, M.C.S., ten Berge, H.F.M., van Larr, H.H., 2001. ORYZA2000: Modeling Lowland Rice. International Rice Research Institute, Metro Manila, Philippines.

[2]DVS is development stage of crop

[3]RCM is regional climate models

Table 4-S2
Phenological development parameters used with TNG67 rice variety for parameterization of ORYZA(v3) model.

Parameters	Abbreviation	Value
Base temperature for development (°C)	TBD	8
Base temperature for juvenile leaf area growth (°C)	TBLV	8
Maximum temperature for development (°C)	TMD	42
Optimum temperature for development (°C)	TOD	30
Development rate in juvenile phase ($^oCd^{-1}$)	DVRJ	0.000524
Development rate in photoperiod-sensitive phase ($^oCd^{-1}$)	DVRI	0.000758
Development rate in panicle development ($^oCd^{-1}$)	DVRP	0.001130
Development rate in reproductive phase ($^oCd^{-1}$)	DVRR	0.001965

Table 4-S3
Statistics for observed and simulated outputs for TNG67 rice variety from calibration of ORYZA(v3) model.

Biomass/LAI	α	β	R^2	$P(t)_1$
Total above ground	185.9	1.034	0.996	0.000
Stem	347.1	0.800	0.927	0.000
Green leaves	-56.8	1.211	0.997	0.000
Dead leaves	28.30	1.440	0.976	0.000
Storage organ	32.84	1.006	0.994	0.000
Leaf Area Index	0.335	1.059	0.992	0.000

α, slope of linear regression between observed and simulated values; β, y-intercept of the linear regression; R^2, coefficient of determination for the linear regression, $P(t)_1$, significant of student *t*-test for the linear regression.

Table 4-S4
Statistics for observed and simulated outputs for TNG67 rice variety from validation of ORYZA(v3) model.

Biomass	α	β	R^2	$P(t)_1$	Mean (sim)	Mean (obs)	$P(t)_2$	SD (sim)	SD (obs)	RMSE (kg ha^{-1})
n =8 (2009 - 2016)										
Yield	7059	0.050	0.001	0.935	7452	7813	0.512	1240	856	1433
Storage organ	6190	0.044	0.001	0.942	6491	6801	0.512	1076	756	1253
Total above ground	9719	0.259	0.054	0.578	1.32E4	1.36E4	0.585	1362	1228	1538
Flowering date	36.61	0.658	0.978	0.000	107	107	0.909	5.60	8.42	2.8
Maturity date	52.64	0.611	0.790	0.003	136	136	0.934	5.66	8.22	3.9
n =5 (excluded 2011, 2014, 2015)										
Yield	4447	0.451	0.790	0.044	7994	7866	0.621	453	892	551
Storage organ	3857	0.452	0.841	0.028	6946	6837	0.624	390	791	477
Total above ground	7267	0.446	0.692	0.081	1.34E4	1.39E4	0.368	793	1479	1043
Flowering date	26.98	0.748	0.977	0.002	107	107	1.000	5.12	6.76	1.7
Maturity date	65.39	0.515	0.857	0.024	136	136	0.737	5.22	9.40	4.5

α, slope of linear regression between observed and simulated values; β, y-intercept of the linear regression; R^2, coefficient of determination for the linear regression; $P(t)_1$, significance of student *t*-test for the linear regression model (non-equal variance); Mean (sim)/(obs), mean of simulated/observed values (kg ha^{-1}); SD (sim)/(obs), standard deviation of simulated/observed values (kg ha^{-1}); $P(t)_2$, significance of student's paired *t*-test of mean (non-equal variance); RMSE, Root mean squared error (kg ha^{-1}; day).

Table 4-S5
Correlation coefficients between accumulated growing degree days and simulated rice yield for 1986-2045 (*, ** indicate significance of the coefficients exceeding 99%, and 99.9 % confidence interval).

Scenario	Planting date	Growth stage	Taichung	Chaiyi	Ilan
Fixed CO2	15 Jan	Vegetative	-0.31	-0.28	-0.04
		Reproductive	-0.37*	-0.15	-0.41*
		Total	-0.41*	-0.26	-0.38*
	30 Jan	Vegetative	-0.20	-0.11	-0.20
		Reproductive	-0.36*	-0.08	-0.46**
		Total	-0.37*	-0.11	-0.47**
	14 Feb	Vegetative	-0.27	-0.34	-0.35*
		Reproductive	-0.28	-0.07	-0.50**
		Total	-0.30	-0.18	-0.53**
Projected CO2	15 Jan	Vegetative	0.02	0.03	0.12
		Reproductive	0.31	0.53**	-0.15
		Total	0.25	0.41	-0.08
	30 Jan	Vegetative	0.07	0.19	-0.05
		Reproductive	0.36*	0.61**	-0.19
		Total	0.32	0.57**	-0.18
	14 Feb	Vegetative	0.28	0.29	-0.12
		Reproductive	0.40*	0.60**	-0.20
		Total	0.39*	0.57**	-0.20

Table 4-S6
Correlation coefficients between accumulated radiation and simulated rice yield for 1986-2045 (*, ** indicate significance of the coefficients exceeding 99%, and 99.9% confidence interval).

Scenario	Planting date	Growth stage	Taichung	Chaiyi	Ilan
Fixed CO2	15 Jan	Vegetative	0.35*	0.26	0.22
		Reproductive	0.69**	0.71**	0.84**
		Total	0.67**	0.64**	0.67**
	30 Jan	Vegetative	0.29	0.18	0.21
		Reproductive	0.66**	0.75**	0.83**
		Total	0.62**	0.62**	0.69**
	14 Feb	Vegetative	0.36*	0.21	0.30
		Reproductive	0.66**	0.66**	0.74**
		Total	0.66**	0.58**	0.68**
Projected CO2	15 Jan	Vegetative	0.12	-0.01	0.15
		Reproductive	0.47**	0.48**	0.74**
		Total	0.36*	0.29	0.56**
	30 Jan	Vegetative	0.01	-0.09	0.16
		Reproductive	0.55**	0.53**	0.75**
		Total	0.35*	0.29	0.60**
	14 Feb	Vegetative	0.08	-0.06	0.25
		Reproductive	0.60**	0.54**	0.71**
		Total	0.44**	0.33*	0.63**

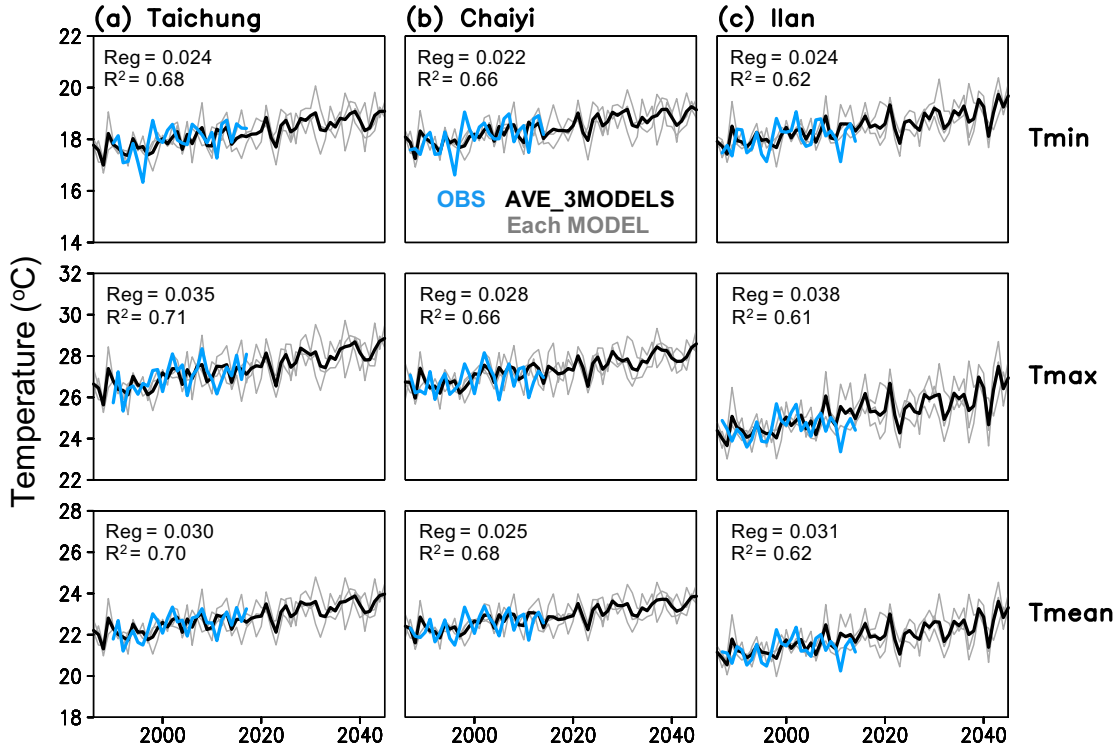

Fig. 4-S1. Seasonal (January–June) observed-temperature (OBS) and projected-temperature from adjusted CORDEX constructed for (a) Taichung, (b) Chaiyi, and (c) Ilan; linear regression coefficients (Reg) and coefficient of determination (R^2) between year and temperature (T_{max}, T_{min}, T_{mean}) are presented in each panel.

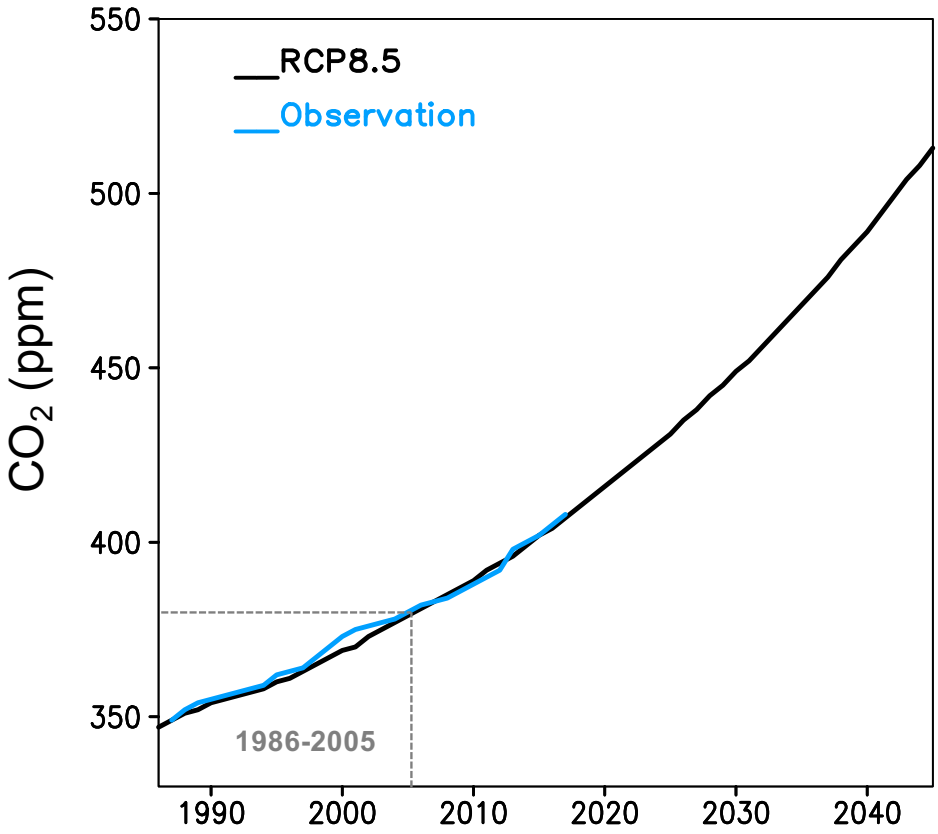

Fig. 4-S2. Annual observed CO_2 and projected CO_2 from RCP 8.5 scenario.

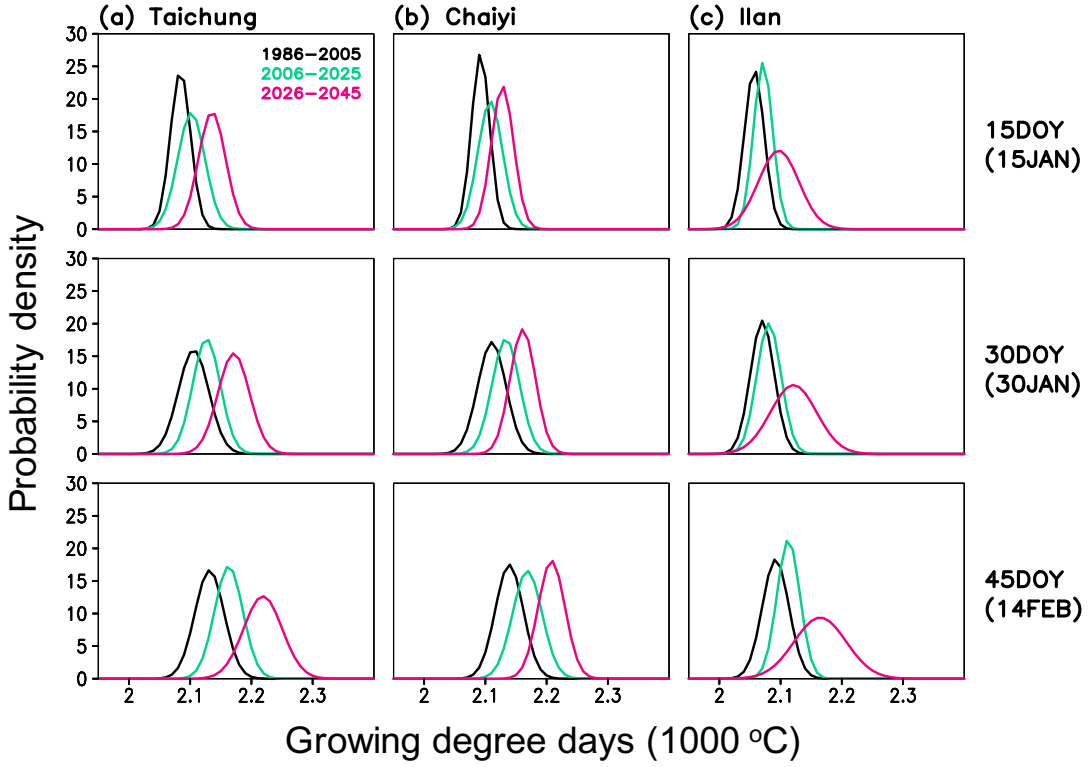

Fig. 4-S3. Probability density function of total growing degree days (GDD) from rice emergence to maturation for three-planting dates (15, 30, 45 day of year) and three periods (1986–2005, 2006–2025, 2026–2045) constructed for (a) Taichung, (b) Chaiyi, and (c) Ilan. The probability density distributions are derived with a bin size of 10 degree-days (°C).

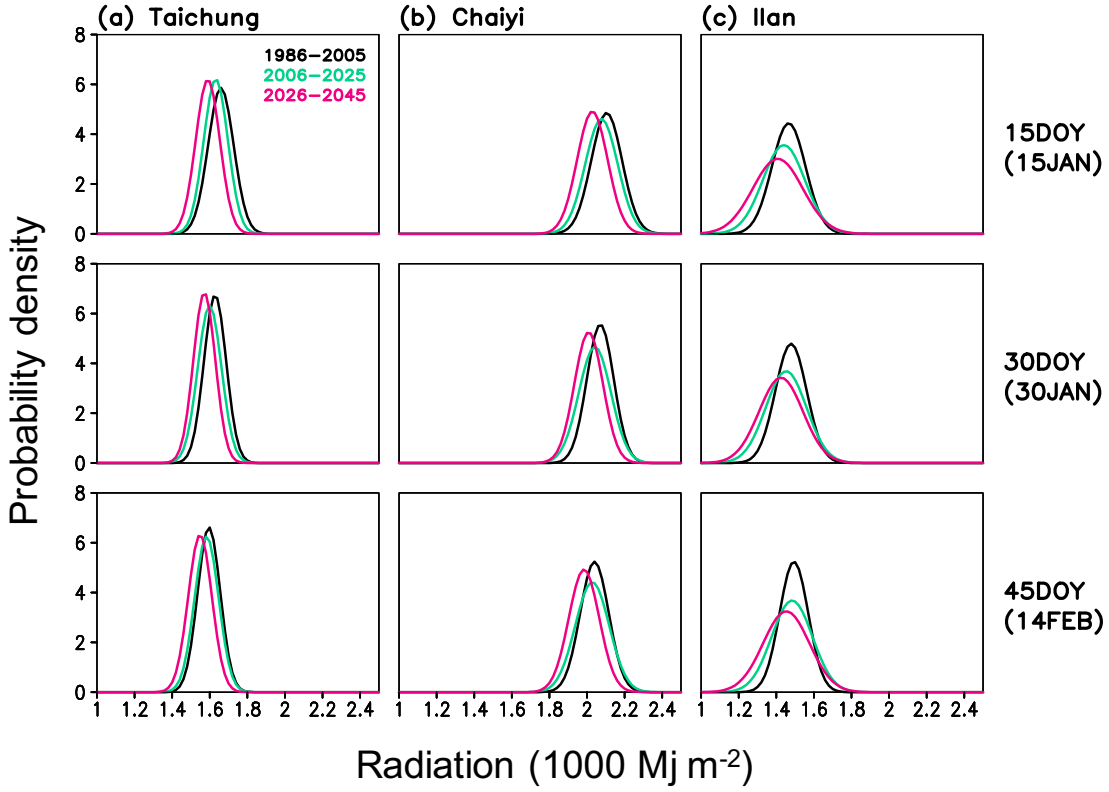

Fig. 4-S4. Probability density function of total radiation from rice emergence to maturation for three-planting dates (15, 30, 45 day of year) and three periods (1986–2005, 2006–2025, 2026–2045) constructed for (a) Taichung, (b) Chaiyi, and (c) Ilan. The probability density distributions are derived with a bin size of 20 (Mj m^{-2}).

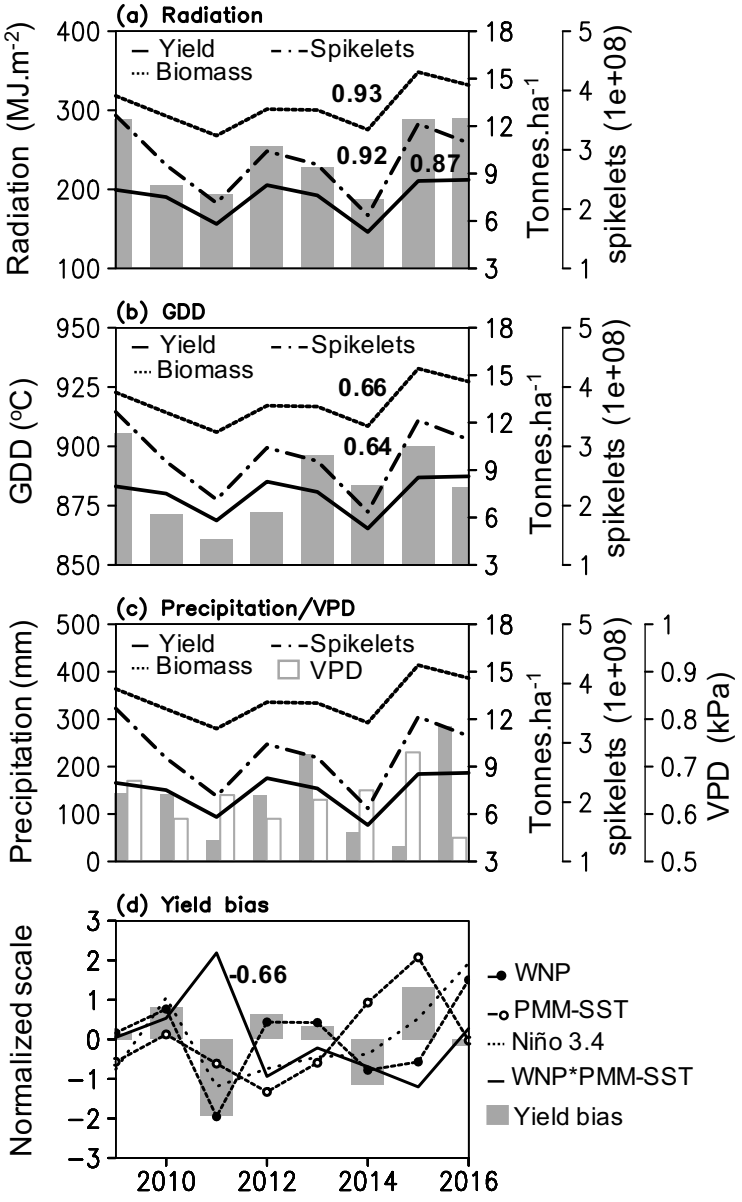

Fig. 4-S5. Time series of yield, biomass and number of spikelets superimposed on (a) total radiation from panicle initiation to flowering stages (DVS0.65 to DVS1.0), (b) growing degree day (GDD) during vegetative phase (DVS0.4), and (c) precipitation and vapor pressure deficit (VPD) during DVS0.4; Panel (d) presents time series of yield bias (simulated – observed yields) and climate indices (WNP, PMM-SST, Niño 3.4, WNP*PMM-SST); number in each panel indicates significant correlation coefficients (r) exceeding 99% ($r > 0.83$) and 90% ($r > 0.62$) confidence interval. [Methodologies to obtain climate indices are followed Promchote et al., 2018; WNP is the western North Pacific, PMM-SST is the Pacific meridional mode – sea surface temperature].

APPENDIX C

PERMISSIONS AND RELEASE LETTERS

License Agreement I: Materials for Chapter 2

February 4th, 2019

Parichart Promchote
760E 900N APT6
Logan, UT 84321

To the Permissions Editor:

I am in the process of preparing my dissertation in the Plants, Soils, and Climate department at Utah State University. I hope to complete my degree program in Climate Science.

The article "The 2011 great flood in Thailand: Climate diagnostics and implications of climate change", of which I am first author, an which appeared in your journal (1 January 2016, pages 367-379) reports an essential part of my dissertation research. I would like permission to reprint it as a chapter in my dissertation, which may require some revision. Please note that USU sends every thesis and dissertation to ProQuest to be made available for reproduction.

I will include acknowledgment to the article on the first page of the chapter, as shown below. Copyright and permission information will be included in a special appendix. Please let me know if you would like a different acknowledgment.

Please indicate your approval of this request by signing in the space provided, and attach any other form necessary to confirm permission. If you charge a reprint fee for use of an article by the author, please indicate that as well.

If you have any questions, please contact me at the phone number or email below. Thank you for your assistance.

Parichart Promchote
Tel: (1) 435 7743711
parichart.promchote@aggiemail.usu.edu

Herbst, Andrea <aherbst@ametsoc.org> Feb 7, 2019, 1:40 PM
to me, permissions

Dear Parichart,

Thank you for your email. This signed message constitutes permission to use the material requested below.

You may use your JCLI article in your upcoming dissertation with the following conditions:

1. Include the complete bibliographic citation of the original source.
2. Include the following statement with that citation: **© American Meteorological Society. Used with permission.**

If you have any questions or need additional information, please feel free to contact me.

Please note: The requester is responsible for ensuring that AMS holds the copyright for the material they wish to reuse. If the material in an AMS journal is credited to another source, they must obtain permission or license from that source directly. That material may not be used without permission or license from the copyright holder.

Best,

Andrea Herbst
Peer Review Support Associate
Permissions Specialist

American Meteorological Society
617.226.3982
www.ametsoc.org

License Agreement II: Materials for Chapter 3

JOHN WILEY AND SONS LICENSE TERMS AND CONDITIONS

Feb 04, 2019

This Agreement between Ms. Parichart Promchote ("You") and John Wiley and Sons ("John Wiley and Sons") consists of your license details and the terms and conditions provided by John Wiley and Sons and Copyright Clearance Center.

License Number
4522170827767
License date
Feb 04, 2019
Licensed Content Publisher
John Wiley and Sons
Licensed Content Publication
International Journal of Climatology
Licensed Content Title
A seasonal prediction for the wet–cold spells leading to winter crop damage in northwestern Taiwan with a combined empirical–dynamical approach
Licensed Content Author
Parichart Promchote, S.-Y. Simon Wang, Yuan Shen, et al
Licensed Content Date
Jul 12, 2017
Licensed Content Volume
38
Licensed Content Issue
2
Licensed Content Pages
13
Type of use
Dissertation/Thesis
Requestor type
Author of this Wiley article
Format
Print and electronic
Portion
Full article
Will you be translating?
No
Title of your thesis / dissertation
LINKAGE OF CLIMATE DIAGNOSTICS IN PREDICTIONS FOR CROP PRODUCTION: COLD IMPACTS IN TAIWAN AND THAILAND
Expected completion date
May 2019
Expected size (number of pages)
135
Requestor Location
Parichart Promchote
760E 900N APT6
LOGAN, UT 84321
United States
Attn: Parichart Promchote
Publisher Tax ID
EU826007151
Total
0.00 USD

Terms and Conditions

ACTION, WHETHER FOR BREACH OF CONTRACT, BREACH OF WARRANTY, TORT, NEGLIGENCE, INFRINGEMENT OR OTHERWISE (INCLUDING, WITHOUT LIMITATION, DAMAGES BASED ON LOSS OF PROFITS, DATA, FILES, USE, BUSINESS OPPORTUNITY OR CLAIMS OF THIRD PARTIES), AND WHETHER OR NOT THE PARTY HAS BEEN ADVISED OF THE POSSIBILITY OF SUCH DAMAGES. THIS LIMITATION SHALL APPLY NOTWITHSTANDING ANY FAILURE OF ESSENTIAL PURPOSE OF ANY LIMITED REMEDY PROVIDED HEREIN.

- Should any provision of this Agreement be held by a court of competent jurisdiction to be illegal, invalid, or unenforceable, that provision shall be deemed amended to achieve as nearly as possible the same economic effect as the original provision, and the legality, validity and enforceability of the remaining provisions of this Agreement shall not be affected or impaired thereby.

- The failure of either party to enforce any term or condition of this Agreement shall not constitute a waiver of either party's right to enforce each and every term and condition of this Agreement. No breach under this agreement shall be deemed waived or excused by either party unless such waiver or consent is in writing signed by the party granting such waiver or consent. The waiver by or consent of a party to a breach of any provision of this Agreement shall not operate or be construed as a waiver of or consent to any other or subsequent breach by such other party.

- This Agreement may not be assigned (including by operation of law or otherwise) by you without WILEY's prior written consent.

- Any fee required for this permission shall be non-refundable after thirty (30) days from receipt by the CCC.

- These terms and conditions together with CCC's Billing and Payment terms and conditions (which are incorporated herein) form the entire agreement between you and WILEY concerning this licensing transaction and (in the absence of fraud) supersedes all prior agreements and representations of the parties, oral or written. This Agreement may not be amended except in writing signed by both parties. This Agreement shall be binding upon and inure to the benefit of the parties' successors, legal representatives, and authorized assigns.

- In the event of any conflict between your obligations established by these terms and conditions and those established by CCC's Billing and Payment terms and conditions, these terms and conditions shall prevail.

- WILEY expressly reserves all rights not specifically granted in the combination of (i) the license details provided by you and accepted in the course of this licensing transaction, (ii) these terms and conditions and (iii) CCC's Billing and Payment terms and conditions.

- This Agreement will be void if the Type of Use, Format, Circulation, or Requestor Type was misrepresented during the licensing process.

- This Agreement shall be governed by and construed in accordance with the laws of the State of New York, USA, without regards to such state's conflict of law rules. Any legal action, suit or proceeding arising out of or relating to these Terms and Conditions or the breach thereof shall be instituted in a court of competent jurisdiction in New York County in the State of New York in the United States of America and each party hereby consents and submits to the personal jurisdiction of such court, waives any objection to venue in such court and consents to service of process by registered or certified mail, return receipt requested, at the last known address of such party.

WILEY OPEN ACCESS TERMS AND CONDITIONS

Wiley Publishes Open Access Articles in fully Open Access Journals and in Subscription journals offering Online Open. Although most of the fully Open Access journals publish open access articles under the terms of the Creative Commons Attribution (CC BY) License only, the subscription journals and a few of the Open Access Journals offer a choice of Creative Commons Licenses. The license type is clearly identified on the article.

The Creative Commons Attribution License

The Creative Commons Attribution License (CC-BY) allows users to copy, distribute and transmit an article, adapt the article and make commercial use of the article. The CC-BY license permits commercial and non-

Creative Commons Attribution Non-Commercial License

The Creative Commons Attribution Non-Commercial (CC-BY-NC)License permits use, distribution and reproduction in any medium, provided the original work is properly cited and is not used for commercial purposes.(see below)

Creative Commons Attribution-Non-Commercial-NoDerivs License

Permission to Reprint from Co-author: Chapter 3

April 1st, 2019

Parichart Promchote
760E 900N APT6
Logan, UT 84321

Dear Dr. Ming-Hwi Yao:

I am in the process of preparing my dissertation in the Plants, Soils, and Climate department at Utah State University. I hope to complete my degree program in Climate Science.

I am requesting your permission to include as a chapter in my dissertation for the paper: A seasonal prediction for the wet-cold spells leading to winter crop damage in northwestern Taiwan with a combined empirical-dynamical approach, published in International Journal of Climatology, 2018 (38: 571-583), which you are listed as co-author. A citation information will appear on the first page of this chapter, and a copy of this permission letter will be included as an appendix to the dissertation.

Please indicate your approval of this request by signing in the space provided. If you have any questions, please contact me at the email below.

Thank you for your cooperation,
Parichart Promchote
Email: parichart.promchote@aggiemail.usu.edu

I hereby give permission to Parichart Promchote to reprint the requested article in her Dissertation.

Signed: _____

Date: April 1, 2019.

CURRICULUM VITAE

Parichart Promchote
(email: parichart.pr@ku.th)

Education

M.Sc. (Agricultural Development), The University of Copenhagen, Denmark
M. de Sci. et Tech. (Agronomie-Agroalimentaire), Montpellier SupAgro – Institue des Régions Chaudes, France
M.S. (Agriculture-Plant Physiology and Crop Production), Kasetsart University, Thailand
B.S. (Agriculture-Agronomy) with honors, Kasetsart University, Thailand

Academic Work Experience

Lecturer, Department of Agronomy, Kasetsart University, Thailand (2009–present)

Study Awards and Grants

Graduate Student Researcher of the Year, Department of Plants, Soils and Climate (PSC), Utah State University (2018)
People's Choice Awards—most innovative poster at the student poster symposium, PSC Showcase (2017 and 2018)
PSC internship travel grants: National Chung Hsing University, Taichung, Taiwan (2016 and 2017)
PSC presentation travel grant: Special seminar entitled Extreme Events Facing Thailand, Bangkok, Thailand (2016)
National Oceanic and Atmospheric Administration (NOAA) student travel grant: Climate Diagnostics & Prediction Workshop, Denver, Colorado (2015)
Royal Thai Government PhD scholarship (2014–2019)

Publications

Xu, C., B.M. Buckley, P. Promchote, S.-Y. S. Wang, N. Pujimonng, W. An, M. Sano, T. Nakatsuka, and Z. Guo, 2019: Increased variability of Thailand's Chao Phraya River peak-season flow and its association with ENSO variability: Evidence from tree ring $\delta^{18}O$. *Geophys. Res. Lett.* (in press).

Mukherjee, A., S.-Y. S. Wang, and P. Promchote, 2019: Examination of the climate factors that reduced wheat yield in northwest India during the 2000s. *Water*, **11**, 343, doi: 10.3390/w11020343.

Promchote, P., S.-Y. S. Wang, Y. Shen, P.G. Johnson, and M.-H. Yao, 2018: A seasonal prediction for the wet-cold spells leading to winter crop damage in northwestern Taiwan with a combined empirical-dynamical approach. *Int. J. Climatol.*, **38**, 571–583, doi: 10.1002/joc.5194.

Huang, W.-R., S.-H. Wang, M.-C. Yen, N.-H. Lin, and P. Promchote, 2016: Interannual variation of springtime biomass burning in Indochina: Regional differences, associated atmospheric dynamical changes, and downwind impacts. *J. Geophys. Res. Atmos.,* **121**, 10016–10028, doi: 10.1002/2016JD025286.

Promchote, P., S.-Y. Wang, and P. G. Johnson, 2016: The 2011 Great Flood in Thailand: Climate Diagnostics and Implications from Climate Change. *J. Climate,* **29**, 367–379, doi: 10.1175/JCLI-D-15-0310.1.

Wang, S.-Y., P. Promchote, H. T. Luu, B. Buckley, R. Li, R. R. Gillies, T. Q. T. Nguyen, B. Guan, and T. T. Monh, 2015: Changes in the autumn precipitation and tropical cyclone activity over Central Vietnam and its East Sea. *Vietnam J. Earth Sci.*, **36**, 1–7.